# The Hillslope Hydrology of a Mountain Pasture: The Influence of Subsurface Flow on Nitrate and Ammonium Transport

Nicolas P. Zegre

Thesis submitted to the faculty of the Virginia Polytechnic Institute and State University in partial fulfillment of the requirements for the degree of

MASTER OF SCIENCE
In
Forestry

Approved:

_____
W. Michael Aust, Chair

_____
Saied Mostaghimi

_____
James M. Vose

July 22, 2003

**Keywords**: hillslope hydrology, subsurface flow, vadose zone hydrology, hydrologic modeling, nutrient transport, riparian zone

# The Hillslope Hydrology of a Mountain Pasture: The Influence of Subsurface Flow on Nitrate and Ammonium Transport

**Nicolas P. Zegre**

## Abstract

Nonpoint source (NPS) pollution is possibly the greatest form of contamination to our nation's waters. Nutrient pollutants, such as nitrate and ammonium, often enter aquatic ecosystems through surface and subsurface hydrological transport that drain agricultural watersheds. The over-abundance of nitrogen within these watersheds is easily transported to receiving stream and rivers, and result in aquatic ecosystem degradation. In response to the problem of nutrient loading to aquatic ecosystems, ecosystems scientists and federal and state governments have recommended the use of streamside management zones (SMZ) to reduce the amount of NPS pollutants. A small agricultural watershed in southwestern North Carolina was utilized to quantify subsurface transport of nitrate and ammonium to a naturally developing riparian area along Cartoogechaye Creek.

Vertical and lateral transport of nitrate and ammonium were measured along three transect perpendicular to the stream. Transects were instrumented with time domain reflectometry (TDR) and porous cup tension lysimeters to monitor soil water and nutrient flux through the pasture and riparian area located at the base of the watershed. The HYDRUS 2-D flow and transport model was used to predict and simulate subsurface flow. Predicted flow was coupled with observed field nutrient data to quantify nutrient flux as a function of slope location. HYDRUS 2-D was capable of simulating subsurface

flow (saturated and unsaturated) as a function of observed soil physical properties (bulk density, saturated hydraulic conductivity, particle size distribution, water retention characteristics) and climatic data (precipitation, air temperature, wind speed, etc.).

The riparian area was effective in reducing the amount of nonpoint source pollution to a naturally developing riparian area from an agricultural watershed. Dramatic decreases in both $NO_3^-$-N and $NH_4^+$-N in upland pasture water were observed within the riparian area. Seasonal percent reductions of $NO_3^-$ from the pasture to riparian area in subsurface water within the study watershed are as follows: summer (2002) = 456%; fall (2002) = 116%; winter (2003) = 29%; spring = 9%, pasture and riparian, respectively.

# Acknowledgements

I would like to sincerely thank my advisor and committee chair, Dr. W, Michael Aust and chair member and mentor, Dr. James M. Vose of the Coweeta Hydrologic Laboratory and Dr. Saied Mostaghimi. Both Dr. Aust, Dr. Vose, and Dr. Mostaghimi allowed me to work with complete autonomy, through the trials, tribulations, and success of the project. I am also very grateful for their ability to allow me to fail, process, and recover with their full confidence of my ability to function as a developing scientist. I especially thank Dr. Aust and Dr. Vose for their dynamic personalities and continued humor. Thanks is also given to the entire faculty and staff of the Department of Forestry, especially Tracey Sherman, for their logistical and administrative support.

I am forever grateful to the scientists and staff of the Coweeta Hydrologic Laboratory for their continued assistance during my employment at the lab and my graduate work at Virginia Tech. A special thanks is given to Dr. Mark Riedel for his unconditional guidance during the project. Though Dr. Riedel was not officially on my committee, he offered invaluable support, technical guidance, and humor that certainly assisted my understanding and desire to study hydrologic sciences. Dr. Jennifer Knoepp, Dr. Robert Hubbard, Jim Deal, and Julie Moore should also be recognized for their valuable assistance.

A very special thanks to Dr. Gaber Hassan, of Dr. Ray Reneaux's lab in the Crop and Soil Environmental Sciences for his continued support and assistance of the HYDRUS 2-D flow model. I recognize Dr. Ray Hicks of the Department of Forestry and Dr. Richard Thomas of Biology, both at West Virginia University, for introducing me to the world of research. Mark Eisenbeis and Dr. Andy Scott are also recognized for their unconditional support.

Finally, I am so grateful of the continued support of my entire family, Andrea, David, Coralie, Jessica, and Ellie for supporting me in my adventures of obtaining all of my dreams, past, present, and future. Their support and calming words often helped me recognized reality and what is truly significant in life

# Table of Contents

# List of Tables

# List of Figures

# Chapter 1: Introduction

Southwestern North Carolina and most of the mid-Appalachian region of the United States have been influenced by a variety of anthropogenic activities including row crop agriculture, livestock grazing, forest harvesting, mining, and other natural resource extractions in an attempt to provide society's natural resources needs (Yarnell, 1998). In the most recent decades, population and development have increased substantially, offering new and possibly unsustainable impacts on the local ecosystems (Yarnell, 1998).

Although the amount of land dedicated to farming and livestock has decreased over the last 50 years, the influence of such activities is still present. Typical to the mid-Appalachian region, these practices have primarily occurred in the more fertile soils of the valleys and toe-slopes of the mountains (United States Department of Agriculture, 1996). These areas are also the headwaters of streams and rivers throughout the southern United States.

The presence of cattle, the increased use of nitrogen fertilizers, and the removal of vegetation along the stream banks of these headwater areas have increased the amount of nitrogen and other nutrients being transported and deposited in the rivers and streams (Dissmeyer, 2000). In an attempt to reduce the amount of non-point source (NPS) pollution inputs to these waterways, federal and state agencies have advocated the use of Best Management Practices (BMP), such as riparian areas, to trap and sequester nutrients and sediments before reaching water (Bosch et al., 1994; Schultz et al., 1994).

It is well documented that riparian areas play a significant role in filtering both surface and subsurface waters of sediment, nutrients, and chemical pollutants (agrochemical, fertilizers, etc.) to aquatic ecosystems (Bosch et al., 1994; Peterjohn and Correll, 1984;

Schultz et al., 1994; Vought et al., 1995). These vegetative buffers also offer terrestrial and aquatic habitat, shade for streams, re-oxygenation of water, and stream bank stability.

Understanding water and pollutants movement through upland soil to the riparian areas is imperative to developing management practices, protocol, and legislation to protect both terrestrial and aquatic ecosystems. There have been considerable research efforts in understanding how pollutants move through saturated zones of terrestrial ecotones, but field studies investigating transport of water and pollutants through unsaturated or vadose zone media is lacking (Dahm et al., 1998; Yeakley et al., 2003).

There are a number of transport parameters that control water movement through unsaturated and saturated media, such as soil physical (soil type, extent, properties, etc.) and mechanical (saturated and unsaturated hydraulic conductivity, bulk density, porosity, etc.) properties, preferential flow (mole/worm holes, rooting channels, confining layers), storm flux, intensity, volume, and duration of precipitation events, and exchange with saturated media. Nitrate transport, the focus of this research, is commonly linked to the lateral subsurface movement of water in soils (Cooper, 1990; Hill, 1996; Hubbard and Sheridan, 1983). Though overland flow is a dominant part of nitrate transport in mountain pastures, research has shown that water (and nitrate) can move laterally in the subsurface as a result of a confining soil layer or geologic structure. The purpose of this project is to gain better understanding of upslope, subsurface hydrological functions and transport of nitrate to a naturally developing riparian area.

## Goal and Objectives of Project

The overall goal of this project was to quantify transport of water, $NO_3^-$, and $NH_4^+$ from pastureland via subsurface pathways to riparian areas in order to evaluate the utility of

riparian buffers. Hydrologic dynamics were quantified through the integration of observed field hydrologic and nutrient transport activity and the HYDRUS 2-D model to simulate and predict subsurface contributions of nutrients to a receiving riparian area. The understanding of this goal will help to better understand the importance of riparian zone function, and the need for riparian restoration in enhancing stream water quality.

The following specific objectives have been identified as important steps for achieving the overall objectives:

1. Quantify primary subsurface drainage within the current study site (upslope, within riparian area, and interaction of riparian area and river).
2. Improve understanding of groundwater transport and the interactions of $NO_3^-$ and $NH_4^+$ with groundwater, riparian area, and river.
3. Understanding hydrologic interactions of riparian area and stream.

# Literature Review

## *Riparian Zones*

Researchers have documented that riparian zones play a significant and beneficial role in natural ecotones (Dillaha et al., 1988; Schultz et al., 1994). Riparian zones have multiple definitions but generally can be defined as the vegetative interface between terrestrial and aquatic ecosystems. These transitional zones provide important links between the terrestrial upland ecosystem and aquatic stream or lake ecosystems (Schultz et al., 1994). Two specific types of riparian zones are forest riparian zones that have large woody herbaceous cover and trees and vegetative filter strips (VFS) that are primarily composed of grasses and herbaceous cover. Riparian zones are often characterized by hydrology, vegetation, and soils (Hill, 1996; Lowrance et al., 1984; Swanson et al., 1982).

## *Riparian Function*

A primary characteristic of the riparian zone is the three-dimensionality of water and solute movement through the soil as well as the biogeochemical processes that occur within these soils. Hill (1996) reviewed hydrological processes and nitrate removal and noted that riparian zones are three-dimensional features of the landscape and that inadequate attention has been given to its three-dimensional nature and subsurface flow paths (Torres et al., 1999). The efficiency of the riparian area that is maintained for solute removal must have a width that is determined by subsurface flow path-length (Torres et al., 1999). Other variables, such as total drainage area, slope, upland vegetation, and soil characteristics and properties all influence the efficiency of riparian zones to filter pollutants. Lowrance et al. (1983), in a study of waterborne nutrient budgets for an agricultural riparian zone, noted that the relative size of upland area devoted to fields, forests, and pastures affected nutrient inputs

and the filtering capacity of the streamside forest. Riparian zones that efficiently remove nitrate often have landscapes with impermeable soil layers near the soil surface (Hill, 1996).

An important function of riparian areas in both the agricultural and forest setting is to reduce the loading of non-point source pollution (NPSP). Many chemical and physical processes occur within the riparian area. Both nitrogen and phosphorous are efficiently removed at the ecotone between upland groundwater and surface water (Dahm et al., 1998). Bosch et al. (1994) found that the concentration and loading of nitrogen and phosphorous in both surface and subsurface runoff were reduced after moving through a riparian zone. In a Coastal Plain riparian zone, Lowrance (1992) noted that year round root growth and nitrogen uptake, combined with fine root biomass and leaf litter in or near the soil surface, was responsible for the nitrogen filtering capacity of these riparian zones. Research has shown that chemical changes in water moving from the upland ecosystem through riparian zones and into surface streams suggest that these areas are major sites of nutrient transformation (Dahm et al., 1998; Hedin et al., 1995; Hill, 1996; Mulholland, 1993; Triska et al., 1990). Filtering and retaining sediments, immobilization, storing, and transforming chemical inputs from uplands, maintaining streambank stability, modifying stream environments, and providing water storage and recharge of subsurface aquifers are just a few of the riparian ecosystem processes that are linked to protection of water quality (Schultz et al., 1994). As noted earlier, nitrate is transported during overland and subsurface flow. Much research has been focused on the transport of nitrate ($NO_3^-N$) due to its ability to readily dissolve and be transported in water. Riparian zones typically act as sinks for nutrients in solution moving along subsurface hydrologic paths (Yeakley et al., 2003) as well as for sediments and nutrients suspended in overland flow. Haycock and Pinay (1993) observed that nitrate

retention in groundwater was at maximum within the first few meters of both P*oplar spp*. and grass riparian zones on the Leach River in the United Kingdom. This study also indicated that the riparian zones were especially durable sinks for nitrate during winter months. Biogeochemical processes and microbial activity within the riparian area sequester and transform nitrogen into nitrogen gases such as nitrous oxide ($N_2O$) and nitric oxide (NO). Gaseous loss typically occurs through microbial denitrification (Lowrance et al., 1983).

The efficacy of re-establishing riparian zones to filter surface and subsurface nutrients from water components has been seen in many studies in both the Coastal Plain and mid-Appalachian areas of the eastern United States (Lowrance, 1992; Lowrance et al., 1983; Peterjohn and Correll, 1984; Yeakley et al., 1994; Yeakley et al., 2003). In a study of hillslope nutrient dynamics following upland riparian vegetation removal, Yeakley et al. (2003) showed that the removal of vegetation generally increases nutrient exports to streams. On a forested hillslope with large tree uprooting (following Hurricane Opal, October 1995), the authors observed large increases of $NO_3^-$ N in soilwater (500x), smaller increases in groundwater $NO_3^-$ N (4x), and streamwater $NO_3^-$ N (2x). Studies conducted at the Hubbard Brook Experimental Forest in New Hampshire showed that the removal of vegetation (through clearcutting) in forested watershed increased nutrient export ($NO_3^-$, $Ca^{++}$, $Mg^{++}$, $Na^+$, and $K^+$) to a receiving stream (Likens et al., 1969).

## *Hillslope Hydrology*

Lowrance at al. (1983) noted that the three sources of water contributing to a riparian area are precipitation, subsurface movement from uplands area, and surface movement from upland areas. The rate at which water from the uplands moves on the surface and in the subsurface to a riparian area or river is dependent on storm intensity and duration, soil

characteristics, antecedent soil moisture, slope, and vegetation. Yeakley et al. (1998) noted that there are two primary physiographic factors that control soil moisture on a hillslope: soil properties and topography.

### *Soil Characteristics*

Soil pore size distribution can influence the specific path that water will follow. The greater the percentage of inter-connected macropores (effective porosity), the higher probability that water molecules will flow laterally through the soil. Such surface soil properties as bulk density and infiltration will influence a soil's ability to transport water through macropores. In a study of the Walker Branch Watershed in Eastern Tennessee, researchers concluded that preferential flow through both the meso and macropores was the predominant mechanism of stream flow generation (Wilson et al., 1990). Contributions of subsoil water came from various pore sizes as a function of a changing stage of the hydrograph (climbing vs. falling limb of the hydrograph). In this specific scenario, it appears that water continued to move through meso and macropores during the rise and fall of soil volumetric water. As soil water content increased with increase stage on the hydrograph, water moved rapidly through macropores as a result of differences in pressure gradient. As the water content decreased, the path of water moving through macro and mesopores became more tortuous, thus reducing contributions to the stream hydrograph. In a similar study in New Zealand, Mosley (1982) noted that approximately 40% of precipitation on a hillslope moves rapidly downslope though macropores.

In Luxmoore and Ferrand's (1993) study of pore-scale analysis of preferential flow, the authors noted that soil-water contact time is significantly modified by pore-scale soil-water dynamics. In describing their connect-disconnect hypothesis, they contended that

subsurface flow path lengths are highly dynamic aspects of the landscape that may vary seasonally or within single storm events.

### *Lateral Flow*

The role of subsurface flow from hillslopes, as described by Freeze (1972), is to maintain wet soil water conditions near stream regions. Subsurface water primarily contributes to the baseflow of a stream, but typically does not contribute directly to increased stream stage. The presence of wet soil on the streambank reduces the force of the matrix pull of water from the unsaturated, upslope soils.

Subsurface flow can occur though both saturated and unsaturated conditions. Under saturated conditions, water primarily moves downslope as a function of pressure and gravimetric gradients. During unsaturated conditions, water moves through the soil media under matric and gravitational forces. In a study of waterborne nutrient budgets of an agricultural watershed, Lowrance et al. (1983) observed that 96% of water emerging from a watershed moved as subsurface flow. Though unsaturated or vadose zone flow is considerably slower than saturated contribution flow, it is an integral part of water inputs to receiving streams. In a study of storm flow paths in the Walker Branch Watershed, it was shown that vadose flow is the dominant component at peak discharge (Mulholland, 1993).

On slopes with permeable surface soils, the degree of permeability decreases with increased soil depth. The presence of this impermeable soil layer or bedrock can influence a large proportion of storm flow inputs (Anderson and Burt, 1990). Zaslavsky and Sinai (1981) noted that there is physical evidence of shallow unsaturated flow moving nearly parallel to a soil's surface and in layered soil, lateral downslope flow develops quickly during wetting and continues for a considerable length of time after the storm has stopped. The influence of an

impermeable subsoil horizon or geologic layer can limit soil depth and cause rapid transport of water and solutes through soil media. The presence of an impermeable layer reduces vertical infiltration and induces subsurface lateral flow. Lateral flow above an agrillic horizon can be a significant transport mechanism of nutrients and agrochemicals to riparian areas (Bosch et al., 1994). Bosch et al. also noted that unsaturated flow occurred during dry periods. Water moved downslope as a function of the high water demand of the riparian forest. Research conducted by Whipskey (1965), De Vries and Chow (1978), and others have also shown that preferential flow occurs through unsaturated conditions in the soil matrix (Wilson et al., 1990). Xu et al. (2000) found that water movement in a wetland actually changed direction and moved toward mature forests following harvest in a relatively flat South Carolina wetland. The water table was higher below the harvested stand than the mature stand prior to harvesting, but increased below the mature stand after harvesting. This increase in water table was a result of reduced water loss (Et) compared to water loss from surface evaporation at the harvested site.

As noted earlier, antecedent moisture conditions play a significant role in determining whether lateral flow occurs on the surface or subsurface. In a study of hillslope nutrient dynamics of a pine plantation soil, Gaskin et al.(1989) observed that in dry conditions the greatest lateral flow occurred in the Ap-horizon. During wet conditions, high lateral flow occurred primarily in the BA and Bt-horizons (Gaskin et al., 1989). The high flow during wet periods in the Bt-horizons of the study soils may be attributed to the vertical movement of high volume of water reaching the somewhat impermeable layers. When the percolating water reached the confining layer, water was forced to flow laterally downslope.

Wilson et al. (1990) studied the hydrology of a forested hillslope during storm events and noted that there was a lag time between the rise of subsurface flow and the rapid decrease in soil water potential. The authors hypothesized that this lag might be attributed to the time required for water to move vertically through the soil to an impermeable Bt-horizon. The water must first perch on the impermeable clay layer before lateral flow will occur.

### *Variable Source*

The duration and intensity of a storm may influence surface and subsurface water movement. The concept of Hewlett's (Hewlett and Troendle, 1975) variable source watershed illustrates how water accumulates in different areas of a watershed, eventually connecting and producing surface and saturated subsurface flow contributions to a stream (Anderson and Burt, 1990). As the variable areas within a watershed become saturated, they will eventually connect. However, the connection of the variable areas is a function of antecedent moisture conditions, precipitation volume, and duration of input (Hippert and Troendle, 1998; Yeakley et al., 1994).

There have been mixed research results as to the degree of contribution of subsurface storm inputs to stream stage. However, it is understood that subsurface flow contributes to the baseflow of streams. Various researchers, such as Dunne and Black (1970) and Weyman (1970; 1973) have found that the influence of storm flow contributions from subsurface sources does not readily influence stream storm stage (Wilson et al., 1990). In contrast, Corbett (1979) concluded that subsurface storm flow from hillslopes was the primary (75-95%) source of storm flow (Wilson et al., 1990).

### *Storm Flux and Intensity*

The interaction of storm intensity, duration, and antecedent soil moisture influences water and nutrient transport on the surface and the subsurface. If a storm is relatively mild, with pre-existing dry soil conditions, much of the water may move downslope across the surface horizon. During times of dry conditions or when surface pores may be plugged, the surface soil may be hardened, thus reducing infiltration and vertical percolation. As precipitation impacts the surface, the accumulated water will move downslope. As the duration of a storm increases, water will slowly accumulate in the area of deposition, eventually moistening the soil surface, improving infiltration (Hippert and Troendle, 1998). If precipitation deposits on a pre-wetted (but not saturated) soil surface, water will infiltrate and theoretically moves vertically into the subsurface horizon. As water accumulates in the subsoil, the forces of a pressure differential between the source soil, and the downslope unsaturated soil will result in subsurface lateral flow. As a precipitation storm continues, and soil water volumetric content increases (towards saturation), water will be forced to travel as overland flow.

The duration and intensity of a storm may rapidly drive nitrate and other water borne nutrients through a watershed (Hill, 1996). In a livestock pasture or agricultural setting, sources of nitrogen, such a manure, urea, and fertilizer, may move rapidly overland as a result of high volume precipitation. The surface water may interact directly with and transport nutrients, bypassing the impedance and sequestration of vegetation and soil resistance. In a study of hillslope nutrient dynamics following vegetation disturbance, Yeakley et al. (2003) observed that an increase of $NO_3^-$ concentration following storm disturbance was observed in soilwater, groundwater, and streamwater. Dillaha et al. (1988) found similar results in a southwestern Virginia soil. They observed that high intensity

storms were primarily responsible for pollutant transport even though the high intensity storms were only responsible for 17% of the total precipitation. Haycock and Pinay (1993) found similar results in groundwater under grass and poplar (*Liquidamber spp.*) riparian zones. They observed that the concentration of $NO_3^-$ increased at peak discharge only on the rising limb of the hydrograph.

### *Water Mass Balance*

Research has shown that the intuitive mass balance method may be used to determine watershed inputs to receiving waters. A general water mass balance may be expressed through the following equation: [Inputs $_{(precipitation)}$ - Outputs $_{(\Sigma\ [surface,\ subsurface,\ soil\ water\ storage,\ Et)}$] = Discharge from watershed. Gaskin et al. (1989) used a mass balance to estimate water flux as the residual of the mass balance equation. Lowrance et al. (1983) applied an input/output mass balance to calculate the amount of water that moved through an agricultural riparian zone to the Little River Watershed in southern Georgia. The objective of the study was to derive a water balance for the riparian zone by estimating the water volume from upland sources required to change the receiving stream observed flow. The authors note that there must be enough input of water (bulk precipitation and water entering from uplands) to first satiate evapotranspiration and soil water storage requirements, then produce surface and subsurface lateral flow, before observable changes in stream flow are to exist.

The efficacy of using the mass balance approach to calculating water flux can again be seen in Russell and Ewel's (1985) study of leaching from a tropical inceptisol. The researchers compared three approaches to determining leached nutrients in soil water. Of the three approaches (Darcy Flow equation, water balance, and zero-tension lysimeters), the

authors concluded that the mass balance was most accurate, primarily due to the other techniques sample only components of soil water flow (Russell and Ewel, 1985).

Though the mass balance approach to determining water inputs from contributing watersheds does not differentiate between individual surface and subsurface flow mechanism, it does provide actual amounts of water flux coming from a watershed. This technique can prove beneficial when nutrient/pollutant flux is desired. However, a physical mass balance is very difficult to apply to smaller watersheds where both saturated and unsaturated flow significantly contribute to watershed discharge.

Two components of hillslope hydrology are the movement of water in both saturated and unsaturated states. Though the concept of unsaturated flow (vadose zone flow) violates Darcy's principle of laminar flow, researchers have shown that unsaturated flow is an integral component of hillslope hydrology (Anderson et al., 1997; Jackson, 1992; Pang et al., 2000; Vogeler et al., 1997). Interest in unsaturated flow processes has increased in recent years due to the increased concern that the quality of the subsurface environment has been adversely affected by agricultural, industrial, and municipal activities (Simunek et al., 1999).

There have been significant field studies focused on saturated transport processes and nutrient transport, but due to the complex nature of unsaturated flow processes, field observation studies are often inadequate in describing unsaturated flow. As a result, mathematical models have been developed to iteratively solve for unsaturated flow (Mailhol et al., 2001; Pang et al., 2000; Simunek et al., 1999). Once such model, HYDRUS 2-D (Simunek et al., 1999), formally know as SWMS 2-D, has received much attention. This model has been used to analyze water and solute movement in unsaturated, partially saturated or saturated porous media (Simunek et al., 1999).

## *Nutrients*

There have been considerable research efforts to quantify nutrient loss from both agricultural and forested watersheds (Lowrance et al., 1983; Peterjohn and Correll, 1984; Schultz et al., 1994; Swanson et al., 1982; Yeakley et al., 2003). Such mechanisms as solute transport, biogeochemical transformation, nutrient sequestration, and reduction of nutrient inputs have received attention in an effort to reduce NPS pollution to receiving waters. Lowrance at al. (1983) observed that streamside forests were effective in sequestering nitrogen, phosphorus, calcium, and magnesium. The authors also observed that the removal of the riparian zone, via conversion to cropland, increased $NO_3^-$ and $NH_4^+$ loads by 800% (1983). Haycock and Pinay (1993) observed nitrate dynamics under grass and poplar vegetated riparian buffers in their study of groundwater $NO_3^-$ transport. The authors concluded that in a grass riparian buffer, the riparian area was efficient in water $NO_3^-$ -N retention if flow was routed through the subsurface, irrespective of loading rates. The implementation and use of riparian buffers can reduce the overall loading of nutrients and sediments to streams and rivers, but the specific characteristics and behavior of each nutrient must be considered.

Nitrogen dynamics in forested and agricultural watersheds has received attention due to the high mobility and transport of soluble nitrogen. The primary sources of nitrogen input in agricultural watersheds are atmospheric deposition, organic matter decomposition, fertilizers, and livestock waste ($NO_3^-$ and $NH_4^+$) (Fisher and Binkley, 2000). However, nitrate ($NO_3^-$) and ammonium ($NH_4^+$) are often lost from agricultural watershed through surface and groundwater transport and denitrification (Lowrance, 1992).

Studies have indicated that subsurface flow is a primary transport mechanism of nitrogen loss from agricultural watersheds (Dahm et al., 1998; Haycock and Pinay, 1993; Hubbard and Sheridan, 1983; Lowrance et al., 1983; Peterjohn and Correll, 1984). Hubbard and Sheridan (1983) found that subsurface $NO_3^-$ concentration was 19 times greater than surface $NO_3^-$ concentration in soils with significant leaching. The study also revealed that $NO_3^-$ concentration was generally low unless favorable surface runoff conditions occurred. In a study of nutrient dynamics in an agricultural watershed, Peterjohn and Correll (1984) observed that of the total nitrogen lost from a riparian forest at the bottom of the agricultural watershed, 75% was lost through groundwater flow, thus concluding that subsurface flow is a major pathway of nitrogen losses from the riparian forest to stream. Hubbard and Sheridan (1983) observed similar results in a small, upland Coastal Plain watershed. Of the total input of nitrogen, 99% of $NO_3^-$ was lost through subsurface flow.

## References


Anderson, M.G., and T.P. Burt. 1990. Subsurface Runoff, p. 368-380, *In* M.G. Anderson and T.P Burt, ed. Process Studies in Hillslope Hydrology. John Wiley and Sons Ltd., West Essex, England. p. 539.

Anderson, S.P., W.E. Dietrich, D.R. Montgomery, R. Torres, M.E. Conrad, and K. Loague. 1997. Subsurface flow paths in a steep, unchanneled catchment. Water Resourc. Res. 33:2637-2653.

Bosch, D.D., R.K. Hubbard, L.T. West, and R.R. Lowrance. 1994. Subsurface flow patterns in a riparian buffer systems. Trans. Am. Soc. Agric. Engrs. 37:1783-1790.

Cooper, A.B. 1990. Nitrate depletion in the riparian zone and stream channel of a small headwater catchment. Hydrobiologia 202:13-26.

Corbett, E.S. 1979. Hydrologic evaluation of the stormflow generation process on a forested watershed. Univ. Microfilms Int., 300 N. Zeeb Rd., Ann Arbor, MI, 48106.

Dahm, C.N., N.B. Grimm, P. Marmonier, H.M. Valett, and P. Vervier. 1998. Nutrient dynamics at the interface between surface waters and groundwaters. Freshwater Biol. 40:427-451.

De Vries, J., and T.L. Chow. 1978. Hydrologic behavior of a forested mountain soil in coastal British Columbia. Water Resour. Res. 5:935-942.

Dillaha, T.A., J.H. Sherrard, D. Lee, S. Mostaghimi, and V.O. Shanholtz. 1988. Evaluation of vegetative filter strip as a best management practice for feed lots. Journal WPCF 60:1231-1238.

Dissmeyer, G.E. 2000. Drinking Water from Forests and Grasslands: a synthesis of the scientific literature. Gen. Tech. Rep. SE US Dep. Agric. For. Srv. South For. Exp. Stn. SRS-39. United States Department of Agriculture Forest Service, Asheville. p. 246.

Dunne, T., and R.D. Black. 1970. Partial area contributions to storm runoff in a small New England watershed. Water Resour. Res. 6.

Fisher, R.F., and D. Binkley. 2000. Ecology and Management of Forest Soils. John Wiley and Sons, Inc., New York. p. 489.

Freeze, R.A. 1972. Role of subsurface flow in generating surface runoff : Upstream source areas. Water Resour. Res.8:1272-1283.

Gaskin, J.W., J.F. Dowd, W.L. Nutter, and W.T. Swank. 1989. Vertical and lateral components of soil nutrient flux in a hillslope. J. Environ. Qual. 18:403-410.

Haycock, N.E., and G. Pinay. 1993. Groundwater nitrate dynamics in grass and poplar vegetated riparian buffer strips during winter. J. Environ. Qual. 22:273-278.

Hedin, L.O., J.J. Armesto, and A.H. Johnson. 1995. Patterns of nutrient loss from unpolluted, old-growth temperate forests: Evaluation of biogeochemical theory. Ecology 76:493-509.

Hewlett, J.D., and C.A. Troendle. 1975. Nonpoint and diffused water sources: A variable source area problem. Proceedings of a symposium on watershed management:21-46.

Hill, A.R. 1996. Nitrate removal in stream riparian zones. J. Environ. Qual. 25:743-755.

Hippert, A.R., and C.A. Troendle. 1998. Streamflow Generation by Variable Source Area Springer-Verlag, New York. p. 111-127.

Hubbard, R.K., and J.M. Sheridan. 1983. Water and nitrate-nitrogen losses from small, upland, coastal plain watershed. J. Environ. Qual. 12:291-295.

Jackson, R. 1992. Hillslope infiltration and lateral downslope unsaturated flow. Water Resour. Res. 28:2533-2539.

Likens, G.E., F.H. Bormann, and N.M. Johnson. 1969. Nitrification: Importance to nutrient losses from a cutover forested ecosystem. Science 163:1205-1206.

Lowrance, R.R. 1992. Groundwater nitrate and denitrification in a coastal plain riparian forest. J. Environ. Qual.21:401-405.

Lowrance, R.R., R.L. Todd, and L.E. Asmussen. 1983. Waterborne nutrient budgets for the riparian zone of an agricultural watershed. Agric. Ecosyst. & Environ. 10:371-384.

Lowrance, R.R., R.L. Todd, and L.E. Asmussen. 1984. Nutrient cycling in an agricultural watershed: I. Phreatic Movement. J. Environ. Qual. 13:22-32.

Luxmoore, R.J., and L.A. Ferrand. 1993. Toward pore-scale analysis of preferential flow and chemical transport, p. 45-60, *In* D. Russo and G. Dagan, ed. Water Flow and Solute Transport in Soils: Developments and Applications. Springer-Verlag, New York, NY. p. 306.

Mailhol, J.C., P. Ruelle, and I. Nemeth. 2001. Impact of fertilisation practices on nitrogen leaching under irrigation. Irrig. Sci. 20:139-147.

Mosley, M.P. 1982. Subsurface flow velocities through selected forest soils, South Island, New Zealand. J. Hydrol. 55:65-92.

Mulholland, P.J. 1993. Hydrometric and stream chemistry evidence of three storm flowpaths in Walker Branch Watershed. J. Hydrol. 151:291-316.

Pang, L., M.E. Close, J.P.C. Watt, and K.W. Vincent. 2000. Simulation of picloram, atrazine, and simazine leaching through two New Zealand soils and into groundwater using HYDRUS-2D. J. Contaminant Hydrol. 44:19-46.

Peterjohn, W.T., and D.L. Correll. 1984. Nutrient dynamics in an agricultural watershed: Observations on the role of riparian forests. Ecology 65:1466-1475.

Russell, A.E., and J.J. Ewel. 1985. Leaching from a tropical Andept during big storms: A comparison of three methods. Soil Sci. 139:181-189.

Schultz, R.C., T.M. Isenhart, and J.P. Colletti. 1994. Riparian Buffer Systems in Crop and Rangelands. Agroforestry and Sustainable Systems: Symposium Proceedings August 1994. p. 13-27.

Simunek, J., M. Sejna, and M.T.van Genuchten. 1999. The Hydrus-2D Software Package for Simulating the Two-Dimensional Movement of Water, Heat, and Multiple Solutes in Variably-Saturated Media. p. 227.

Swanson, F.J., S.V. Gregory, J.R. Sedell, and A.G. Campbell. 1982. Land-Water Interactions: The Riparian Zone, p. 267-291, *In* R. L. Edmonds, ed. Analysis Of Coniferous Forest Ecosystems In The Western United States. Hutchinson Ross Publishing Company, Stroudsburg, PA. p. 419.

Torres, R., B. Fornwalt, and J. Morris. 2003. Effects of topography on subsurface flow path-length through riparian zones: Implications for buffer efficiency. Water Resourc. Res. *In Review*.

Triska, F.J., J.H. Duff, and R.J. Avanzino. 1990. Influence of exchange flow between the channel and hyporheic zone on nitrate production in a small mountain stream. Can. J. Fish. Aquat. Sci. 47:2099-2111.

United States Department of Agriculture, Natural Resources Conservation Service. 1996. Soil Survey of Macon County, North Carolina. p. 322.

Vogeler, I., D.R. Scotter, S.R. Green, and B.E. Clothier. 1997. Solute movement through undisturbed soil columns under pasture during unsaturated flow. Aust. J. Soil Res. 35:1153-1163.

Vought, L.B.M., G. Pinay, A. Fuglsang, and C. Ruffinoni. 1995. Structure and function of buffer strips from a water quality perspective in agricultural landscapes. Landscape and Urban Plann. 31:323-331.

Weyman, D.R. 1970. Throughflow on hillslopes and its relation to the stream hydrograph. Bull. Int. Assoc. Sci. Hydrol.15:25-33.

Weyman, D.R. 1973. Measurements of the downslope flow of water in a soil. J. Hydrol. 20:267-288.

Whipskey, R.Z. 1965. Subsurface stormflow from forested slopes. Bull. Int. Assoc. Sci. Hydrol. 10:74-85.

Wilson, G.V., P.M. Jardine, R.J. Luxmoore, and J.R. Jones. 1990. Hydrology of a forested hillslope during storm events. Geoderma 56:119-138.

Xu, Y.J., J.A. Burger, and W.M. Aust. 2000. Responses of surface hydrology to soil disturbance and site preparation in a lower coastal plain wetland. New Zealand Journal of Forest Science 30:250-265.

Yarnell, S.L. 1998. The Southern Appalachians: A History of the Landscape Gen. Tech. Rep. SRS-18. Gen. Tech. Rep. SE US Dep. Agric. For. Serv. South For. Exp. Stn., Asheville, NC. p. 45.

Yeakley, J.A., J.L. Meyer, and W.T. Swank. 1994. Hillslope Nutrient Flux During Near-Stream Vegetation Removal I. A Multi-Scaled Modeling Design. Water, Air, & Soil Pollut. 77:229-246.

Yeakley, J.A., W.T. Swank, L.W. Swift, G.M. Horneberger, and H.H. Shugart. 1998. Soil moisture and controls on a southern Appalachian hillslope from drought through recharge. Hydrology and Earth Systems Sciences 2:41-49.

Yeakley, J.A., B.W. Argo, D.C. Coleman, J.M. Deal, B.L. Haines, B.D. Kloeppel, J.L. Meyer, W.T. Swank, and S.F. Taylor. 2003. Hillslope nutrient dynamics following upland riparian vegetation disturbances. Ecosystems 6:154-167.

Zaslavsky, D., and G. Sinai. 1981. Surface Hydrology I: In surface transient flow. J. Hydrauil. Div. Am. Soc. Civ. Eng.107:65-93.

# Chapter 2: Methods and Materials

## Site Description

### *Study Site*

The study watershed is located approximately 13 kilometers west of the town of Franklin, Macon County, North Carolina on the Slagle Farm (Figure 2-1). This area of southwestern North Carolina is in the Blue Ridge Mountain physiographic region and is typified by steep granitic slopes to relatively level alluvial flood plains adjacent to primary rivers. The Slagle Farm watershed (N:92355.91 E:27448.47) (Figures 2-2 and 2-3) incorporates approximately 5-ha of drainage, and ranges in elevation from 646 meters at the top ridge to 628 meters at the Cartoogechaye Creek. The watershed is located on private land that has primarily been used for agriculture, with moderate cattle grazing.

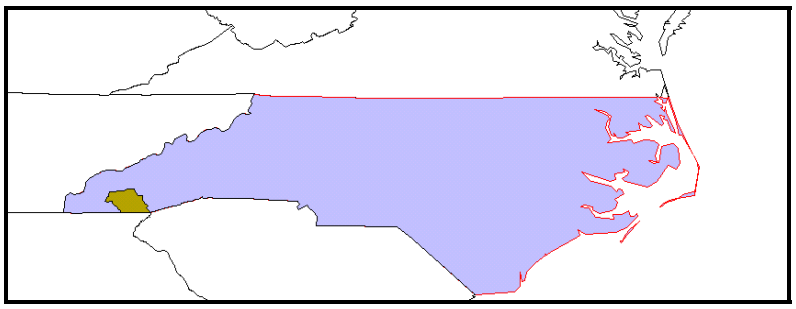

Figure 2-1: Location of Macon County, NC

The area receives an average of 132 cm of precipitation a year. Precipitation is evenly distributed throughout the year, with an average relative humidity of 60% (United States Department of Agriculture, 1996). The average summer temperature is 24° C, with a

maximum temperature of 29° C. The average winter temperature is 4° C, with a minimum of -3° C (United States Department of Agriculture, 1996).

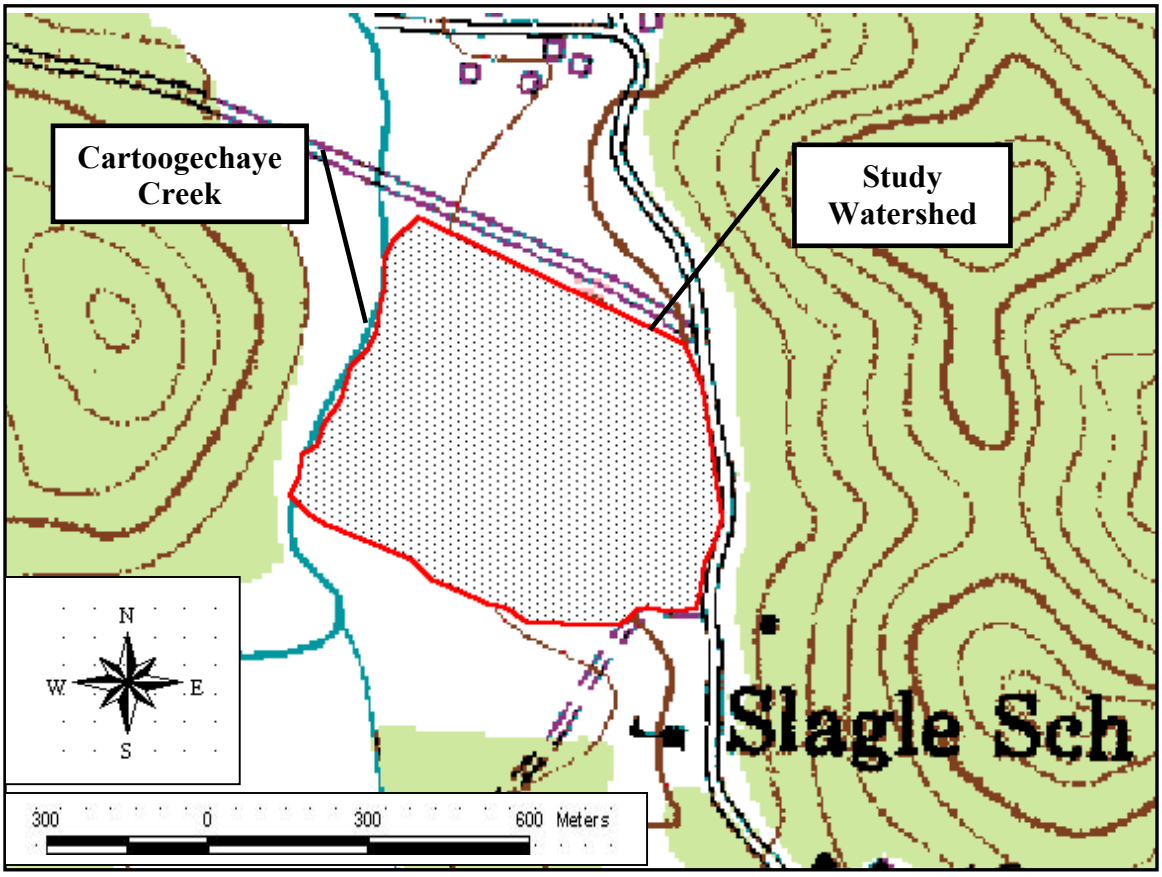


Figure 2-2: Topographic map of the Slagle property where watershed study was conducted.

## *Soil and Site Characteristics*

The site is primarily vegetated with Kentucky Fescue 31 grass, with sparse woody vegetation distributed across the landscape. The pasture is primarily composed of four series of soil. These series are the Braddock, the Saunook, the Rosman, and the Dillsboro series (Figure 2-4) (United States Department of Agriculture, 1996). The Braddock series is primarily located on the strongly sloping (8-15%) and top-slopes of the pasture as well as on the spurs within the drainage. The Braddock clay loam is a well-drained, clayey, mixed, mesic Typic Hapludults. The surface layer is within the top 28 cm of soil and is reddish

brown (Ap-horizon) (United States Department of Agriculture, 1996). The subsoil Bt-horizon is located between 28 and 109 cm, followed by a weathered C-horizon consisting primarily of mica.

Figure 2-3: View of the Slagle watershed and Cartoogechaye Creek looking North

The Saunook series is a very deep, well-drained, moderately permeable soil located on gently sloping (2-8%) mid-sloped areas. The Saunook loam is a fine-loamy, mixed, mesic Humic Hapludults. The surface layer (Ap-horizon) is a dark brown loam and is up to 25 cm deep. The subsoil (Bt-horizon) ranges from 25 cm to 86 cm in depth. The Bt is located atop a weathered C-horizon composed of mica with 15% gravel and 25% cobbles (United States Department of Agriculture, 1996).

The Dillsboro series is a moderately permeable, very deep, well-drained loam that is located mid-slope in the eastern most drainage of the watershed. The Dillsboro loam is a

clayey, mixed, mesic Humic Hapludults found on gentle slopes ranging between 2 and 8%. The surface soil is a dark brown loam up to 30 cm in depth. The subsoil Bt-horizon is a strong brown clay up to 127 cm deep (United States Department of Agriculture, 1996).

The Rosman series is a very deep, well-drained, moderately rapid permeable sandy loam. This series is often found on nearly level (0-2%) slopes adjacent to major streams and is specifically located within the established riparian area of this site. The Rosman is a fine sandy loam that is frequently flooded. This coarse-loamy, mixed, mesic Fluventic Haplumbrepts runs the entire length of the watershed. The surface soil (Ap-horizon) is dark brown and reaches a maximum depth of 41 cm. The subsoil (Bt-horizon) reaches a maximum depth of 145 cm and is typified as a Bt/Bw horizon (United States Department of Agriculture, 1996).

## *Stream Characteristics*

The Slagle Farm drainage discharges into Cartoogechaye Creek (Figure 2-5). Cartoogechaye Creek receives inputs from a total drainage area of 22.3 $km^2$ (Slack et al., 2002). The total length of the creek is 24.8 km, and it meanders approximately north/north east to its confluence with the Little Tennessee River, south of Franklin, NC. The creek has a mixed silt/cobble floor and has undergone drastic channel morphological changes during the last 200 years. The channel segment of the creek directly draining the Slagle Farm originated as a sawmill flume. However, when the mill was abandoned, the Cartoogechaye diverged

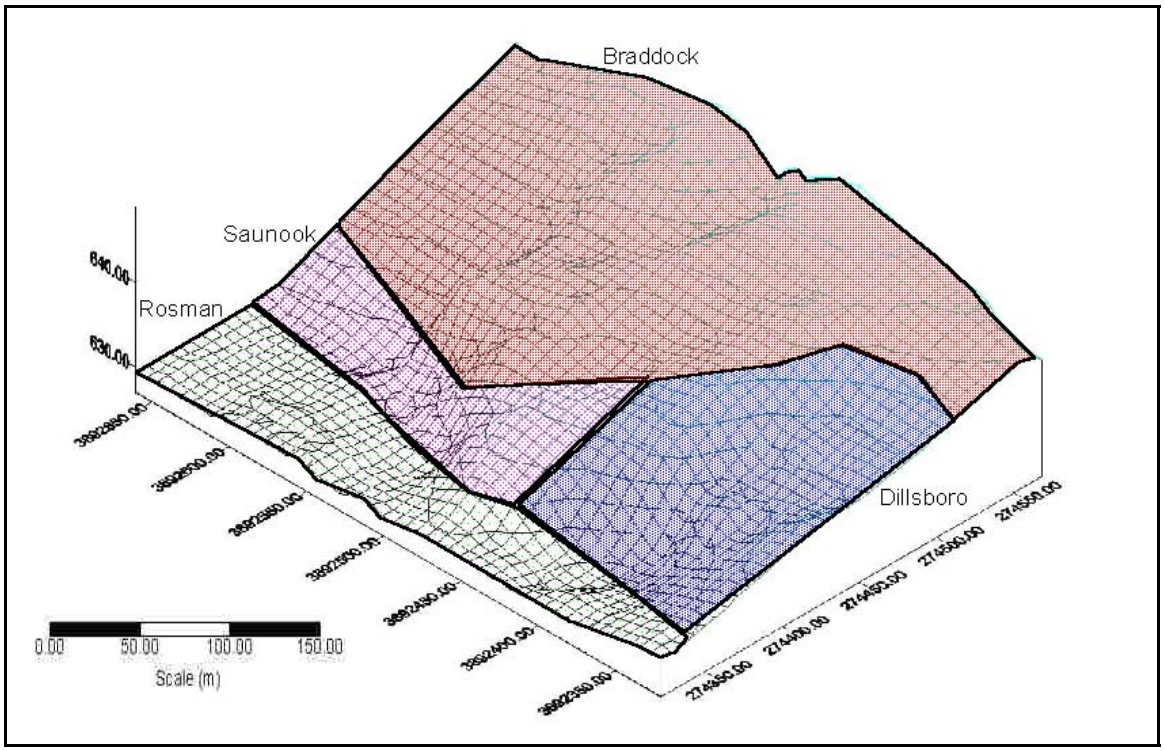


Figure 2-4: Soils map of the Slagle Watershed.

from its original path to create the present day stream channel. Much of the stream bank is a result of over-bank sedimentation and has succumbed to intense erosion. Most of the Cartoogechaye Creek drainage originates from moderately steep pasture and agricultural lands.

# Methods

Table 2-1 explains the specific use of the data illustrated in the Methods section.

## *Delineation of Watershed and Topographic Map*

The delineation of the watershed was conducted on site, with use of USGS 7.5' Franklin, NC quadrangle topographic map (Figure 2-2) and Corvallis Microtechnology, Inc. GPS-HP-L4 global positioning system (GPS) receiver (Corvallis Microtechnology, 1998b).

The survey was conducted to define the smaller watershed that drains into the established riparian study site. The survey established elevation gradients, slopes, and drainage

Figure 2-5: Cartoogechaye Creek at the base of the Slagle Watershed

reference points that aided in quantifying the total drainage area of the study riparian zone. The following steps were taken to determine total area drainage to the riparian zone: GPS X, Y, and Z coordinates were taken at each obvious change in gradient, on the boundary of the watershed. These stations were assigned a station number, consecutive with number and letter, designating location of survey station (1AA, 2,3,1CA, 1CB, etc.). Consecutive numbers were used to designate stations outside of riparian area (1,2,3,etc.), while stations within pre-existing riparian study plots (streamside boundary) were designated by plot number/letter and assigned A for downstream plot corner, and B for upstream plot corner (1AA, 1AB, 2AA, 2AB, etc.).

After the perimeter survey was completed, a more intensive survey was conducted within the watershed to develop a local topographic map for the drainage area. GPS locations were taken at every major change (> 0.5-m) in micro-topographical feature within a 10-m grid. Data collected were used to develop a topographic map, with geodetic correction.

CMT PCGPS 3.7 software was used to correct and process GPS data (Corvallis Microtechnology, 1998a). X, Y, and Z data collected was then processed through Surfer Win 32 Version 6.04 (Golden Software, 1999) to create the topographic map (Figure 2-6). The watershed topographic map assisted in identifying micro-topography and its influence on both surface and subsurface drainage.

## *Sampling Transects*

Transects were established within each of the three significant sub-watershed drainages (identified from contour map) of the study watershed that drain into the study riparian area (Figure 2-6). Transects span the length of the watershed, from ridge tops in pasture, through riparian area, to river (transects were laid in the general direction of subsurface flow to river).

## *Soil Characteristics*

### *Soil Characterization*

Soil profile descriptions were conducted along each transect to characterize master soil horizons. Four sampling stations were located in each transect, representing top-slope, mid-slope, toe-slope, and riparian area. Open-bucket augers were utilized to extract 15 cm segments that were placed in a soil tray for profile delineation. Profiles were delineated based on depth, color, structure, texture, mottles, and roots. A Munsell color chart and the Soil Survey of Macon County, North Carolina (United States Department of Agriculture, 1996) aided in the delineation and classification. The profile descriptions were used to determine specific depths for the eventual placements of lysimeters and time domain reflectometer (TDR) instrument placements. Intact soil core samples were collected from both the Ap- and the Bt-horizons.

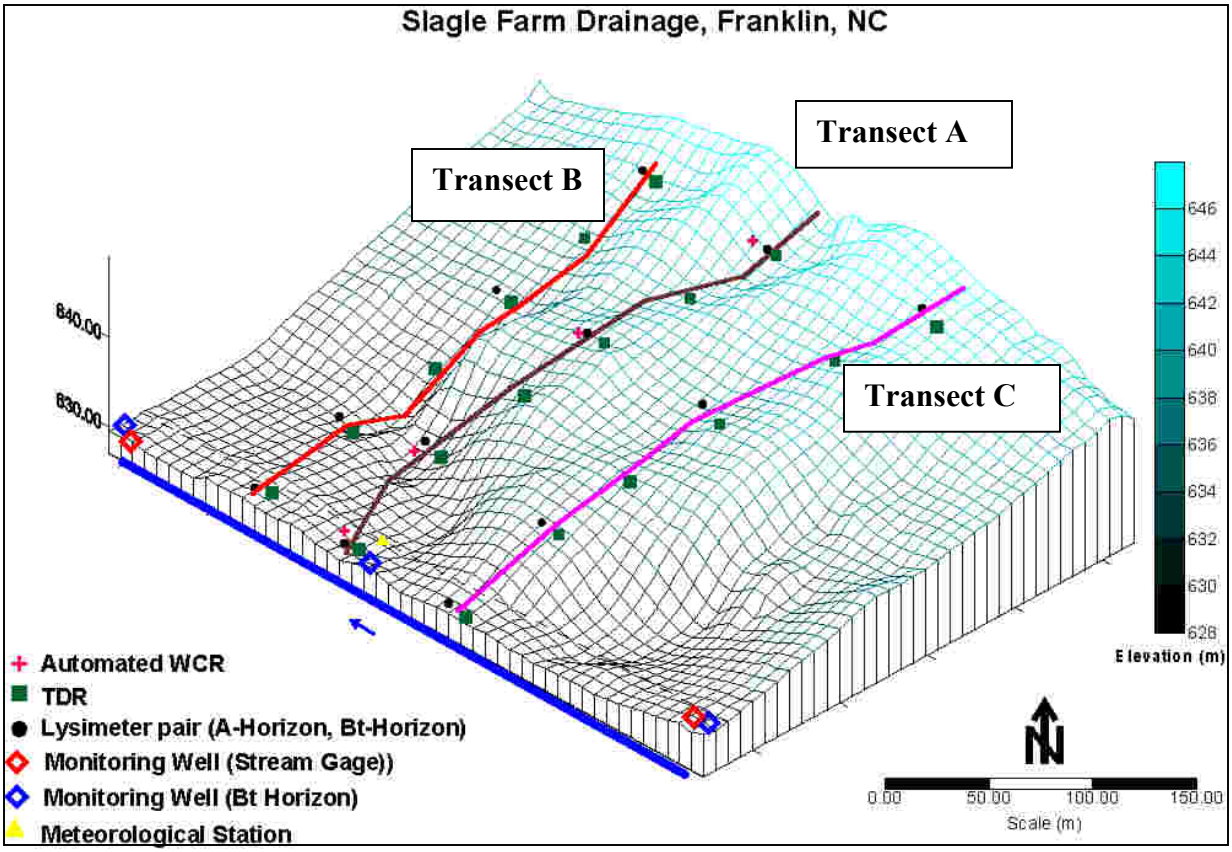


Figure 2-6: Rendered Slagle Watershed topographic map with instrumentation locations.

Three intact soil cores were taken from the Ap- and Bt-horizons at each monitoring station. A total of 24 cores were taken per transect. Core samples were then taken back to the lab and analyzed for total, macro and micro porosity, and saturated hydraulic conductivity and bulk density. Three loose soil samples were also taken from the Ap- and Bt-horizons at each monitoring station. Loose samples were used for water retention curve points at 0.05 MPa, 1.0 MPa, and 1.5 MPa.

### *Total, Micro- and Macro- Porosity Protocol*

Total, micro- and macro- porosities were calculated utilizing a modification of the Water Desorption Method described by Danielson and Sutherland (1986). The soil cores (5.08 cm height by 4.8 cm diameter) were capped and placed in trays flooded with ¼" water,

and soaked for 12 hours. The water level was then increased to just short of flooding the surface of the core and saturated for an additional 12 hours. After the 24-hour saturation period, the water level was increased to flood the surface of the core, then removed and immediately weighed to 0.1 g (saturated weight).

The saturated cores were placed on a tension table, pre-fixed with a 50 cm water column. After approximately 15-30 minutes, the cores were inverted and placed upright on the tension table. After 24 hours, equilibrium was reached. The cores were removed and weighed to 0.1 g. Cores were then placed in an oven, and dried at 105° C for 24 hours, removed, and weighed to 0.1 g (Cassell and Nielsen, 1986; Danielson and Sutherland, 1986).

Equilibrium weight was calculated as:

*(soil weight + cylinder weight + plastic lid) - (cylinder weight + plastic lid)*

Total porosity was calculated as:

*TP (%) = [(2.65-bulk density) / (2.65)] * 100*

Micro-porosity (*MiP*) was calculated by:

*MiP (%) = [(equilibrium weight – cylinder weight) / (cylinder volume)] * 100*

Macro-porosity (*MaP*) was calculated by:

*MaP (%) = total porosity (%) – micro-porosity (%)*

### *Water Retention Curve Development*

Field capacity estimates were calculated using the Small Soil Core method (approximation) described by Cassell and Nielsen (1986). A pressure plate apparatus was used to achieve equilibrium in the soil samples. Initially, the 0.01 MPa ceramic plate was saturated with deionized water. Soil cores were pre-saturated as per the procedure illustrated above. Sixteen core batches were placed on the saturated ceramic plate and pressure was

elevated to 0.003 MPa air pressure. Due to the high clay content of sampled soils, the pressure plate remained under 0.003 MPa air pressure for three days, until equilibrium was achieved. Field capacity (% by weight) was calculated using the equation:

*FC (% weight) = [(weight 0.003 MPa - cylinder weight) / (cylinder weight)] * 100*

Field capacity (% weight) was then used to calculate field capacity (% vol.) via equation:

*FC (% vol.) = FC (% weight) * bulk density*

Water retention values for .01 MPa, .05 MPa, 1.0 MPa, and 1.5 MPa air pressure were achieved through the pressure plate apparatus as illustrated above.

### *Saturated Hydraulic Conductivity*

Saturated hydraulic conductivity was measured and calculated via the Constant-Head Method, as described by Klute and Dirksen (1986). The conductivity was calculated by:

$K_s = (Q/At)(L/H)$,

Where $Q$= weight of water, $A$= cross-sectional area of cylinder, $t$= time, $L$= length of cylinder, $H$= height of constant head

Intact soil cores were saturated as described above. Saturated cores were then attached to a hydraulic conductivity leaching rack as described. Water was then allowed to percolate through cores into a container. Once the system reached equilibrium, the head height ($H$) was recorded. An Erlenmeyer flask was then placed under the core to collect percolate. Approximately 100 ml of water was collected, all the while noting the duration of time ($t$) in seconds for the water to move into the flask. The flask was then weighed to nearest 0.01 g and $Q$ (g) was calculated as the difference between the dry Erlenmeyer flask weight and the weight of the flask with percolate. The cross-sectional area ($A$) and the length ($L$) of the soil core were measured to 0.01 of a cm.

### *Bulk Density*

Bulk density was measured and calculated via the Core Method bulk density sampling technique as described by Blake and Hartge (1986). The soil cores (24) were heated in a drying oven at 105°C for 24 hours. Dried samples were weighed to 0.1 g. The bulk density is the oven-dry mass of the sample divided by the sample volume:

*Bulk Density = cylinder weight / cylinder volume*

### *Particle Size Analysis*

Particle size analysis was calculated through procedures developed by Bouyoucos (1936). Three sub-samples per sampling location were used to calculate an arithmetic mean of particle size per location. Silt and clay percentages were calculated through the following equation:

*% Silt and Clay = (corrected hydrometer (40s) / Oven dry weight) * 100*

Clay percentage was calculated as:

*% Clay = (Corrected hydrometer reading (2hr) / Oven dry weight) * 100*

Sand sieving was used to calculate sand percentage within each sub-sample. Sand was sieved through a series of different sized sieves to determine distribution of sand particles within the soil. Sand percentage was calculated through the following equation:

*% Sand = (sand weight) / Oven dry weight) * 100*

Silt percentage was calculated as:

*% Silt = 100-(% sand + % clay)*

## *Soil Water Analysis*

Four soil water sampling stations were established on each transect. The four sampling stations represented top-slope, mid-slope, toe-slope, and riparian area. Two porous-

cup tension lysimeters were installed at each station, one in the Ap-horizon and one in the Bt-horizon respectively, along each transect. Lysimeters were pressurized to 0.003 MPa and sampled in two-week intervals (Gaskin et al., 1989; Yeakley et al., 2003). Total volume extracted from each lysimeter was recorded for use in soil water chemistry composites. Water samples were analyzed for total N, $NO_3^-$-N, and $NH_4^+$-N through procedures developed by the Coweeta Hydrologic Laboratory (Reynolds and Deal, 1986; Walsh, 1971).

## *Subsurface Flow*

### *Vadose Zone Monitoring*

Subsurface flow within the pasture was monitored via use of non-automated Time Domain Reflectometry (TDR) and automated Water Content Reflectometry (WCR). A Trase System 1, TDR 6050X1 and a series of four Campbell Scientific CS 615 WCRs were used for continuous water content measurement. Two sets of paired stainless steel TDR rods were installed vertically at each monitoring station, with depths of 0-20 cm and 0-50 cm. A ratio method illustrated by Lakel (2000) was used to determine the volumetric moisture percentage for the Bt-horizon independently from the cumulative (both Ap- and Bt-horizons) TDR measurements. The following equation was used for the partition:

*[(Ap-horizon depth of rods)(volumetric moisture % Ap)]+[(Bt-horizon depth)(x)] = (cumulative depth of both horizons)(volumetric moisture % of cumulative horizons)*

Solving for "x" yields the actual volumetric moisture percentage of the Bt-horizon.

TDR measurement occurred bi-weekly throughout the sampling year. Bi-weekly TDR data was used to partition areas of the watershed into separate water content regimes in order to apply continuous Bt -WCR values across the entire watershed. Water Content Reflectometers

were installed along transect A for continuous monitoring (Figure 2-6). A single WCR was installed horizontally at the bottom of the Ap-horizon, above the Bt-horizon at each monitoring location along this transect. All four WCRs were automated through the Campbell Scientific 10X data logger. Water content flux measurements were measured in 5-minute intervals, then averaged hourly and daily for each month.

## *Stream Gauging and Watershed Discharge Monitoring*

Automated Ecotone Water Level wells were installed in the riparian area at the upstream, midway, and downstream areas of the watershed. Both the upstream and downstream locations had two wells, one in the Bt-horizon (approx. 102 cm) and one mounted in the steam (Figure 2-6). Depths of wells were approximate depths of the Bt horizon within the riparian area and water table of the Cartoogechaye Creek. A single well of an approximate depth of 102 cm was installed at the halfway point between the upstream and downstream boundaries of the watershed. The purpose of these automated wells were to record the dynamics of both the stream level and the expected perched water level on the Bt-horizon. Wells were automated to record changes in water table levels every 10 minutes. Stream stage and Bt-horizon water table were used to estimate total discharge into Cartoogechaye Creek from the watershed (Buchanan and Somers, 1969).

### *Stream Stage and Flux*

Stream discharge and watershed discharge to Cartoogechaye Creek was measured and calculated using a cross-sectional stream survey as illustrated by Harrelson et al. (1994). A Laser Level LB-1 was used to measure stream bottom depths. Seven cross-section transects were established within the watershed boundary. Transects were located at areas of relative uniformity of stream width, straightness of stream stretch, between ripples and pools, and

areas void of large boulders and woody debris. Endpoints were established on the left and right sides of the cross-section and pinned with stakes. Endpoints were identified as the outward most reach of the floodplain on each side of the stream. A temporary benchmark (TBM) was also established at each cross-section. An arbitrary elevation of 30 m was assigned to each TBM. A tape was stretched to measure total width of the channel. Total channel width was divided to establish 20 measurement intervals. Horizontal measurements were taped to 0.003 of a meter. Additional measurements were taken at each significant change in stream bottom (change in stream bottom depth, terraces, channels, etc.). Channel depth measurements were measured to 0.003 of a meter. Surveys commenced from river left to river right to ease in graphical plotting. Flood plain left, bank-full left, left edge of water (LEW), channel bottom, right edge of water (REW), bank-full right, and flood plain right were all recorded for each transect.

Recorded stream height data (automated stream recorders) were used to determine height of a constant head boundary for input of the HYDRUS 2-D model. Average monthly values for stream height were calculated as the difference between the down and upstream gages.

## *Meteorological Monitoring*

A meteorological station integrated with a CR 10X (Campbell Scientific) data logger was used to collect data within the watershed. Variables measured were rainfall frequency, volume, intensity, air temperature, and soil temperature. The precipitation data were used to determine total precipitation and storm frequency occurring within the Slagle watershed. Potential evapotranspiration was calculated in the CropWat 4.0 model (Smith et al., 1998). Model inputs were maximum and minimum temperature, relative humidity, wind speed, and

solar radiation. Actual evapotranspiration per time step were calculated through the HYDRUS 2-D model, utilizing precipitation, plant water stress functions, and potential evapotranspiration calculated through CropWat 4.0.

## *Hydrologic Modeling*

Water transport was simulated using the HYDRUS 2-D model (Simunek et al., 1999). HYDRUS 2-D is a Microsoft Windows based modeling platform for the analysis of unsaturated, variably saturated, and saturated flow and solute transport through porous media. The HYDRUS 2-D model numerically solves Richard's equation for saturated-unsaturated water flow. Richard's equation (1), the governing flow and transport equation, is solved numerically using a Galerkin-type linear finite element scheme (Simunek et al., 1999).

$$\textit{Richard's Equation: } \frac{\partial \theta}{\partial t} = \frac{\partial}{\partial x_i}\left[K(K_{ij}^A \frac{\partial h}{\partial x_j} + K_{iz}^A) - S)\right] \quad (1)$$

where $\theta$ is the volumetric water content [$L^3L^{-3}$], $h$ is the pressure head [L], $S$ is a sink term [$T^{-1}$], $x_i$ ($i$=1,2) are the spatial coordinates [L], $t$ is time [T], $K_{ij}^A$ are components of a dimensionless anisotropy tensor $K^A$, and $K$ is the unsaturated conductivity function [$LT^{-1}$] (2) given by

$$K(h,x,z) = K_s(x,z)\, K_r\, h,x,z) \quad (2)$$

Where $K_r$ is the relative hydraulic conductivity and $K_s$ is the saturated hydraulic conductivity [$LT^{-1}$].

HYDRUS 2-D uses unsaturated soil hydraulic properties that are incorporated into the governing flow equation. The user may choose from three different analytical models as described by Brooks and Corey (1966), van Genuchten (1980), and Vogel and Cislerova (1988), to solve for unsaturated soil hydraulic properties. This model incorporates a sink

term for root water uptake (evapotranspiration), and uses an anisotropy tensor to account for an anisotropic medium.

The general construction of the HYDRUS 2-D model can be seen in Figure 3-6. The desired simulation is defined in the pre-processing menus within the HYDRUS 2-D model. Geometry, time information, iteration criteria, soil hydraulic model, water flow parameters, root water uptake, time-variable boundary conditions, and mesh generation are defined within these pre-processing menus. For more detail about procedures and description of the HYDRUS 2-D model, refer to Chapter 3, Model Construction and Inputs).

Table 2-1: Data collection and application the for watershed study.

| Data Collected | Data Use |
|---|---|
| Watershed Survey | define total drainage of study watershed<br>define slope distribution of study watershed<br>establish instrument transect location<br>used to create cross-section transport domain for hydrologic modeling |
| Transect Location | define spatial distribution between instrument locations (TDR, WCR, meteorological station, lysimeters) |
| Soil Characterization | classification of soil series<br>define horizon depths<br>soil physical properties per slope location and horizon :<br>bulk density, saturated hydraulic conductivity, particle size, water retention curve<br>soil physical properties used for model parameterization |
| Soil Water Analysis | monitoring of nitrate and ammonium concentration / mass flux |
| Vadose Zone Monitoring | TDR and WCR:<br>monitor subsurface soil volumetric water flux<br>estimate time dependent water flux for hydrologic modeling boundary conditions<br>used to estimate nutrient flux per soil water volume |
| Stream Gaging | stream stage monitoring for hydrologic modeling boundary conditions |
| Meteorological Station | determine atmospheric conditions within study watershed<br>establish boundary conditions for hydrologic modeling<br>calculate water input (precipitation) and loss (Et, evaporation) |
| Hydrologic Modeling | estimate subsurface water flux within study watershed<br>estimate of water loss and storage (Et, soil water storage) |

# References


Blake, G.R., and K.H. Hartge. 1986. Bulk Density, p. 364-367, *In* A. Klute, ed. Methods of Soil Analysis: Part 1- Physical and Mineralogical Methods, 2 ed. A. Klute, Madison,WI. p. 1188.

Bouyoucos, G.J. 1936. Directions for making mechanical analysis of soil by the hydrometer method. Soil Sci. 42:225-228.

Brooks, R.H., and A.T. Corey. 1966. Properties of porous media affecting fluid flow. J.Irrig. Drainage Div., ASCE Proc. 72:61-88.

Buchanan, T.J., and W.P. Somers. 1969. Techniques of Water-Resources Investigation of the United States Geologic Survey Book 3: Applications of Hydraulics. United States Geologic Survey.

Cassell, D.K., and D.R. Nielsen. 1986. Field Capacity and Available Water Capacity, p. 910-913, *In* A. Klute, ed. Methods of Soil Analysis: Part 1-Physical and Mineralogical Methods, 2 ed. ASA, Inc. and SSSA, Inc., Madison, WI. p. 1188.

Corvallis Microtechnology, Inc. 1998a. PC-GPS. Release 3.7D. Corvallis Microtechnology, Inc., Corvallis, OR.

Corvallis Microtechnology, Inc. 1998b. GPS-HP-L4 Operator's Manual. Corvallis Microtechnology, Inc., Corvallis, OR.

Danielson, R.E., and P.L. Sutherland. 1986. Porosity, p. 450-457, *In* A. Klute, ed. Methods of Soil Analysis: Part 1-Physical and Mineralogical Methods, 2 ed. ASA, Inc. and SSSA, Inc., Madison, WI. p. 1188.

Gaskin, J.W., J.F. Dowd, W.L. Nutter, and W.T. Swank. 1989. Vertical and lateral components of soil nutrient flux in a hillslope. J. Environ. Qual. 18:403-410.

Golden Softwrare, Inc. 1999. User's Guide: Contouring and 3D Surface Mapping for Scientists and Engineers. Release 6.04. Golden Softwrare, Inc., Golden, CO.

Harrelson, C.C., C.L. Rawlins, and J.P. Potyondy. 1994. Stream channel reference sites: an illustrated guide to field techniques. General Technical Report RM-245. U.S. Department of Agriculture, Fort Collins, CO.

Klute, A., and C. Dirksen. 1986. Hydraulic Conductivity and Diffusivity: Laboratory Methods, p. 694-700, *In* A. Klute, ed. Methods of Soil Analysis: Part 1-Physical and Mineralogical Methods, 2 ed. ASA, Inc. and SSSA, Inc., Madison, WI. p. 1188.

Lakel, W.A., III. 2000. Slash Mulching and Incorporation as Mechanical Site Preparation for Pine Plantation Establishment and Subsequent Effects on Soil Moisture and

Site Hydrology, Virginia Polytechnic Institute and State University, Blacksburg, VA. p. 72.

Reynolds, B.C., and J.M. Deal. 1986. Procedures for Chemical Analysis at the Coweeta Hydrologic Laboratory. Coweeta Hydrologic Laboratory, Otto, NC.

Simunek, J., M. Sejna, and M.T.v. Genuchten. 1999. The Hydrus-2D Software Package for Simulating the Two-Dimensional Movement of Water, Heat, and Multiple Solutes in Variably-Saturated Media. p. 227.

Slack, J.R., A.M. Lumb, and J.M. Landwehr. 2002. Station 03500240 Cartoogechaye Creek near Franklin, NC 93-4076. USGS Water Resources.

Food and Agriculture Organization of the United Nations (FAO). 1998. CropWat 4 Windows. Release 4.2. Food and Agriculture Organization of the United Nations (FAO), Rome, Italy.

United States Department of Agriculture, Natural Resources Conservation Service. 1996. Soil Survey of Macon County, North Carolina. p. 322

van Genuchten, M.T. 1980. A closed-form equation for predicting the hydraulic conductivity of unsaturated soils. Soil Sci. Am. J. 44:892-898.

Vogel, T., and M. Cislerova. 1988. On the reliability of unsaturated hydraulic conductivity calculated from the moisture retention curve. Transp. Porous Media 3:1-15.

Walsh, L.M. 1971. Instrumental Methods for Analysis of Soils and Plant Tissue. *In* A. Klute, ed. Methods of Soil Analysis: Part 1-Physical and Mineralogical Methods, 2 ed. ASA, Inc. and SSSA, Inc., Madison, WI. p. 1188.

Yeakley, J.A., B.W. Argo, D.C. Coleman, J.M. Deal, B.L. Haines, B.D. Kloeppel, J.L. Meyer, W.T. Swank, and S.F. Taylor. 2003. Hillslope nutrient dynamics following upland riparian vegetation disturbances. Ecosystems 6:154-167.

# Chapter 3: Hillslope Hydrology of a Mountain Pasture

## Abstract

Soil and hydrologic characteristics of a 5-ha agricultural watershed, located in southwestern North Carolina, were studied to quantify surface and subsurface hydrological dynamics to a developing riparian area. The watershed is composed of four dominant soil series, the Braddock (clay loam), Saunook (loam), Dillsboro (loam), and Rosman (sandy loam), which are all underlain by a less permeable Bt-horizon. Field and laboratory analysis was conducted on the Braddock, Saunook, and Rosman series only, to incorporate this specific project into an existing riparian study within the watershed. The physical and mechanical characteristics of these soils were studied to understand the influence these soils had on surface and subsurface flow processes. The watershed was monitored for approximately eight months with meteorological monitoring, time domain reflectometry (TDR), and stream gaging. A full year of monitoring was desired, but not fulfilled due to instrumentation problems. However, the eight-month monitoring period was sufficient in quantifying water flow and nutrient transport in periods of high flow and minimal plant growth. HYDRUS 2-D was used to simulate water movement in a domain with a depth of 0.2 m for the Ap-horizon and 1.5 m for the Bt-horizon. The model simulated soil water content ($\theta v$) compared reasonably well to observed data.

HYDRUS 2-D provided a good link between unsaturated flow and saturated flow processes. Output from the model were used to quantify the interaction of rainwater with surface and subsurface soil horizons, and to describe specific flow paths between heterogeneous soil materials.

## Introduction

Researchers have documented that riparian zones play a significant and beneficial role in natural ecotones (Dillaha et al., 1988; Schultz et al., 1994). Riparian zones have multiple definitions but generally can be defined as the vegetative interface between terrestrial and aquatic ecosystems. These transitional zones provide important links between the terrestrial upland ecosystem and aquatic stream or lake ecosystems (Schultz et al., 1994). A primary characteristic of the riparian zone is the three-dimensionality of water and solute movement through the soil as well as the biogeochemical processes that occur within these soils. Lowrance at al. (1983) noted that the three sources of water contributing to a riparian area are precipitation, subsurface movement from uplands area, and surface movement from upland areas. The rate at which water from the uplands moves on the surface and in the subsurface to a riparian area or river is dependent on storm intensity and duration, soil characteristics, antecedent soil moisture, slope, and vegetation. Yeakley et al. (1998) noted that there are two primary physiographic factors that control soil moisture on a hillslope: soil properties and topography.

The interaction of soil properties and topography dictate how and when water will move through the watershed from source to discharge. Such soil properties as bulk density, infiltration, saturated and unsaturated hydraulic conductivity, and particle size distribution influence the specific path water will move downslope (McLaren and Cameron, 1996). If the surface soil layer is impermeable, precipitation will either pool or move as lateral flow. If the surface horizon has sufficient infiltration, water may infiltrate and percolate both horizontally or vertically.

There are a number of transport parameters that control water movement through unsaturated and saturated media, such as soil physical properties (soil type, extent, properties, etc.) and mechanical properties (saturated and unsaturated hydraulic conductivity, bulk density, porosity, etc.), preferential flow (mole/worm holes, rooting channels, confining layers), storm flux, intensity, volume, and duration of precipitation events, and exchange with saturated media.

Nutrient transport, the focus of this research, is commonly linked to the subsurface movement of water laterally in soils (Cooper, 1990; Hill, 1996; Hubbard and Sheridan, 1983). Though overland flow is a dominant part of nitrate transport in mountain pastures, research has shown that water (and nitrate) can move laterally in the subsurface as a result of a confining soil layer or geologic structure.

Soil pore size distribution can influence the specific path that water will follow. The greater the percentage of inter-connected macropores (effective porosity), the higher probability that water molecules will flow laterally through the soil. Such surface soil properties as bulk density and infiltration will influence a soil's ability to transport water through macropores. In a study of the Walker Branch Watershed in Eastern Tennessee, researchers concluded that preferential flow through both the meso and macropores was the predominant mechanism of stream flow generation (Wilson et al., 1990). Contributions of subsoil water came from various pore sizes as a function of a changing stage of the hydrograph (climbing vs. falling limb of the hydrograph). In this specific scenario, it appears that water continued to move through meso and macropores during the rise and fall of soil volumetric water. As soil water content increased with increase stage on the hydrograph, water moved rapidly through macropores as a result of

differences in pressure gradient. As the water content decreased, the path of water moving through macro and mesopores became more tortuous, thus reducing contributions to the stream hydrograph. In a similar study in New Zealand, Mosley (1982) noted that approximately 40% of precipitation on a hillslope moves rapidly downslope though macropores.

In Luxmoore and Ferrand's (1993) study of pore-scale analysis of preferential flow, the authors noted that soil-water contact time is significantly modified by pore-scale soil-water dynamics. In describing their connect-disconnect hypothesis, they contended that subsurface flow path lengths are highly dynamic aspects of the landscape that may vary seasonally or within single storm events.

Two components of hillslope hydrology are the movement of water in both saturated and unsaturated states. Though the concept of unsaturated flow (vadose zone flow) violates Darcy's principle of laminar flow, researchers have shown that unsaturated flow is an integral component of hillslope hydrology (Anderson et al., 1997; Jackson, 1992; Pang et al., 2000; Vogeler et al., 1997). Interest in unsaturated flow processes has increased in recent years due to the increased concern that the quality of the subsurface environment has been adversely affected by agricultural, industrial, and municipal activities (Simunek et al., 1999).

There have been several field studies focused on saturated transport processes and nutrient transport, but due to the complex nature of unsaturated flow processes, field observation studies are often inadequate in describing unsaturated flow. As a result, mathematical models have been developed to iteratively solve for unsaturated flow (Mailhol et al., 2001; Pang et al., 2000; Simunek et al., 1999). Once such model,

HYDRUS 2-D (Simunek et al., 1999), formally know as SWMS 2-D, has received much attention. This model may be used to analyze water and solute movement in unsaturated, partially saturated or saturated porous media (Simunek et al., 1999).

The specific objective of this paper is to utilize observed watershed soil, hydrological, and meteorological data to two-dimensionally model both saturated and unsaturated flow processes within the pasture and at the riparian zone interface. The understanding of these flow processes will assist in understanding the hillslope hydrology of the study site, as well as the influence of water flux on nutrient transport.

# Methods

## *Site Description*

The study watershed is located approximately 13 kilometers west of the town of Franklin, Macon County, North Carolina on the Slagle Farm (Figure 2-2). This area of southwestern North Carolina is in the Blue Ridge Mountain physiographic region and is typified by steep granitic slopes to relatively level alluvial flood plains adjacent to primary rivers. The Slagle Farm watershed (N:92355.91 E:27448.47) (Figure 2-2, 2-3) incorporates approximately 5-ha of drainage, and ranges in elevation from 646 meters at the top ridge to 628 meters at the Cartoogechaye Creek. The watershed is located on private land that has primarily been used as agricultural land, with moderate cattle grazing.

The area receives an average of 132 cm of precipitation a year. Approximately 50 % of annual precipitation falls during the months of April and September, with an average relative humidity of 60% (United States Department of Agriculture, 1996). The average summer temperature is 24° C, with a maximum temperature of 29° C. The average winter temperature is 4° C, with a minimum of -3° C (United States Department of Agriculture, 1996).

## *Soil Characteristics*

The site is primarily covered with Kentucky Fescue 31 grass, with sparse woody vegetation distributed across the landscape. The pasture is primarily composed of four series of soil: the Braddock, Saunook, Rosman, and Dillsboro series (Figure 2-4) (United States Department of Agriculture, 1996). The Braddock series is usually located on the strongly sloping (8-15%) and top-slopes of the pasture as well as on the spurs within the

drainage. The Braddock clay loam is a well-drained, clayey, mixed, mesic Typic Hapludults. The surface layer is within the top 28 cm of soil and is reddish brown (Ap-horizon) (United States Department of Agriculture, 1996). The subsoil Bt-horizon is located between 28 and 109 cm, followed by a weathered C-horizon consisting primarily of mica.

The Saunook series is a very deep, well-drained, moderately permeable soil located on gently sloping (2-8%) mid-sloped areas. The Saunook loam is a fine-loamy, mixed, mesic Humic Hapludults. The surface layer (Ap-horizon) is a dark brown loam and is up to 25 cm deep. The subsoil (Bt-horizon) ranges from 25 cm to 86 cm in depth. The Bt is located atop a weathered C-horizon composed of mica with 15% gravel and 25% cobbles (United States Department of Agriculture, 1996).

The Dillsboro series is a moderately permeable, very deep, well-drained loam that is located mid-slope in the eastern most drainage of the watershed. The Dillsboro loam is a clayey, mixed, mesic Humic Hapludults found on gentle slopes ranging between 2 and 8%. The surface soil is a dark brown loam up to 30 cm in depth. The subsoil Bt-horizon is a strong brown clay up to 127 cm deep (United States Department of Agriculture, 1996).

The Rosman series is a very deep, well-drained, moderately rapid permeable sandy loam. This series is often found on nearly level (0-2%) slopes adjacent to major streams and is specifically located within the established riparian area of this site. The Rosman is a fine sandy loam that is frequently flooded. This coarse-loamy, mixed, mesic Fluventic Haplumbrepts runs the entire length of the watershed. The surface soil (Ap-horizon) is dark brown and reaches a maximum depth of 41 cm. The subsoil (Bt-horizon)

reaches a maximum depth of 145 cm and is typified as a Bt/Bw horizon (United States Department of Agriculture, 1996).

### *Stream Characteristics*

The Slagle Farm drainage discharges into Cartoogechaye Creek (Figure 2-5). Cartoogechaye Creek receives inputs from a total drainage area of 22.3 $km^2$ (Slack et al., 2002). The total length of the creek is 24.8 km, and meanders approximately north/north east to its confluence with the Little Tennessee River, directly south of Franklin, NC. The creek has a mixed silt/cobble bottom and has undergone drastic channel morphological changes during the last 200 years. The channel segment of the creek draining the Slagle Farm originated as a sawmill flume. However, when the mill was abandoned, the Cartoogechaye diverged from its original path to create the present day stream channel. Much of the stream bank is a result of over-bank sedimentation and has succumbed to intense erosion. Most of the Cartoogechaye Creek drainage originates from moderately steep pasture and agricultural lands.

## *Watershed Delineation and Sample Transects*

The delineation of the watershed was conducted on site, with use of USGS 7.5' Franklin, NC quadrangle topographic map (Figure 2-2) and Corvallis Microtechnology, Inc. PC5-L global positioning system (GPS) receiver (Corvallis Microtechnology, 1998b). The survey was conducted to define the smaller watershed that drains into an established riparian study site. The established elevation gradients, slopes, and drainage reference points that aided in quantifying the total drainage area of the study riparian zone.

After the perimeter survey was completed, a more intensive survey was conducted within the watershed to develop a local topographic map for the drainage area. GPS locations were taken at every major change (> 0.5-m) in micro-topographical feature within a 10-m grid. Data collected were used to develop a topographic map, with geodetic correction. CMT PCGPS 3.7 software (Corvallis Microtechnology, 1998a) was used to correct and process GPS data. X, Y, and Z data collected was then processed through Surfer Win 32 Version 6.04 (Golden Software, 1999) to create the topographic map (Figure 3-1). The watershed topographic map assisted in identifying micro-topography and its influence on both surface and subsurface drainage.

Transects were established within the primary sub-watershed drainage patterns (identified from contour map) of the watershed (Figure 3-1). A total of three transects were established within each primary sub-watershed individual drainage regimes, which drain into the study riparian area. Transects span the length of the watershed, from ridge tops in pasture, through riparian area, to river (transects were laid in the general direction of subsurface flow to river).

## *Field and Laboratory Measurements*

### *Soil Characterization*

Soil profile descriptions were conducted along each transect to characterize master soil horizons. Four sampling stations were located in each transect, representing top-slope, mid-slope, toe-slope, and riparian area. Profiles were delineated based on depth, color, structure, texture, mottles, and roots. A Munsell color chart and the Soil Survey of Macon County, North Carolina (United States Department of Agriculture, 1996) aided in the delineation and classification. The profile descriptions were used to

determine specific depths for the placements of lysimeters and TDR instrumentation placements. Intact soil core samples were collected from both the Ap and the Bt horizons.

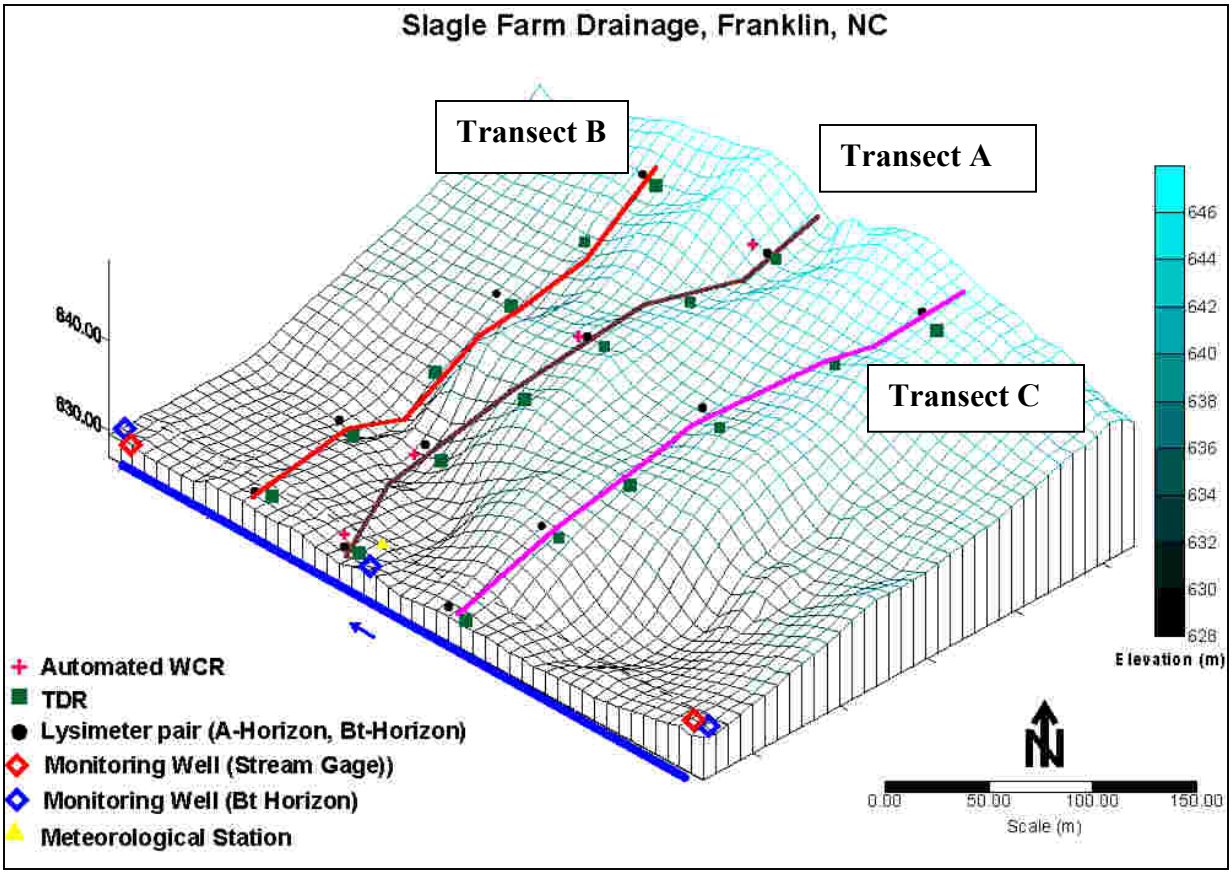


Figure 3-1: Rendered Sagle Farm Watershed topographic map with instrumentation Locations

Three intact soil core sub-samples and three loose soil sub-samples were taken from the Ap and Bt horizons at each monitoring station. Samples were then analyzed in the lab for soil physical and mechanical properties.

Particle size distribution was determined using the dispersion method illustrated by Bouyoucos (1936). Sand, silt, and clay percentages were calculated for each sample location, top-slope, mid-slope, toe-slope, and riparian area, respectively. Total, macro and micro porosity was calculated by the Danielson and Sutherland method (1986), while the constant head method was used to calculate saturated hydraulic conductivity (Klute

and Dirksen, 1986). Bulk density was determined by the intact core method (Blake and Hartge, 1986). Water retention characteristic curves were calculated via the small core method for each sample location, and averaged to soil series (Cassell and Nielsen, 1986). Pressure potentials of 0.005 MPa, 0.03 MPa .01 MPa, .05 MPa, 1.0 MPa, and 1.5 MPa were used to develop high-resolution curves. Water retention curves were fitted using RETC (Simunek et al., 1999), and unsaturated soil hydraulic parameters were derived (Table 3-2).

Transects were instrumented with four pairs of porous-cup tension lysimeters. Lysimeters pairs, in the Ap (20 cm) and Bt (50 cm) horizons, were located on the top-slope, mid-slope, toe-slope, and riparian zone (approximately 125 m spacing). Volumetric water content ($m^3/m^3$) was estimated via time domain reflectometry (TDR) (Topp and Davis, 1985) at measurement locations installed along each transect from riparian area to top-slope. TDR rods (3-mm diameter) were inserted vertically, 5 cm apart for the 20-cm and 50-cm depths, corresponding to Ap and Bt-horizon depths, respectively. Four automated water content reflectometers (Campbell Scientific CS-615) were installed along transect A at the top-slope, mid-slope, toe-slope, and riparian zone. Water content reflectometers were installed horizontally on top of the Bt horizon and automated with a Campbell Scientific 10x datalogger.

TDR and lysimeter measurements were conducted bimonthly. TDR and lysimeter measurements occurred from August 2002 to March 2003. Lysimeters were evacuated to -0.03 MPa, and were analyzed for total N, $NO_3^-$-N, and $NH_4^+$-N through procedures developed by the Coweeta Hydrologic Laboratory (Reynolds and Deal, 1986; Walsh,

1971). WCR recorded volumetric water content ($m^3/m^3$) in 5-minute intervals, and averaged hourly to account for the influence of storm flux.

### *Meteorological Monitoring*

A meteorological station integrated with a CR 10X (Campbell Scientific) data logger was used to collect meteorological data within the watershed. Variables measured were rainfall frequency, volume, intensity, air temperature, and soil temperature. Additional meteorological data was collected at the Coweeta Hydrologic Laboratory, approximately 20 km away from the study site. Data collected were minimum and maximum temperature, relative humidity, wind speed, and solar radiation. The precipitation data was used to determine total precipitation and storm frequency occurring within the Slagle watershed.

### *Stream Monitoring*

Stream discharge and watershed discharge to Cartoogechaye Creek was measured and calculated using a cross-sectional stream survey as illustrated by Harrelson et al. (1994). A Laser Level LB-1 was used to measure stream bottom depths. Seven cross-section transects were established within the watershed boundary. Transects were located at areas of relative uniformity of stream width, straightness of stream stretch, between ripples and pools, and areas void of large boulders and woody debris. Stream height data was recorded at the upstream and downstream boundaries of the watershed using Ecotone water level loggers. Measurements were recorded in 10-minute intervals to aid in developing boundary conditions for hydrologic modeling.

## *Hydrologic Analysis*

### *Model Description*

Water transport were simulated using the HYDRUS 2-D model (Simunek et al., 1999). HYDRUS-2D is a Microsoft Windows based modeling platform for the analysis of unsaturated, variably saturated, and saturated flow and solute transport through porous media. The HYDRUS 2-D model numerically solves Richard's equation for saturated-unsaturated water flow. Richard's equation (1), the governing flow and transport equation, is solved numerically using a Galerkin-type linear finite element scheme (Simunek et al., 1999).

$$\textit{Richard's Equation: } \frac{\partial \theta}{\partial t} = \frac{\partial}{\partial x_i}\left[K(K_{ij}^A \frac{\partial h}{\partial x_j} + K_{iz}^A) - S)\right] \quad (1)$$

where $\theta$ is the volumetric water content [$L^3L^{-3}$], $h$ is the pressure head [L], $S$ is a sink term [$T^{-1}$], $x_i$ ($i$=1,2) are the spatial coordinates [L], $t$ is time [T], $K_{ij}^A$ are components of a dimensionless anisotropy tensor $K^A$, and $K$ is the unsaturated conductivity function [$LT^{-1}$] (2) given by

$$K(h,x,z) = K_s(x,z)\, K_r\, h,x,z) \quad (2)$$

Where $K_r$ is the relative hydraulic conductivity and $K_s$ is the saturated hydraulic conductivity [$LT^{-1}$].

HYDRUS 2-D uses unsaturated soil hydraulic properties that are incorporated into the governing flow equation. The user may choose from three different analytical models as described by Brooks and Corey (1966), van Genuchten (1980), and Vogel and Cislerova (1988), to solve for unsaturated soil hydraulic properties. This model incorporates a sink term for root water uptake (evapotranspiration), and uses an anisotropy tensor to account for an anisotropic medium.

The general construction of the HYDRUS 2-D model can be seen in Figure 3-2. The desired simulation is defined in the pre-processing menus within the HYDRUS 2-D model. Geometry, time information, iteration criteria, soil hydraulic model, water flow parameters, root water uptake, time-variable boundary conditions, and mesh generation are defined within these pre-processing menus.

The conditions menu is used to assign various boundary conditions to the generated mesh (representing watershed, cross section, water column, etc.). Menu options within the conditions menu are used to characterize the generated mesh for soil materials distribution, root distribution, initial water content or pressure head conditions, sub-region distribution for spatially explicit mass water balances, and observation node locations. A brief description of the available condition menus taken from the HYDRUS 2-D reference manual are presented below in Table 3-1.

### *Model Construction and Inputs*

*Space and time discretizations*. A cross-section of the Slagle Farm watershed was created from the survey data used to create the 3-D topographic map. Average elevations per slope location were calculated across the slope perpendicular to Cartoogechaye Creek. X, Y, and Z data were imported into the MeshGen menu of HYDRUS-2D to create the cross-section. The size of the model domain for the cross-section was 206 m in width with a total depth (slope top to creek) of 20 m. The finite element grid consisted of a total of 11,954 nodes and 21,907 elements.

Water flow was simulated for 212 days, representing August 2002 to March 2003. This time duration was used to represent the total period of which onserved field data was collected. Individual days were scaled up to four-day intervals for a simulation period of

53 units. Time discretizations were as follows: initial time step 1 X $10^{-1}$ day, minimum time step 1 X $10^{-2}$ day, and maximum time step 5 days.

*Water Flow Paramters*. As noted earlier, to determine soil hydraulic properties, representative soil horizons were sampled at depths of 20 cm and 50 cm (Ap- and Bt-horizons, respectively). Sampling occurred along each transect, at the top-slope, mid-slope, toe-slope, and riparian area (Figure 3-1). Three samples were taken from each horizon, and an arithmetic mean was calculated per horizon and slope location. Particle size analysis (Bouyoucos, 1936) was used to calculate sand, silt, and clay percentages for each sample location, and an arithmetic mean was calculated per horizon and slope location. Water retention curves and saturated hydraulic conductivity (Ksat) were calculated in the laboratory using methods of Cassell and Nielsen (1986) and the constant head method described by Klute and Dirksen (1986), respectively. Water retention curves were fitted using RETC (van Genuchten et al., 1991), and soil hydraulic parameters were derived (Table 3-2).

A modified form of van Genuchten's unsaturated hydraulic conductivity equation (1980), as described by Vogel and Cislerová (1988), was used to calculate the unsaturated hydraulic properties for the water flow parameters of each soil horizon per classification used in the HYDRUS 2-D model (Table 3-3).

As noted earlier, HYDRUS 2-D utilizes a sink term ($S$) to account for root water uptake. This term represents the volume of water removed per unit time from a unit volume of soil due to plant water uptake (Simunek et al., 1999).

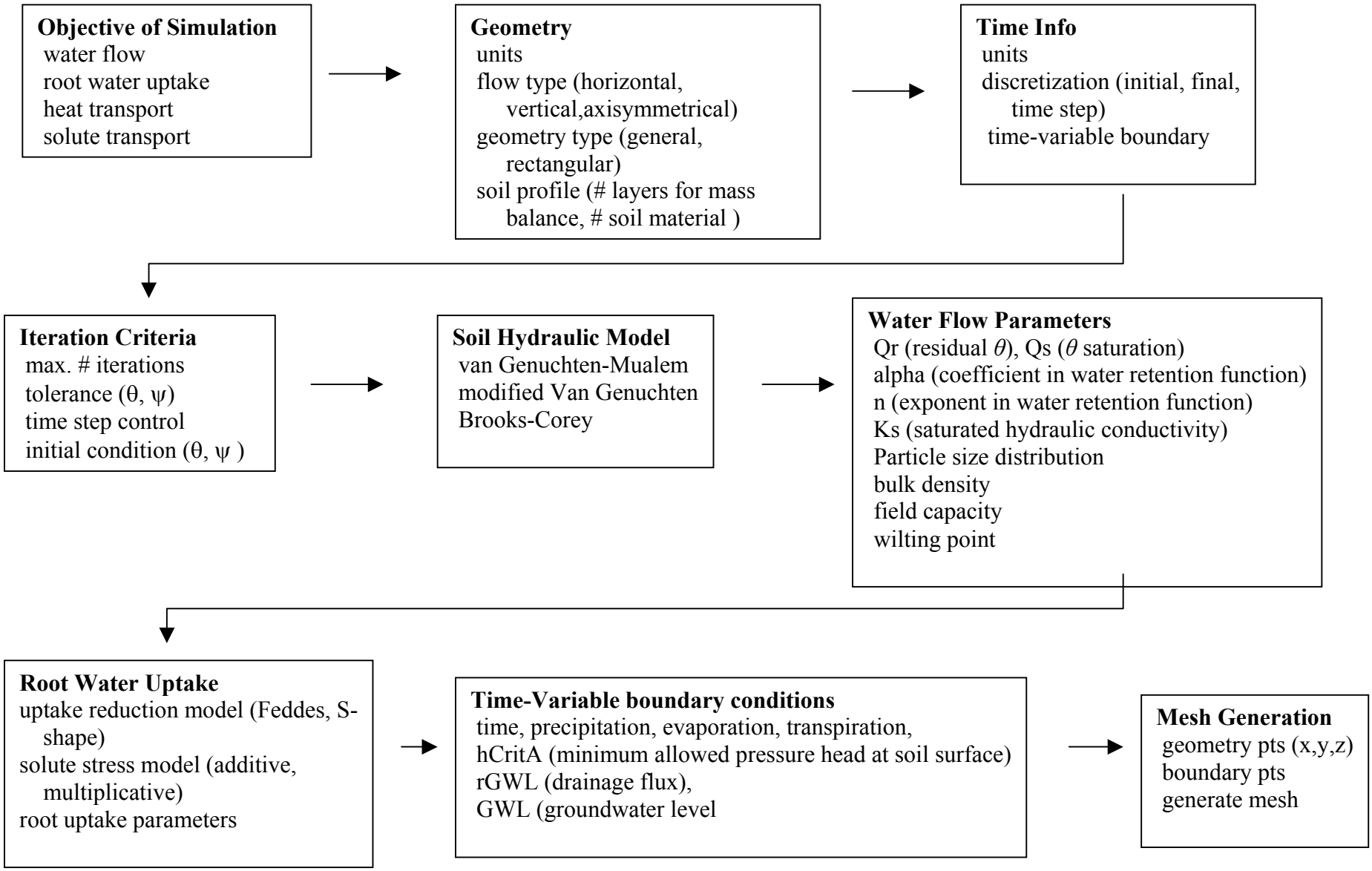


Figure 3-2: Pre-processing menu commands for HYDRUS 2-D flow and transport simulation.

Table 3-1: HYDRUS 2-D model conditions menu commands for parameter and boundary condition assignment.

| Condition | Description of menu commands |
|---|---|
| Water flow boundary conditions | specifies BC for water flow |
| Solute transport boundary conditions | specifies BC for solute transport |
| Heat transport boundary conditions | specifies BC for heat transport |
| Material distribution | specifies spatial distribution of soil materials |
| Root distribution | specifies root water uptake distribution |
| Nodal recharge | specifies spatial distribution of nodal recharge |
| Scaling Factors | specified spatial distribution of scaling factors for hydraulic conductivity, pressure head, water content |
| Initial conditions | specifies starting conditions for water flow, heat and/or solute transport |
| Local anisotrophy | specifies spatial distribution of local anisotrophy |
| Sub-regions | specifies spatial distribution of mass balance calculations |
| Observation nodes | specifies nodes for output of pressure head, water content, concentration at each time step |
| Drains | specifies nodal points representing tile drains |

Table 3-2: Soil hydraulic values each horizon for Braddock (Bra), Saunook (Sau), and Rosman (Ros) soils used in HYDRUS 2-D simulation *.

| Soil | Horizon | Theta S | FC | WP | BD | Ksat | Sand | Silt | Clay |
|---|---|---|---|---|---|---|---|---|---|
| | | ($m^3/m^3$) | ($m^3/m^3$) | ($m^3/m^3$) | $Mg/cm^3$ | cm/hr | (%) | (%) | (%) |
| Bra | A | 41.61 | 35.44 | 19.21 | 1.28 | 8.37 | 52.27 | 22.6 | 25.13 |
| Bra | B | 41.56 | 38.87 | 18.83 | 1.36 | 2.22 | 48.76 | 23.8 | 27.42 |
| Sau | A | 43.22 | 36.25 | 16.87 | 1.11 | 19.45 | 57.37 | 24.3 | 18.33 |
| Sau | B | 41.62 | 35.95 | 18.61 | 1.3 | 3.89 | 45.22 | 26.5 | 28.3 |
| Ros | A | 45.21 | 39.21 | 18.14 | 1.16 | 24.39 | 59.69 | 24.4 | 15.9 |
| Ros | B | 50.44 | 48.89 | 19.35 | 1.11 | 6.89 | 46.47 | 27 | 26.55 |

* Theta S - saturated soil water content; FC - field capacity (0.003 MPa); WP - wilting point (1.50 MPa); BD - bulk density; Ksat - saturated hydraulic conductivity.

Table 3-3: Water flow parameters defined from unsaturated hydraulic properties for Ap- and Bt-horizons per soil series*.

| Soil | Horizon | Qr | Qs | Alpha | n | Ks | l | Qm | Qa | Qk | Kk |
|---|---|---|---|---|---|---|---|---|---|---|---|
| | | ($cm^3/cm^3$) | ($cm^3/cm^3$) | | | m/d | | | ($cm^3/cm^3$) | ($cm^3/cm^3$) | |
| Bra | A | 0.06 | 0.47 | 0.93 | 1.35 | 0.25 | 0.5 | 0.47 | 0.06 | 0.47 | 0.25 |
| Bra | B | 0.07 | 0.46 | 0.34 | 1.52 | 0.10 | 0.5 | 0.46 | 0.07 | 0.46 | 0.10 |
| Sau | A | 0.06 | 0.50 | 0.75 | 1.41 | 0.64 | 0.5 | 0.50 | 0.06 | 0.50 | 0.64 |
| Sau | B | 0.07 | 0.47 | 0.69 | 1.39 | 0.18 | 0.5 | 0.47 | 0.07 | 0.47 | 0.18 |
| Ros | A | 0.06 | 0.50 | 0.52 | 1.47 | 0.52 | 0.5 | 0.50 | 0.06 | 0.50 | 0.52 |
| Ros | B | 0.09 | 0.53 | 0.14 | 1.95 | 0.21 | 0.5 | 0.53 | 0.09 | 0.53 | 0.21 |

* Variables are defined as: *Qr* =residual water content $\theta$, *Qs* = saturated water content $\theta$, *alpha* = parameter in the soil water retention function [$L^{-1}$], *n* = parameter in soil water retention function, *Ks* = saturated hydraulic conductivity [$LT^{-1}$], *Qm* = parameter $\theta m$ in soil water retention function, *Qa* = $\theta a$ in soil water retention function, *Qk* = soil water content $\theta k$ corresponding to *Kk*, *Kk* = measured value of the hydraulic conductivity corresponding to $\theta k$ [$LT^{-1}$].

The sink term *S* (3), as defined by Feddes et al. (1978) is:

$$S(h) = a(h)S_p \quad (3)$$

where the water stress response function *a(h)* is a prescribed dimensionless function (Richard's equation) of the soil water pressure head ($0 \leq a \leq 1$), and $S_p$ is the potential water uptake rate [$T^{-1}$]. The Feddes model (1978) was used to calculate the water stress

response function. Root water uptake parameters used for this calculation were based on plant water stress function for fescue grass (Table 3-4). A time-variable boundary condition was utilized in this simulation to account for the distribution of water input and outputs. Input was defined as gross precipitation deposition specifically at the Slagle Farm watershed. Outputs in the time-variable boundary condition were defined as transpiration and evaporation as a function of time (daily). Potential evapotranspiration was calculated through the separate model CropWat 4 (Smith et al., 1998). CropWat 4 (Smith, 1999) uses the Penman-Monteith methods for calculating reference crop evapotranspiration. Latitude, longitude, and elevation, as well as daily arithmetic means of maximum temperature, minimum temperature, relative humidity, wind speed, and global radiation were used as input values for CropWat 4 evapotranspiration calculations (Table 3-5). Daily outputs of evapotranspiration rates were then imported into the time-variable boundary conditions editor in HYDRUS 2-D, and coupled with precipitation and minimum allowed pressure head at the soil surface, to calculate the water flow interactions of root water uptake and evaporation.

Table 3-4: Feddes parameters used to define root water uptake (water stress response function) for fescue grass*.

| Po | Popt | P2H | P2L | P3 | R2H | R2L |
|---|---|---|---|---|---|---|
| (m) | (m) | (m) | (m/d) | (m) | (m/d) | (m/d) |
| -0.1 | -0.25 | -2 | -8 | -153 | 0.005 | 0.001 |

* Values defined as: *Po* =pressure head below which roots start to extract water from the soil, *Popt* = pressure head below which roots extract water at the minimum possible rate, *P2H* = limiting pressure head below which roots can no longer extract water at the max. rate, P2L = similar to *P2H*, but for potential transpiration rate of *r2L*, *P3* = pressure head below which root water uptake ceases (WP), *R2H* = potential Et rate set at 0.5 cm/day, *R2L* = potential Et rate set at 0.1 cm/day.

*Boundary and Initial Conditions*. Water flow boundary conditions were defined for the finite element grid based on observed water flow characteristics of the Slagle Farm watershed. As noted above, a cross-section of slope mean elevations was used to create the grid. Three water flow characteristics, consisting of an atmospheric boundary condition, a constant pressure boundary condition for stream head, and a no flux boundary condition along the base and vertical boundaries of the finite grid representing "no flow " were distributed accordingly along the cross-section.

Table 3-5: Mean monthly atmospheric conditions for the Slagle Farm watershed.

| Month | maximum temperature (deg.C) | minimum temperature (deg.C) | humidity (%) | wind speed (Km/d) | sun shine (Hours) | solar raiation (MJ/m2/d) | PEt (m/month) |
|---|---|---|---|---|---|---|---|
| August | 22.6 | 21.2 | 77.9 | 76 | 8.5 | 21.6 | 0.615 |
| September | 20.4 | 19.4 | 85.5 | 85.5 | 7.1 | 20.3 | 0.827 |
| October | 15.3 | 14.3 | 90.8 | 77.8 | 7.1 | 20.4 | 0.566 |
| November | 7.5 | 6.3 | 76.5 | 127 | 7.2 | 20 | 0.449 |
| December | 5 | 3.8 | 70.2 | 140 | 7.4 | 19.9 | 0.365 |
| January | 2.3 | 1 | 61.4 | 156.4 | 8.5 | 21.9 | 0.211 |
| February | 5.5 | 4.3 | 73.8 | 145.2 | 6.5 | 19.5 | 0.322 |
| March | 11.4 | 10 | 72 | 133.1 | 6.6 | 19.9 | 0.420 |
| Average | 11.3 | 10 | 76 | 117.6 | 7.4 | 13.6 | 0.472 |

The atmospheric boundary condition, a time-dependent variable consisting of precipitation, precipitation rate, and evaporation at the soil surface, was applied to the surface of entire transport domain except for the furrow representing the stream channel. As noted earlier, the atmospheric boundary conditions were calculated through input variables in the time-variable boundary conditions menu. A constant pressure head boundary condition was assigned to the surface of the stream furrow. The value of the constant pressure head boundary condition at a particular node is given by the initial value of the pressure head. For this particular simulation, the assigned pressure head of 0.544 m was calculated as the average stream stage height. A no flux boundary condition

was assigned to the base of the cross-section, representing the relative impermeability of the C-horizon located below the Bt-horizon. A no flux boundary is specified for impermeable boundaries where the flux is zero perpendicular to the boundary. A no flux boundary was also assigned to the vertical boundaries of the finite element grid.

The Slagle Farm watershed is primarily composed of three soil series, the Braddock clay loam, Saunook loam, and Rosman sandy loam (Figure 2-4). It is apparent that these soils and their individual horizons are distributed as a function of slope. As a result, the material distributions menu was utilized to assign individual soil series to their respective locations along the slope. It was necessary to delineate and distribute individual soil series and horizons due to their differing soil properties (Table 3-2 and 3-3). The average depth of the Ap- and Bt-horizons were 20 and 50 cm, respectively. A total of eight soil materials were assigned within the finite element mesh to represent the Ap- and Bt-horizons for the Braddock top-slope and mid-slope locations, the Saunook for toe-slope, and Rosman for the riparian area.

The sub-region distribution menu was used to specify the spatial distribution of desired mass balance calculations. Water mass balance calculations are carried out in these sub-regions, as well as over the entire domain. Eight sub-regions were assigned with spatial similarity to material distribution to partition water flow based on soil series and horizon. The individual mass balances calculated for each sub-region assist in quantifying flow processes within individual soil layers. Flow processes within these different soil layers are necessary in order to calculate soil water and nutrient contributions from one soil series and horizon to the next.

The root water uptake spatial distribution menu was used to distribute the influence of plant water uptake of fescue across the flow domain. The maximum root water uptake distribution is time independent (scaled to a potential Et rate), and reflects the distribution in the root zone of roots that are actively involved in water uptake (Simunek et al., 1999). As noted earlier, root water uptake was calculated through the Feddes model (Feddes et al., 1978), in the pre-processing menu of water flow parameterization. Fescue may have a total rooting and water uptake depth of 1.5 m (Johns, 1989). Root water uptake was distributed across the flow domain to a maximum depth of 1.5 m.

The water flow initial conditions menu is used to specify the initial conditions for water flow by defining the initial spatial distribution of the water content over the flow domain (Simunek et al., 1999). Values for water flow initial conditions were obtained from observed water content values from field TDR locations (Figure 3-1). Initial conditions for this simulation were derived from water contents of sampling locations per horizon across each transect. An arithmetic mean of values (by TDR location) for early August 2002 was used to establish pre-simulations criteria. Initial water content values were then distributed across the flow domain, relative to soil series and horizon.

Observations nodes were designated in the flow domain to represent lysimeter sample locations per soil series and horizon. A total of eight observations nodes were assigned relative to each lysimeter location within individual soil series and horizon. These nodes are used to specify observations points for output of water content at each time step within the flow domain.

# Results and Discussion

## *Mechanical and Physical Soil Properties*

Soil mechanical and physical properties analyzed in this study were bulk density, saturated hydraulic conductivity, total, macro-, and micro-porosity, particle size analysis, and water retention curve development. Individual bulk density values for the Braddock series soil (top and mid-slope locations) (Figure 2-4) Ap-horizon ranged from 1.06 $Mg/m^3$ to 1.47 $Mg/m^3$, while Bt-horizon values ranged from 1.13 $Mg/m^3$ to 1.66 $Mg/m^3$, with an arithmetic mean of 1.28 $Mg/m^3$, and 1.36 $Mg/m^3$ (Table 3-6). Individual values for the Saunook series soil (toe-slope locations) (Figure 2-4) Ap-horizon ranged from 0.82 $Mg/m^3$ to 1.38 $Mg/m^3$, with an arithmetic mean of 1.12 $Mg/m^3$, while Bt-horizons values ranged from 1.07 $Mg/m^3$ to 1.43 $Mg/m^3$, with an arithmetic mean of 1.30 $Mg/m^3$ (Table 3-6). The riparian area soil series (Rosman) (Figure 2-4) Ap-horizon had individual bulk density values ranging from 0.97 $Mg/m^3$ to 1.46 $Mg/m^3$, with an arithmetic mean of 1.16 $Mg/m^3$, while the Bt-horizon had individual values of 0.88 $Mg/m^3$ to 1.47 $Mg/m^3$, with an arithmetic mean of 1.10 $Mg/m^3$ (Table 3-6).

Particle size analysis for the Braddock, Saunook, and Rosman soil series are presented in Table 3-7. Mean values for Ap-horizons for sand were 52 %, 55 %, and 54 % (Braddock, Saunook, Rosman series, respectively) with Bt-horizon means of 50 %, 51 %, and 51 %. Mean silt values for the Ap-horizon were 20 %, 25 %, and 30 %, with 23 %, 26 %, and 26 % for Bt-horizons. Mean clay values were 27 %, 20 %, and 16 % for the Ap-horizon, with 27 %, 22 %, and 23 % for Bt-horizons (Braddock, Saunook, Rosman series, respectively).

Table 3-6: Bulk Density and saturated hydraulic conductivity (Ksat) mean values per soil series and horizon (Bra = Braddock, Sau = Saunook Ros = Rosman) *.

| Soil | Horizon | mean bulk density (Mg/cm3) | saturated hydraulic conductivity (cm/hr) |
|---|---|---|---|
| Bra | Ap | 1.28 (.09) | 8.37(10.7) |
| Bra | Bt | 1.36 (.08) | 2.22(2.2) |
| Sau | Ap | 1.12(.20) | 19.45(12.6) |
| Sau | Bt | 1.30(.09) | 3.89(4.7) |
| Ros | Ap | 1.16(.10) | 24.39(12.1) |
| Ros | Bt | 1.10(.21) | 6.89(3.8) |

(* Standard deviations in parenthesis.)

Table 3-7: Mean sand, silt, and clay percentages per soil series and horizon *.

| Soil | Horizon | Sand (%) | Silt (%) | Clay (%) |
|---|---|---|---|---|
| Bra | Ap | 52 (7.4) | 20 (5.0) | 27 (5.4) |
| Bra | Bt | 50 (9.5) | 23 (2.5) | 27 (8.0) |
| Sau | Ap | 55 (5.0) | 25 (6.1) | 20 (3.7) |
| Sau | Bt | 51 (11.6) | 26 (3.2) | 22 (10.3) |
| Ros | Ap | 54 (12.4) | 30 (7.9) | 16 (6.2) |
| Ros | Bt | 51 (11.5) | 26 (5.3) | 23 (6.7) |

( * Standard deviations in parenthesis.)

Bulk density values for the Bt-horizons of the Braddock and Saunook soil series were greater than the Ap-horizons. The increase of bulk density from the Ap- to the Bt-horizon may be attributed to pedogenic processes or terrestrial and microbial activity. Such processes as eluviation (movement of material out of a horizon) and illuviation (movement of a material into a horizon) can remove smaller particle of clay out of the Ap-horizon, depositing them into the Bt-horizon (Fisher and Binkley, 2000). Studies conducted by Wilson et al. (1990) in a forested hillslope and Hill (1996) in a riparian zone adjacent to agricultural land, observed similar results.

Though the particle density of clay is smaller than that of sand, clay particles have greater surface area (due to the mineralogical constitution of clay), packing more particles into a smaller area, thus increasing bulk density. Packing of soil particles also may influence bulk density. Packing refers to how soil particles align within a given soil volume (Fetter, 2001). In heterogenic soils made of sand, silt, and clay, the heavier particles (sand) settle under gravity. Smaller particles, such as silt or clay, will fill in the voids left between individual sand particles, resulting in an increase of total mass per unit volume. This can be seen in the particle size distribution of the Braddock, Saunook, and Rosman soils (Table 3-7). Clay and silt percentages increased from the Ap- to the Bt-horizon in each of the three soils.

It is interesting to note that the bulk densities of the Ap-horizons were less than the Bt-horizons, even though this horizon receives greater compaction as a result of cattle grazing. This may be attributed to the influence of root penetration and turn over in this surface horizon. Once established in the shallow sub-soil, roots will continue to grow and slough, adding organic matter to this horizon and reducing bulk density (Fisher and Binkley, 2000). The influence of freezing and thawing cycles, as well as the shrinking and swelling of soils with mixed mineralogy may also reduce bulk density in surface horizons. Such terrestrial creatures as shrews, moles, and earthworms also aid in churning and aerating the surface soil horizon. This surface horizon may be desirable to earthworms and microbial populations due to the deposition of cattle manure and urea.

The bulk density for the Rosman series (riparian area) did not show the same trend of increased bulk density in the Bt-horizon. This phenomenon may be attributed to the influence of particle deposition within the riparian zone. As sediment is transported

in overland flow into the riparian area, the vegetation reduces the velocity of flow, resulting in sediment deposition. Over time, fine sediments will eluviate from the surface horizon into the sub-soil. However, overland flow and sediment deposition may be episodic (function of storm frequency and intensity), resulting in a continual deposition of fine sediments in the riparian area.

Mean saturated hydraulic conductivity values are shown above in Table 3-6. Ap-horizon values for the Braddock, Saunook, and Rosman soil series were 8.37 cm/hr, 19.45 cm/hr, and 24.39cm/hr, respectively. Mean values for Bt-horizons of the Braddock, Saunook, and Rosman were 2.22 cm/hr, 3.89 cm/hr, and 6.89 cm/hr, respectively.

Mean total, macro-, and micro-porosity values are presented in Table 3-8. Total porosity means for Ap-horizons of the Braddock, Saunook, and Rosman series were 51.57%, 57.94%, and 56.10%, while Bt-horizon values were 48.70%, 50.80%, and 58.30%. Macro-porosity mean values for Ap-horizons were 13.18%, 19.13%, and 13.73%, with 8.02%, 12.08%, and 9.56% for Bt-horizons. Micro-porosity mean values for Ap-horizons were 38.49%, 38.81%, and 42.37%, with 41.05%, 38.74%, and 48.74% for the Bt-horizons.

Saturated hydraulic conductivity and macro-porosity was greater in the Ap-horizon in each of the three soils. This is what was expected due to the influence of particle size distribution and bulk density. Fisher and Binkley (2000) attributed this reduction of hydraulic conductivity to the influence of material layering with different textures. The authors noted that the influence of different parent material and pedogenic processes could result in silt or clay pans on top of a restrictive horizon, such as a Bt-

horizon. This characteristic is often detected in Utlisols. As noted earlier, the clay content and bulk densities of the Bt-horizon were greater. Particle size distribution and bulk density may also influence the distribution of macro-pores to micro-pores. The increase of macro-pores directly influences saturated hydraulic conductivity by moving water under non-capillary force. Water flow in the macro-pores flows under reduced tortuosity than in micro-pores, thus increasing saturated hydraulic conductivity.

Water retention curves for the three soil series present in the Slagle Farm watershed are presented in Figure 3-3. Mean point values for each pressure potential are presented in Table 3-9. The water retention capacity of a soil is primarily attributed to the particle

Table 3-8: Mean total, macro-, and micro-porosity values for the Braddock, Saunook, and Rosman soil series.

| Soil | Horizon | Total (%) | Macro (%) | Micro (%) |
|---|---|---|---|---|
| Bra | Ap | 51.67 (3.4) | 13.18 (1.9) | 38.49 (2.2) |
| Bra | Bt | 48.7 (3.2) | 8.02 (2.1) | 41.05 (2.4) |
| Sau | Ap | 57.94 (7.6) | 19.13 (2.6) | 38.81 (5.5) |
| Sau | Bt | 50.80 (3.5 | 12.08 (1.7) | 38.72 (2.3) |
| Ros | Ap | 56.1 (3.7) | 13.73 (3.8) | 42.37 (1.9) |
| Ros | Bt | 58.30 (7.9) | 9.56 (1.6) | 48.74 (6.4) |

( * Standard deviations in parenthesis.)

size distribution within the soil matrix. Water is held more tightly to clay particles than sand or silt, due to the mineralogical structure of clay (McLaren and Cameron, 1996; Stephens, 1996). Water is held through cohesion of water molecules to one another, and adhesion of water to clay particles. As a result, water content is often greater in soil horizons with high clay content. This is illustrated by the more gradual curve reflecting a

more uniform pore size distribution within the Bt-horizons (McLaren and Cameron, 1996).

Table 3-9: Mean water content values at various pressure potentials for water retention curve development by soil series and horizon. Pressure values represent the pressure at which soil samples were subjected to determine water content at various pressures. Standard deviations in parenthesis adjacent to mean water content values.

| Soil | Horizon | 0.00 (Mpa) | 0.0005 (Mpa) | 0.003 (Mpa) | 0.10 (Mpa) | 0.50 (Mpa) | 1.00 (Mpa) | 1.50 (Mpa) |
|---|---|---|---|---|---|---|---|---|
| Bra | Ap | 41.61 (1.6) | 38.49 (2.2) | 35.44 (1.8) | 31.72 (3.2) | 25.44 (2.5) | 20.93 (3.4) | 19.21 (2.5) |
| Bra | Bt | 41.56 (2.8) | 41.05 (2.4) | 38.87 (2.3) | 34.10 (3.2) | 25.41 (2.9) | 21.41 (3.3) | 18.83 (3.7) |
| Sau | Ap | 43.22 (6.6) | 38.81 (5.5) | 36.25 (3.8) | 30.60 (2.4) | 23.09 (3.0) | 18.76 (2.0) | 16.87 (2.2) |
| Sau | Bt | 41.62 (3.1) | 38.72 (2.3) | 35.95 (3.3) | 31.44 (3.8) | 25.87 (2.0) | 21.67 (2.1) | 18.61 (2.5) |
| Ros | Ap | 45.21 (3.3) | 42.37 (1.9) | 39.21 (2.6) | 32.51 (1.0) | 24.51 (0.9) | 19.89 (8.1) | 18.14 (6.4) |
| Ros | Bt | 50.44 (7.6) | 48.74 (6.4) | 48.89 (6.3) | 43.03 (6.6) | 37.36 (5.6) | 21.22 (1.6) | 19.35 (1.9) |

This trend was relatively consistent between the Ap- and Bt-horizons of the Braddock, Saunook, and Rosman series (Figure 3-3). The Ap-horizons generally had greater water content at lower pressures, while the Bt-horizons had higher water content at higher pressures. The occurrence of higher water content at lower pressures in the Ap-horizons may be attributed to the influence of organic matter in this surface horizon. Organic matter absorbs and stores water in a relatively free state, which may be available for root water uptake. As pressure increases, water content is often reduced in soils or horizons with lower clay percentages (Ap), while water content will be higher in soils with high clay content (Bt). This trend is illustrated in Figure 3-3. It is interesting to note that the water content for the Braddock series Ap-horizon is slightly greater than the Bt-horizon at higher pressures (Figure 3-3). This is may be attributed to the standard deviations of the Braddock Ap- and Bt-horizons.

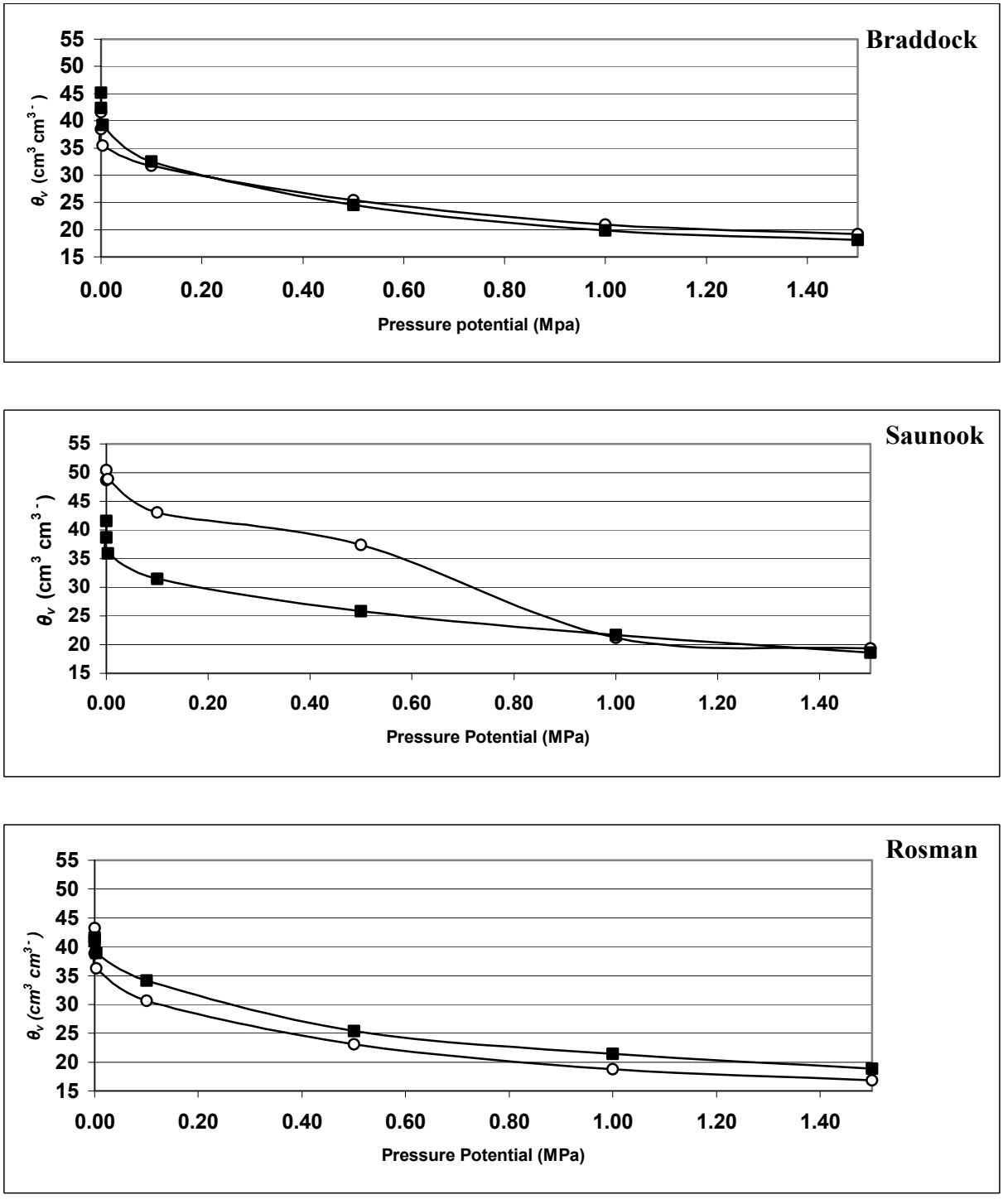


Figure 3-3: Water retention curves for the Slagle Farm soils per series and horizon: Ap-(circle) Bt-horizon (square).

## *Hydrologic Characteristics*

### *Observed*

Hydrological activity of the Slagle Farm watershed was characterized in the field through use of time domain reflectometry (TDR), stream gaging, and meteorological monitoring. These characteristics were then incorporated into HYDRUS 2-D model to quantify subsurface water flux as a function of atmospheric conditions, soil water activity, and discharge to Cartoogechaye Creek. TDR, coupled with automated water content reflectometers (WCR), were used to monitor soil water content of the vadose zone. Observed soil volumetric water content values in Figure 3-4 are presented as observed mean $\theta_v$ for all transects for the top-slope (Braddock series), mid-slope (Braddock series), toe-slope (Saunook series), and riparian area (Rosman series) locations. Meteorological inputs per month and average evapotranspiration for the Slagle Farm watershed are presented in Table 3-5. Gross precipitation is presented in Figure 3-6, and Figure 3-8 shows monthly stream heights for Cartoogechaye Creek. Observed soil volumetric water content ($\theta v$) in the Bt-horizon was consistently higher than the Ap-horizon (Figure 3-4). This was expected due to the higher clay contents of the Bt-horizons (Table 3-7) and plant root water uptake. The plate-like structure of clay holds water more tightly than silt and sand. As a result, in periods with drier conditions, $\theta v$ in soils with high clay content is often higher than soils with low clay (McLaren and Cameron, 1996). The influence of vegetation above of the Ap-horizon also may have contributed to a smaller $\theta_v$ than in the Bt-horizon. Though root density and distribution were not measured in this study, it is reasonable to assume that the Ap-horizon is primary source of water for the grass root water uptake. As a result of root water uptake, and decreased clay content (than the Bt-horizon) to hold water more tightly, the Ap-horizon

water was taken up by plants through evapotranspiration. The influence of evapotranspiration can easily be seen by comparing $\theta_v$ for the Ap- and Bt-horizons of the riparian area (Figure 3-4). There is a dramatic difference of $\theta_v$ between these two horizons. $\theta_v$ for the Ap-horizon ranged from 0.15 to 0.22 $cm^3$ $cm^{3-}$, while the Bt-horizon had values of 0.35 to 0.54 $cm^3$ $cm^{3-}$. The increase of $\theta_v$ from the Ap- to the Bt-horizon can be attributed to increased evapotranspiration in the Ap-horizon and a hyporheic recharge of water to the Bt-horizon from the stream. Vegetation in the riparian area has been excluded from cattle grazing and is less degraded than vegetation in the pasture area.

Soil $\theta_v$ for the Ap-horizon was highest for the mid-slope area of the pasture. This area is less steep than the top-slope, and is the area of preferred grazing. The top-slope Ap-horizon had the second highest $\theta_v$, followed by the toe-slope, and riparian area. The top-slope has the greatest slope that results in subsurface flow within the Ap-horizon to the mid-slope area. The low values of toe-slope $\theta_v$ may be attributed to a matrix pull of water towards the riparian area (function of root water uptake of vegetation in the riparian area). The highest $\theta_v$ for the Bt-horizons occurred in the riparian area. As noted above, this is attributed to the influence of hyporheic recharge from the stream and possibly to the greater depth of this subsurface horizon. Root depth may be limited from deep penetration due to the anaerobic conditions within this saturated area.

### *Simulated Hydrology*

Figure 3-5 suggests that simulations for water content agreed well with the general trend of observed $\theta_v$, but individual values across seasonal durations varied considerably. Simulated $\theta_v$ was consistently higher than the observed $\theta_v$ in each of the

four sampling locations (top-slope, mid-slope, toe-slope, and riparian area). For following discussions, top-slope, mid-slope, toe-slope, and riparian area represent the Braddock (top and mid-slope), Saunook, and Rosman series, respectively.

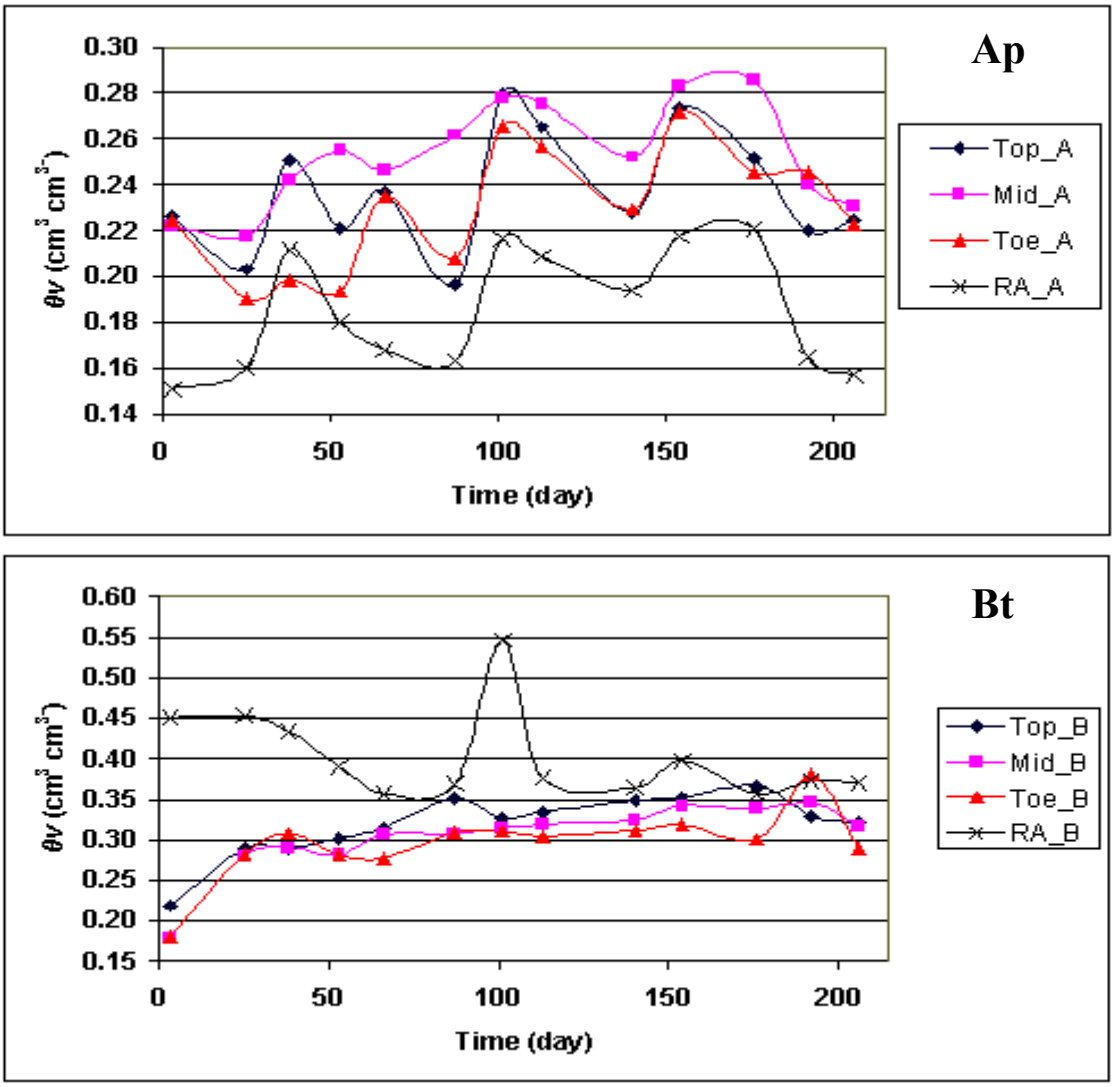


Figure 3-4: Observed $\theta_v$ by slope location (Top, Mid, Toe, RA) for the Ap- and Bt-horizons of the study watershed. Time scale: Aug. (1-18), Sep. (19-48), Oct. (49-79), Nov. (80-109), Dec. (110-134), Jan. (135-161), Feb. (162-182), and Mar. (183-212).

In general, simulated Bt $\theta_v$ matched well with the general trend of observed $\theta_v$. An average relative error of 11.25 % was calculated between observed and simulated $\theta_v$ for the Bt-horizons of the top-slope, mid-slope, toe-slope, and riparian area. However,

simulated $\theta_v$ for the Ap-horizon was significantly higher than observed $\theta_v$. An average relative error of 47.5 % was calculated between observed and simulated $\theta_v$ for each of the slope locations of the Ap-horizons. High simulated Ap-horizon $\theta_v$ is most likely attributed to how the HYDRUS 2-D model regards infiltration of rain water. Only one boundary condition can be assigned to specific nodes (surface nodes in this scenario) within the model flow domain. As noted in the water flow parameters section of Methods and Materials, a time-variable atmospheric condition was assigned surface horizons of the domain. When using atmospheric boundary conditions at the soil surface, HYDRUS 2-D allows all water to infiltrate (Simunek et al., 1999). As a result of this assumption, all of the water (minus evaporation) is moved into the surface horizon (Ap) thus resulting in increased soil $\theta_v$.

When one considers the hydrologic dynamics of a watershed, the entire hydrologic budget must be considered. The interaction of inputs of precipitation, removal of water by evapotranspiration, and discharge to a stream all influence the dynamics of the water budget. Soil water storage is directly affected by precipitation and evapotranspiration. The highest precipitation for the duration of the study occurred in late September 2002 (days 39-46) (Figure 3-6). The highest actual evapotranspiration rates also occurred in these months (Figure 3-7).

It should be noted that "actual Et" is the simulated amount of AEt. In-field AEt was not measured in this study. High precipitation also occurred in late December (days 122-134) of the same year. However, evapotranspiration was lower in December than September. Partitioning the components of the hydrograph may help to further explain hydrologic dynamics within the watershed. Though precipitation was greatest for

September 2002, soil $\theta_v$ and stream stage were the lowest. This may be attributed to the higher rates of evapotranspiration for this period. The period of November and December 2002 showed the second highest rates of precipitation, as well as increasing discharge to Cartoogechaye Creek (Figure 3-8). Though total precipitation was lower for the December period, stream stage was greater than the September event. Analysis of soil $\theta_v$ in Figure 3-5 shows that $\theta_v$ was greatest for both horizons of the pasture soils for the same period. Though the amount of total precipitation was greater for September than December, water in September was lost through plant water uptake (evapotranspiration).

An integral part of understanding the hydrologic dynamics of a watershed is the quantification of subsurface flow between heterogeneous soil materials and layers. To satiate this objective, HYDRUS 2-D was utilized to simulate water volume within specific soil series and layers, as well as the flux of water between different materials. These data will help illustrate how and when water will move through the subsoil. The quantification of the volume of water and flux of water in and between different soil media may be used, among other applications, to determine flow path, water sequestration, and pollutant transport (nutrients). The latter will be illustrated in Chapter 4 of this paper.

Within the HYDRUS 2-D model, the user has the ability to manipulate time information to achieve desired time-step resolution or desired output print interval. For the specific scenario described in this paper, desired output print interval was scaled to the lysimeter sampling time interval, approximately 14-days, while minimum time-step interval was $1 \times 10^{-2}$ day. Recall that the print time interval is used simply to specify at

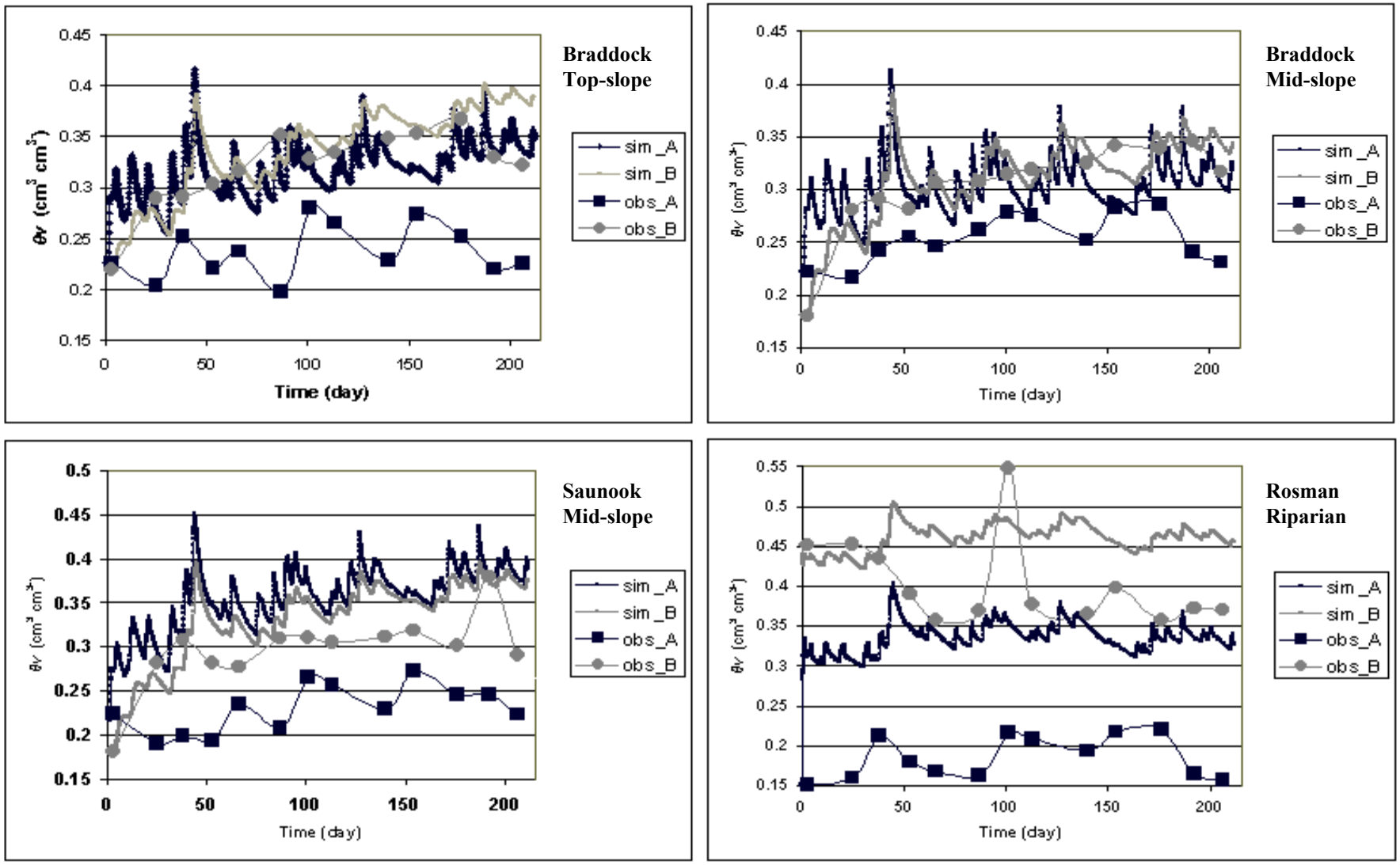


Figure 3-5: Simulated ("sim") and observed ("obs") $\theta_v$ for Braddock top-slope, Braddock mid-slope, Saunook toe-slope, and Rosman riparian. (Time scale: Aug. (1-18), Sep. (19-48), Oct. (49-79), Nov. (80-109), Dec. (110-134), Jan. (135-161), Feb. (162-182), and Mar. (183-212).)

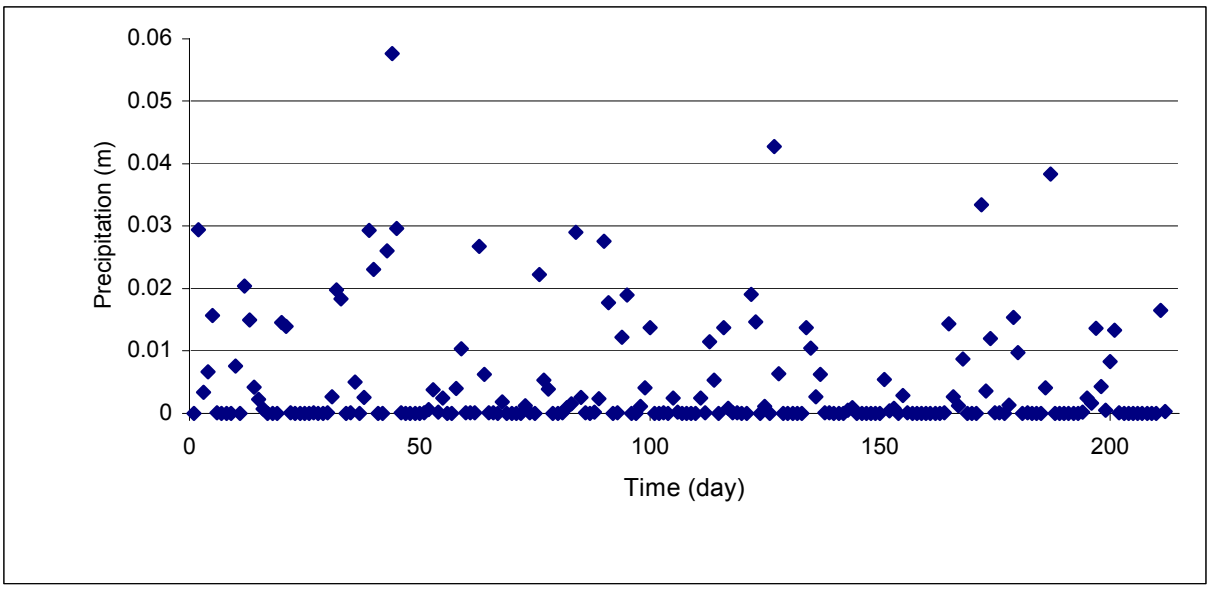


Figure 3-6: Daily precipitation for study watershed from August 2002 (day 0) to March 2003 (day 212).

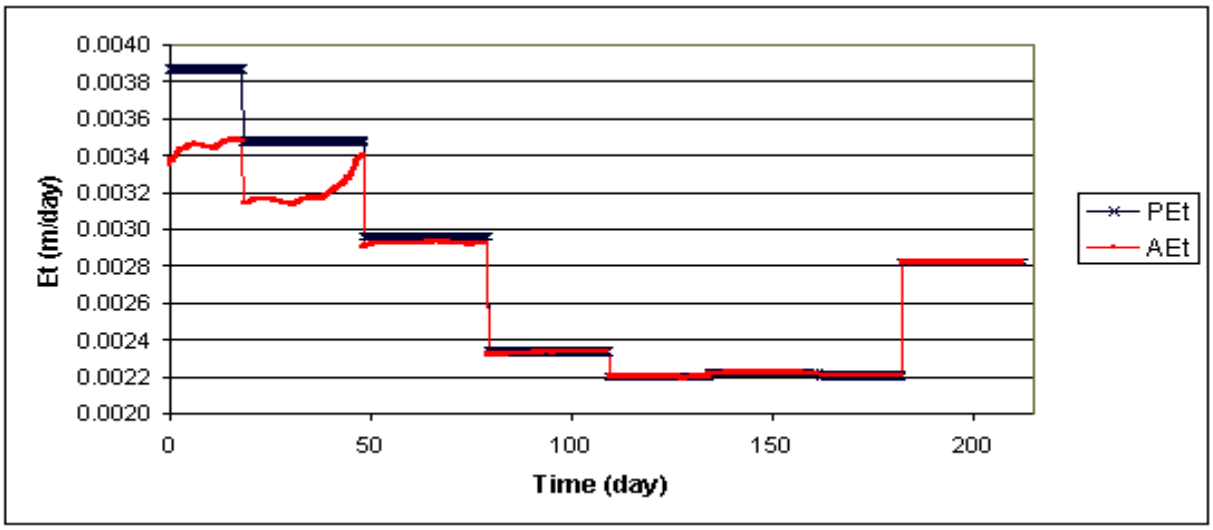


Figure 3-7: Daily Potential (PEt) and Actual (AEt) evapotranspiration rates for the study watershed.

which times detailed information about the pressure head, water content, flux, and water balances are printed. The time-step interval is used to define the minimum time increment between individual calculations. A print time interval of 15 (14-day intervals for 212 days) was

used in this simulation to match water volume and flux per sub-region (soil series and layer) to lysimetry data (Chapter 4). However, water volume and flux is calculated on a 1 x $10^{-2}$ day for every day over the entire simulation period (212 days).

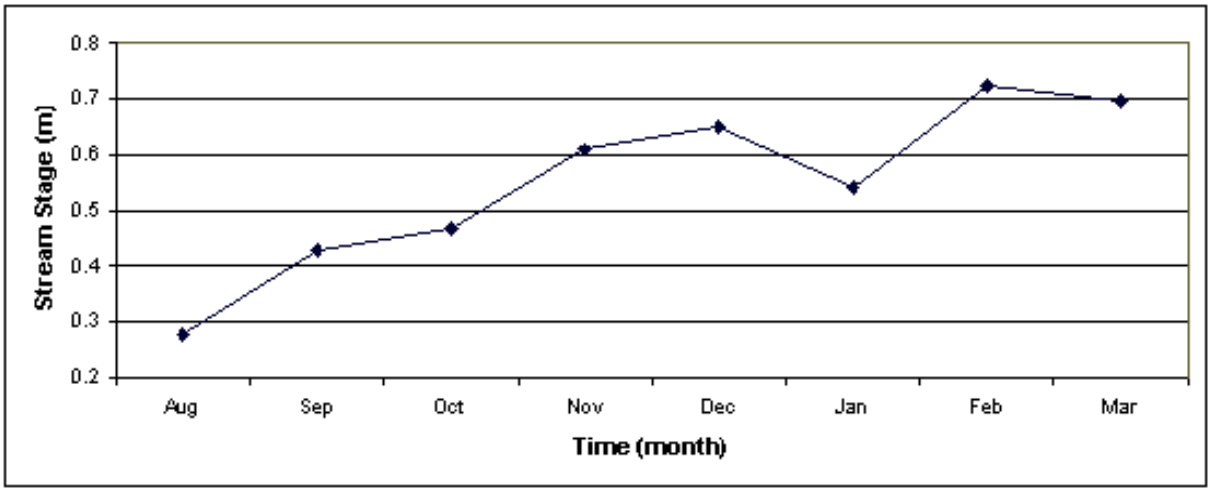


Figure 3-8: Mean monthly* stream stage of the Cartoogechaye Creek.
* (Aug: day 1-18; Sep: 19-48; Oct: 49-79; Nov: 80-109; Dec: 110-143; Jan: 135-161; Feb: 162-182; Mar: 183-212)

Figure 3-9 shows the total volume of inflow for the study watershed. Inflow is defined as the change in the volume of water per time in the total transport domain or predefined sub regions (Simunek et al., 1999). Watershed inflow in Figure 3-9 is the sum of all sub region materials (Ap- and Bt-horizon per soil series). Inflow is the summation of water (precipitation) entering (positive) the system as well as leaving (negative) the flow domain (Et, evaporation, soil water storage). Peak inflow occurred during the days leading to and on day 44 (late September). This dramatic increase of inflow into the watershed corresponds well with precipitation input previous to, and on day 44, as well as on day 84 (Figure 3-6).

### *Seasonal Influence on Water Flow*

Due to a variety of equipment malfunctions, a complete year of sampling was not attained. However, the total monitoring period, late August 2002 to March 2003, captured the four distinct seasons. Summer was covered by days 1 to 48, days 49 to 109 were used for fall, days 110 to 182 were used for winter, and spring was characterized by days 183-212. In an attempt to characterize periods of potentially high precipitation with low surface resistance (low vegetation surface friction, and low evapotranspiration), much of the monitoring period occurred during the fall and winter seasons.

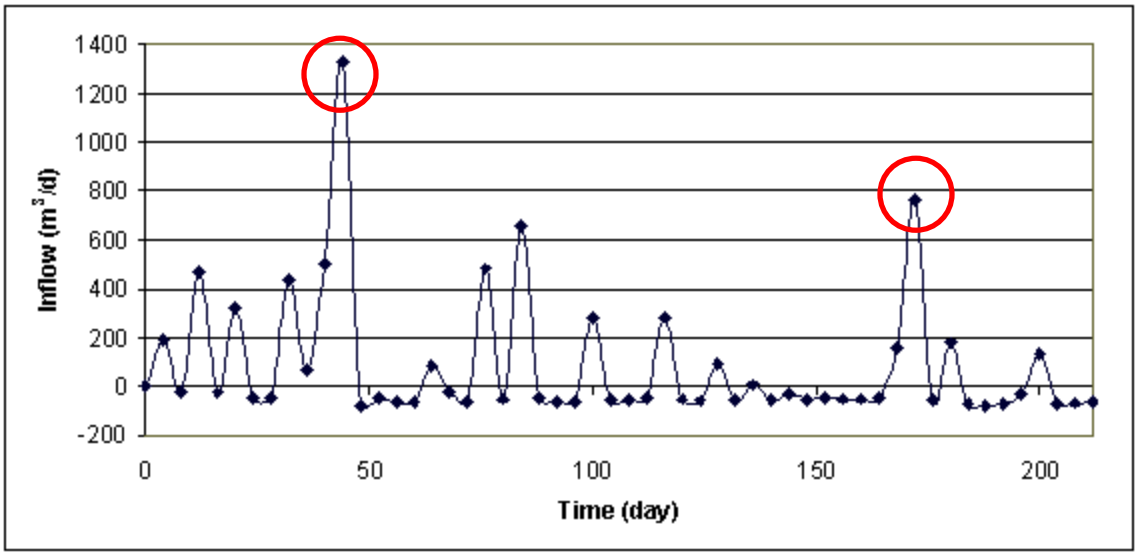


Figure 3-9: Inflow rates of water within the study watershed flow domain.
(Circles show example of the increase of inflow that corresponds to increased input of precipitation.)

Though precipitation was highest for the summer season (1- 48) (Figures 3-6), average stream stage was lowest (Figure 3-8). This is most likely attributed to high evapotranspiration during this season (Figure 3-7). The summer season was characterized as the growing season for fescue, resulting in high root water uptake. In the drier times of this season, pasture Bt-horizons generally had higher $\theta_v$ than Ap-horizons (Figure 3-5). Simulated $\theta_v$ for the pasture soils

followed this general trend. However, in periods of high precipitation, simulated $\theta_v$ was often higher for Ap-horizons. This reversal of simulated Ap- and Bt-horizon $\theta_v$, again, is attributed to Et occurring primarily in the Ap-horizons during drier times, while in periods of high precipitation, water was perched above the less permeable Bt-horizon. Observed $\theta_v$ did not follow this trend, which may be attributed to a bimonthly collection interval for observed $\theta_v$. Simulated $\theta_v$ had a much higher time-step interval (calculated at $1 \times 10^{-2}$ day), which shows a higher trend of simulated $\theta_v$.

The fall season (days 49-109) showed average stream stage increasing (Figure 3-8). Though precipitation for this season was lower than the summer season (Figures 3-6), Et was significantly lower (Figure 3-7). The decreased rate of Et resulted in less water uptake, resulting in increased water discharge to Cartoogechaye Creek. Again, observed $\theta_v$ for the Bt-horizon was greater than the Ap-horizon (Figure 3-5). Simulated $\theta_v$ for the pasture soils Ap- and Bt-horizons seem to alternate higher $\theta_v$, which may be attributed to wetting and drying fronts moving through the watershed (function of lower precipitation and Et).

The winter season (days 110-182) had the highest stream stage (Figure 3-8) that may be attributed to intense, sporadic storms (Figure 3-6) and the lowest Et for the four seasons (Figure 3-7). Observed and simulated $\theta_v$ for the Bt-horizon was significantly higher than the Ap-horizon (Figure 3-5). Again, this is attributed to very low Et rates.

Average stream stage for the spring season (183-212) was still relatively high, but had decreased from the winter season (Figure 3-8). More frequent and intense precipitation events were observed during this season (Figures 3-6), and Et began to rise (Figure 3-7). The increased Et, a result of fescue entering the growing season, again, started to uptake water into plant roots.

This, coupled with increased surface resistance (from plants reducing the velocity of surface water), resulted in the initiation of stream stage decrease. Observed $\theta_v$ for the Ap-horizon dropped below $\theta_v$ for the Bt-horizon (Figure 3-5). Simulated $\theta_v$ for the Bt-horizon again climbed significantly higher than simulated Ap-horizon $\theta_v$.

### *Storm Event vs. Dry Period*

Two specific time periods were selected to illustrate the dynamics of the Slagle Farm watershed. Days 40 to 48 (late September) will be used to illustrate the response of the watershed to high precipitation, while days 156 to 164 (late January to early February) will be used to illustrate flow dynamics under dry conditions (Table 3-10). These two specific conditional periods represent the maximum and minimum precipitation inputs over the entire simulation period. The objective of these two scenarios is to draw correlations between precipitation, soil volumetric water content ($\theta_v$), and evapotranspiration (AEt). Graphical outputs of each period will be presented to illustrate how water moves through each soil series (material distribution) and horizon (Ap- and Bt-horizon).

The "wet" period, encompassing day 40 to 48, had a total precipitation input of 0.1364 m for the 5-ha watershed and an average AEt of 603.22 $m^3$/day. Total precipitation for the "dry" (156-164) period was 0.0002m, with an average AEt of 121.60 $m^3$/day. Soil $\theta_v$ for the wet and dry periods be seen in Figures 3-10 and 3-11. Average $\theta_v$ per slope location and horizon are presented in Table 3-11. The day previous to each period is presented to show an "initial" condition for each scenario. Figure 3-10 shows the trend of soil $\theta_v$ during the wet period. The entire system responded to the increase of precipitation. Peak $\theta_v$ occurred on day 44, which

corresponds with peak precipitation (Figure 3-6) and peak inflow (Figure 3-9). During the "wet" period, pasture Ap-horizons generally had higher soil $\theta_v$ than their respective Bt-horizons. However, the riparian Bt-horizon consistently had higher $\theta_v$, which, as discussed earlier, may be a result of hyporheic recharge from Cartoogechaye Creek, and the lack of root water uptake from riparian vegetation. The toe-slope Ap-horizon had the second highest $\theta_v$, which is most likely attributed to water contributions from upslope sources. The rate at which rainwater infiltrates into the surface horizon and percolates into the subsoil horizon is primarily a function of bulk density, macro-porosity, and antecedent moisture conditions (Anderson and Burt, 1990; Anderson et al., 1997; McLaren and Cameron, 1996). If precipitation is greater than infiltration, overland flow or subsurface lateral flow (above a less permeable horizon) may occur (Anderson et al., 1997; Heppell et al., 2000). The top and mid-slope locations consistently had lower soil $\theta_v$. This is mostly likely the result of the influence of slope and increased clay content within the Bt-horizon. As noted above, increased clay creates a less impermeable horizon, resulting in slower percolation and possibly perching of water above the subsoil horizon. This perched water is moved downslope, above the Bt-horizon, under gravity.

Figure 3-11 shows the trend of soil $\theta_v$ during the "dry" period. In general, the Bt-horizons had greater soil $\theta_v$ than Ap-horizons. This was expected due to the tighter bond clay particles have with water molecules. The plate-like structure of clay holds water more tightly than silt and sand. As a result, in periods with drier conditions, $\theta_v$ in soils with high clay content is often higher than soils with low clay (McLaren and Cameron, 1996). Higher $\theta_v$ may also be attributed to the absence of dense rooting within this layer. The high clay content may restrict vertical penetration of fescue roots, thus restricting root water uptake to the Ap-horizons

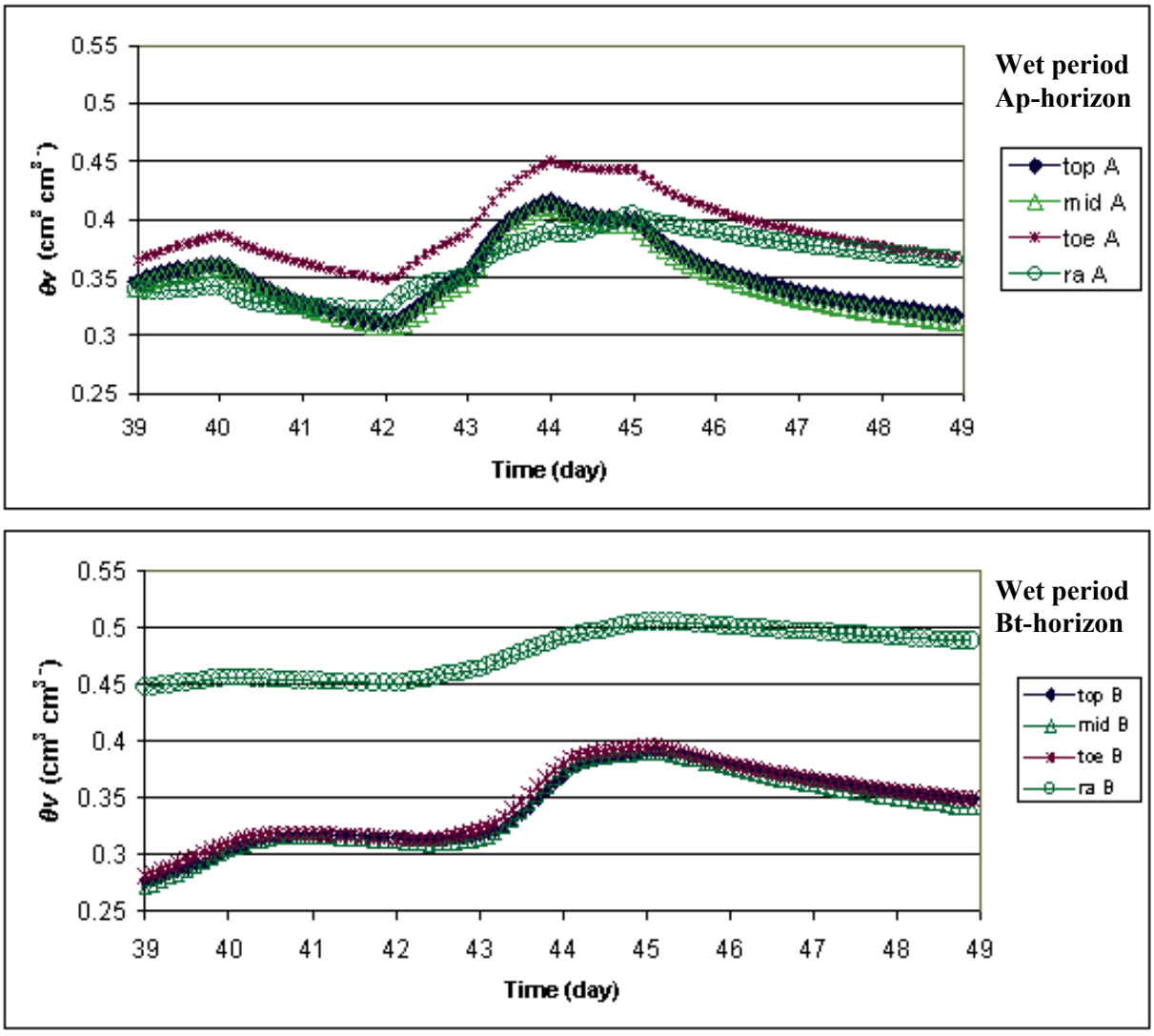


Figure 3-10: Simulated soil $\theta_v$ for watershed during "wet" period per horizon and slope location*.

* Slope locations are defined for Braddock top-slope (top), Braddock mid-slope (mid), Saunook toe-slope (toe), and Rosman riparian (ra).

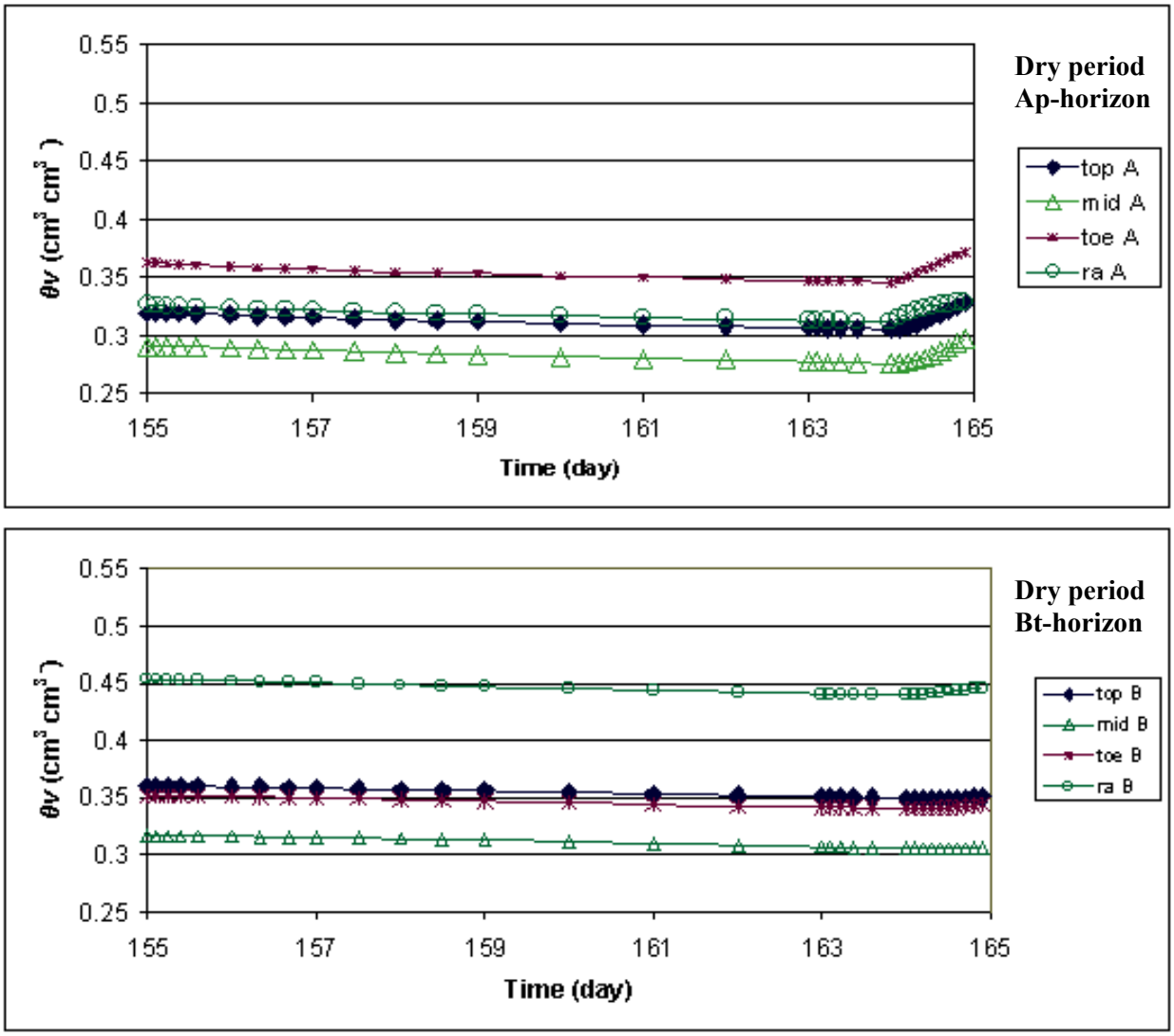


Figure 3-11: Simulated soil $\theta_v$ for watershed during "dry" period per horizon and slope location*.

* Slope locations are defined for Braddock top-slope (top), Braddock mid-slope (mid), Saunook toe-slope (toe), and Rosman riparian (ra).

Table 3-10: Precipitation inputs for "wet period" and "dry period". Precipitation is given for the entire study watershed.

| Wet Period | | Dry Period | |
|---|---|---|---|
| Day | Precipitation | Day | Precipitation |
| | (m) | | (m) |
| 40 | 0.0231 | 156 | 0.0001 |
| 41 | 0 | 157 | 0 |
| 42 | 0 | 158 | 0 |
| 43 | 0.026 | 159 | 0 |
| 44 | 0.0576 | 160 | 0 |
| 45 | 0.0296 | 161 | 0 |
| 46 | 0.0001 | 162 | 0 |
| 47 | 0 | 163 | 0 |
| 48 | 0 | 164 | 0.0001 |

Table 3-11: Average simulated soil $\theta_v$ per slope location and horizon for "wet" and "dry" period.

| Period | top A | top B | mid A | mid B | toe A | toe B | ra A | ra B |
|---|---|---|---|---|---|---|---|---|
| | $cm^3\ cm^{3-}$ | $cm^3\ cm^{3-}$ | $cm^3\ cm^{3-}$ | $cm^3\ cm^{3-}$ | $cm^3\ cm^{3-}$ | $cm^3\ cm^{3-}$ | $cm^3\ cm^{3-}$ | $cm^3\ cm^{3-}$ |
| **Wet** | 0.3525 | 0.3430 | 0.3491 | 0.3398 | 0.3931 | 0.3463 | 0.3628 | 0.4783 |
| **Dry** | 0.3133 | 0.3537 | 0.2837 | 0.3100 | 0.3555 | 0.3452 | 0.3202 | 0.4457 |

An analysis of inflow volumes for these two periods helps to illustrate water flow dynamics within the flow domain. Figure 3-12 shows the inflow volume change for the wet (day 40-48) and the dry (156-164) periods. Inflow volumes are displayed by soil series and horizon for Transect A (Figure 3-1). The general trend of inflow for each slope location increases during the storm, and then falls towards "equilibrium" after the storm has succeeded (day 47-48). The Bt- horizons are consistently higher than Ap- horizons (contrary to $\theta_v$), but this is attributed to the total modeled depth of the Bt-horizon. Average Bt-horizon depth distributed in the model flow domain was approximately 1.5 m, while Ap-horizon depth was 0.2 m. The dry period has inflow values that are slightly negative or at equilibrium for days 155-163, reflecting the absence of precipitation input.

Graphical outputs of the flow domain during each period (wet and dry) are presented in Figures 3-13 to 3-16. Initial conditions (day 0=Aug 2002) are presented in Figure 3-13, followed by Figure 3-24, which are the conditions previous to the large storm (day 38=Sep 2002). Figure 3-15 shows the response of the flow domain to a significant storm (day 52=Oct 2002), and Figure 3-16 shows the response of the flow domain to a drying front (day 163 = Feb 2003).

The movement of water during specified time intervals can be seen in Figures 3-15 to 3-16. The initial conditions were defined as atmospheric and soil $\theta_v$ conditions for time = 0 of the simulation period. The flow domains shown above represent specific intervals also based on atmospheric and $\theta_v$ conditions that were iteratively soled by the HYDRUS 2-D model. The response of the watershed to precipitation inputs, evapotranspiration outputs, soil water storage, and soil $\theta_v$ can be seen from time = 0 to the final display time of time = 163. The initial soil $\theta_v$ is very dry for the pasture areas of the Ap- and Bt-horizons ($\theta_v$ = between 0.15 to 0.20 $cm^3$ $cm^{3-}$). The riparian area Bt-horizon has an approximate $\theta_v$ of 0.45 $cm^3$ $cm^{3-}$, while the AP-horizon of the riparian area has an approximate $\theta_v$ similar to the Ap-horizons of the pasture soils (0.15 to 0.20 $cm^3$ $cm^{3-}$). As noted earlier, the low $\theta_v$ may be attributed to evapotranspiration of fescue distributed across the surface soil horizon. As the watershed received precipitation inputs, soil moved vertically and laterally into the Ap- and Bt-horizons. Figure 3-16 shows how the watershed responded to a dramatic increase of precipitation, and subsequently, how the water moved through the system. As time approached the "dry" period (time = 163), surface horizon $\theta_v$ decreased, and water moved vertically into the Bt-horizon. The simulation results of the HYDRUS 2-D model matched reasonably well to observed $\theta_v$ (Figure 3-16), and satiated what one would expect to see.

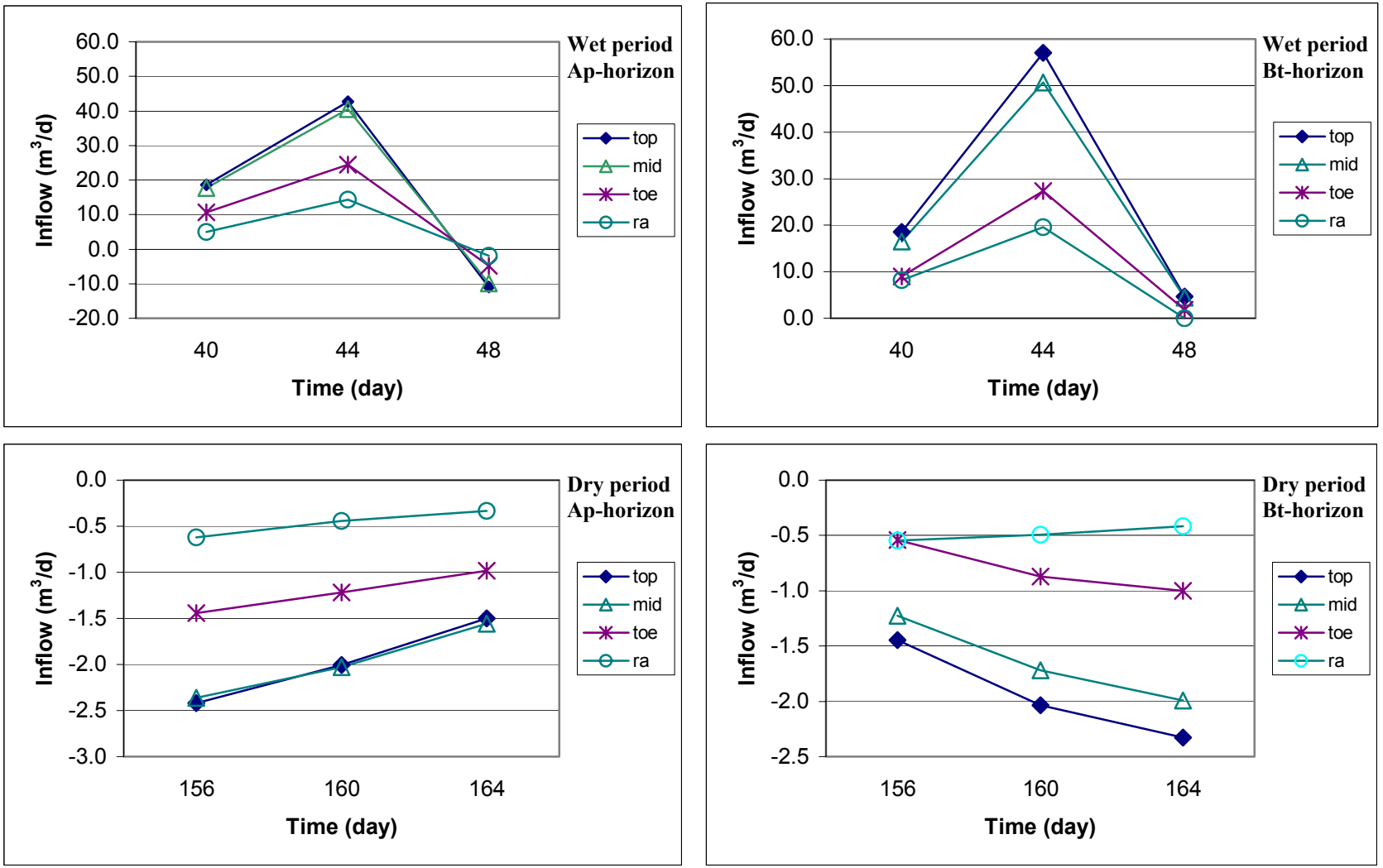


Figure 3-12: Inflow water volumes of study watershed during the "wet" and "dry" periods.

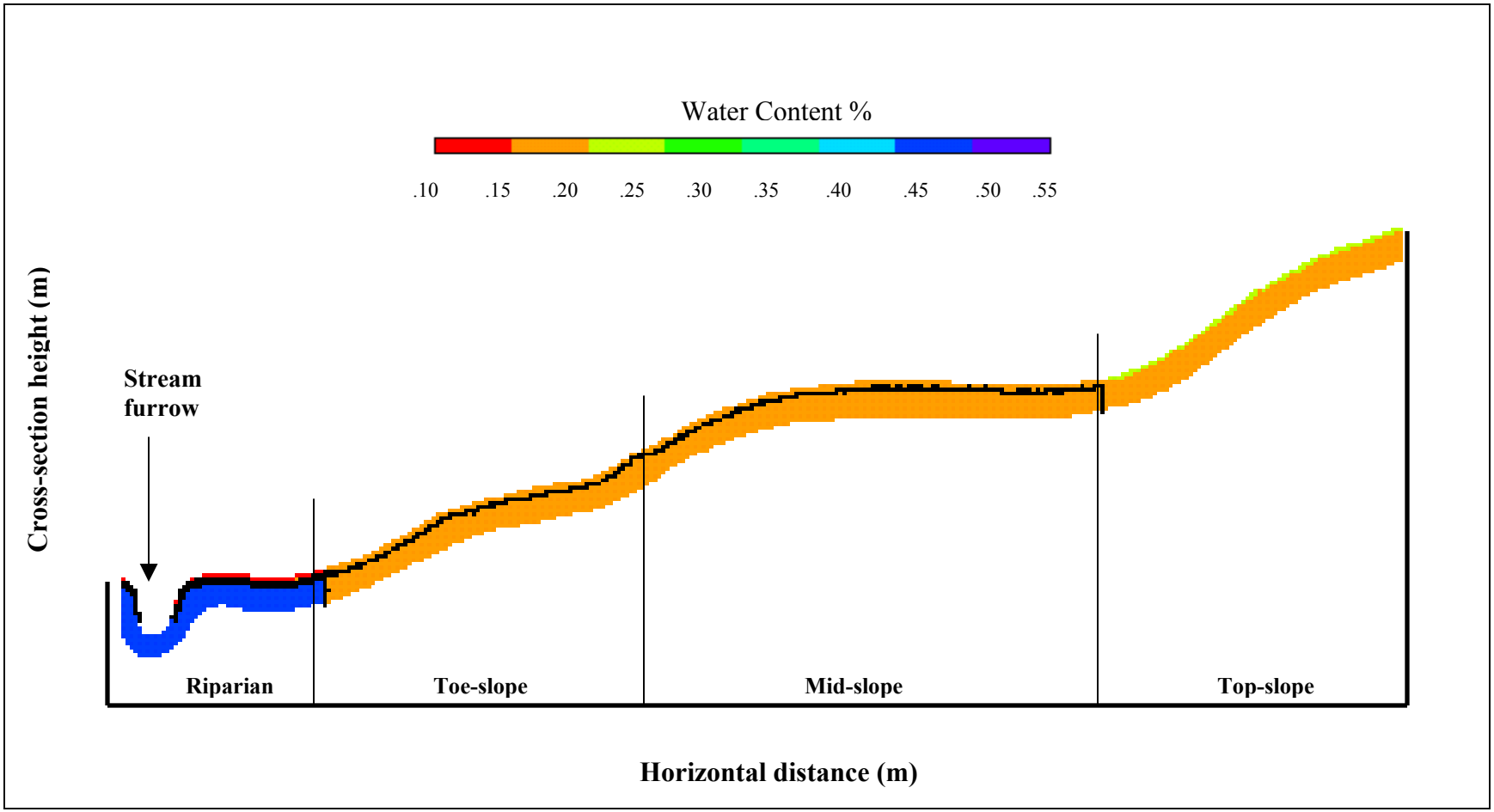


Figure 3-13: Initial conditions of $\theta_v$ for the flow domain time cross-section of the study watershed time = 0 (August 2002).

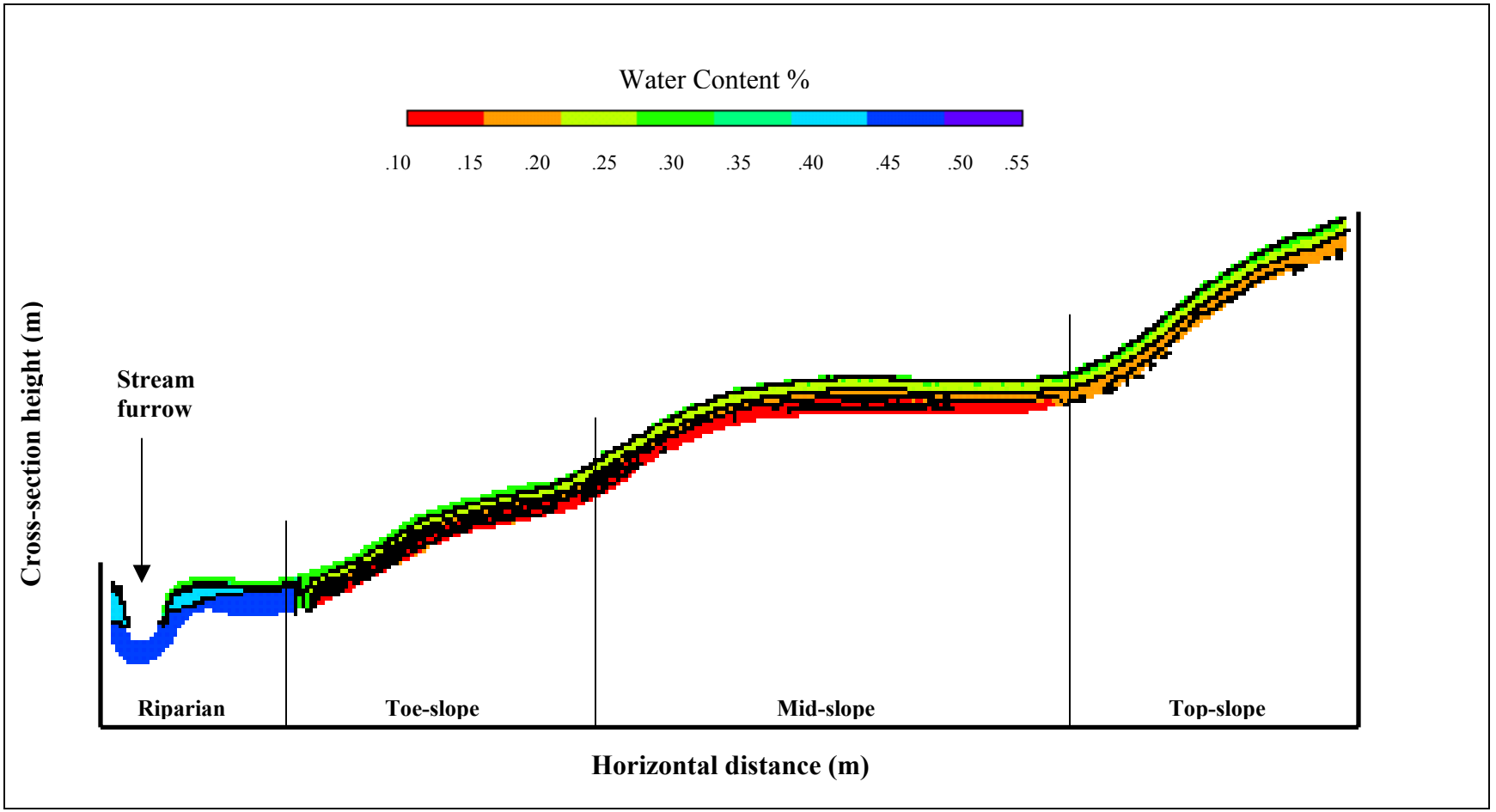


Figure 3-14: $\theta_v$ previous to "wet" period for the flow domain time cross-section of the study watershed time = 38 (mid-Sep 2002).

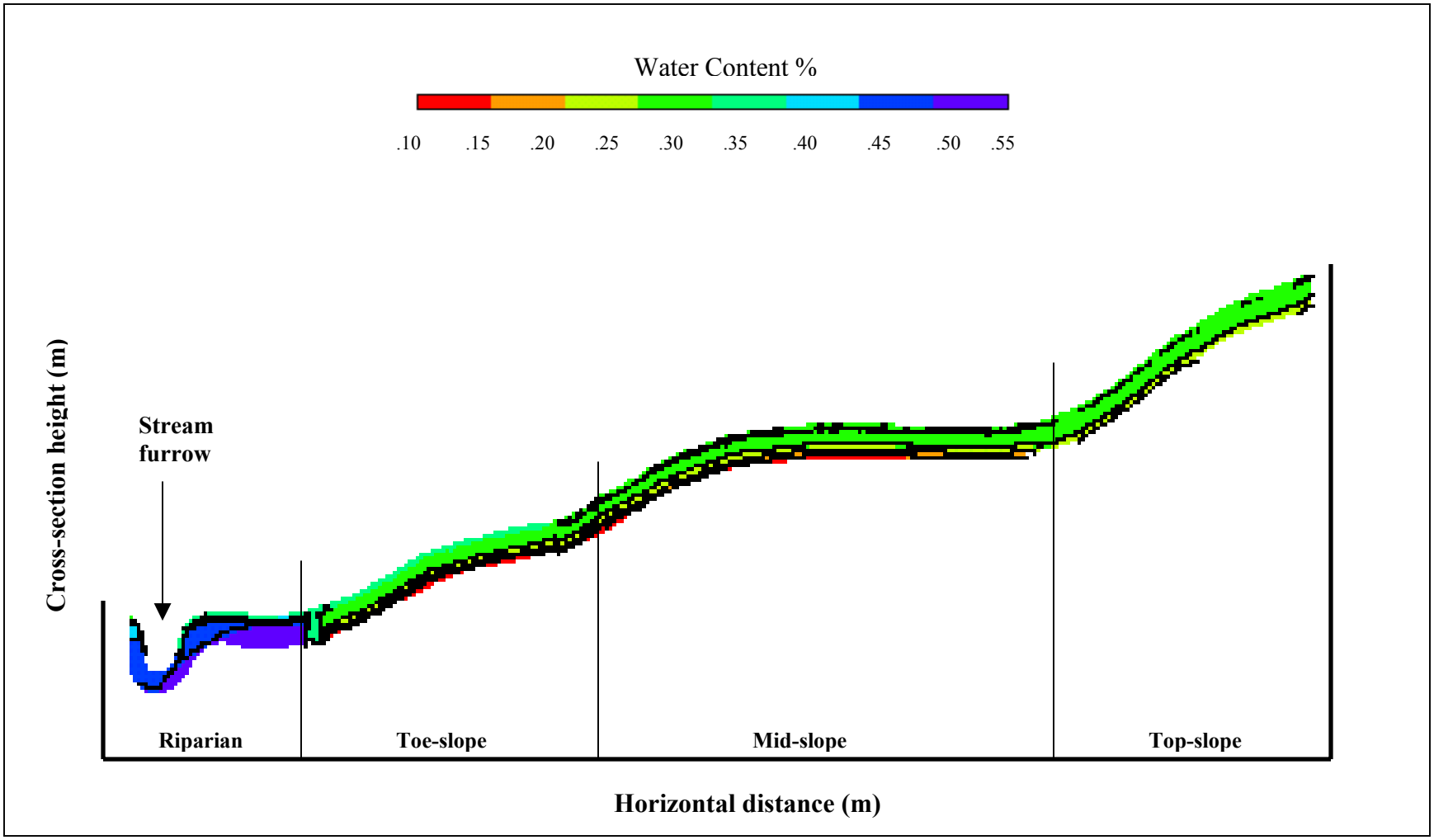


Figure 3-15: Influence of storm on $\theta_v$ for "wet" period for the flow domain cross-section of the study watershed time = 52 (Oct 2002).

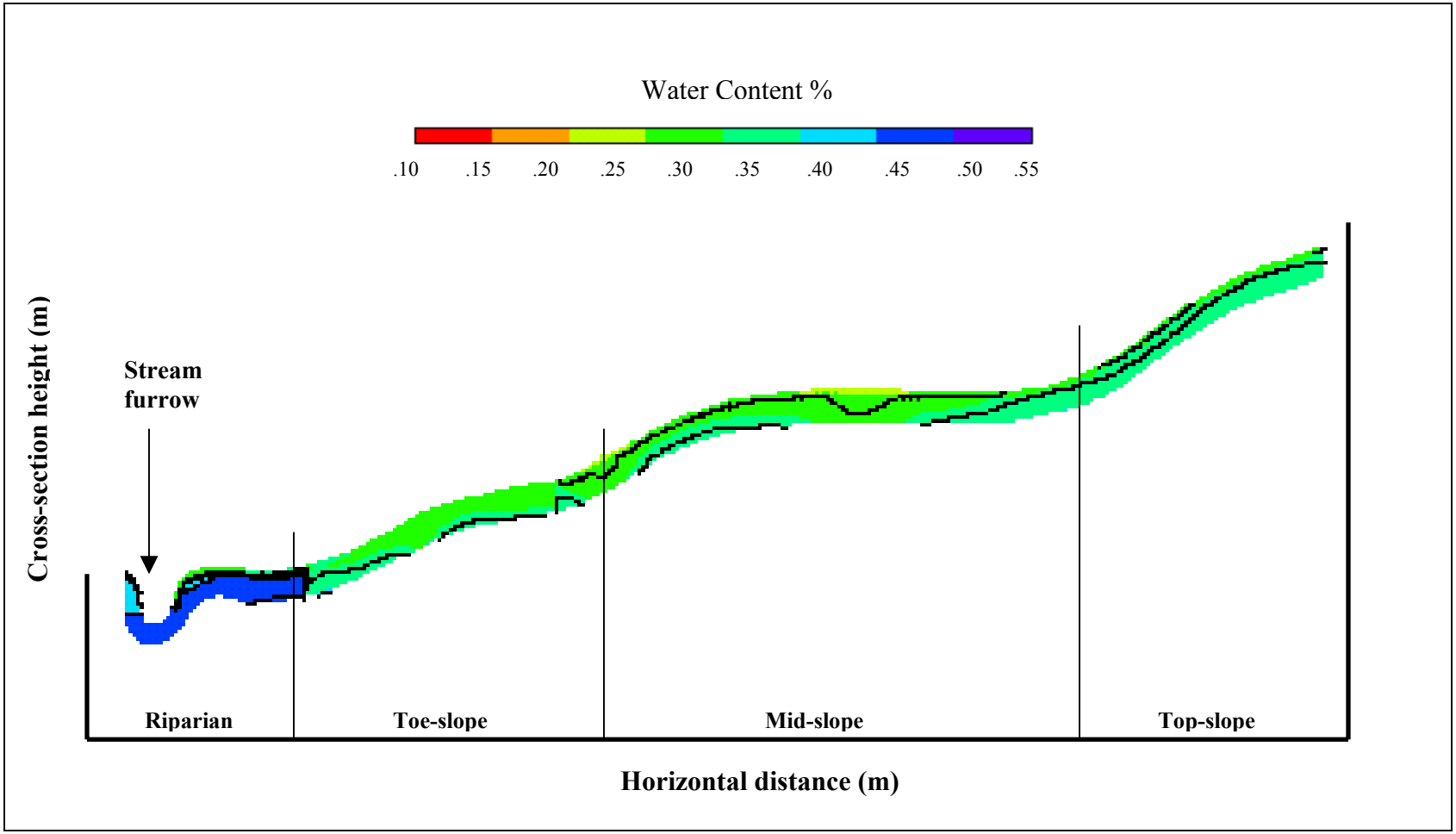


Figure 3-16: $\theta_v$ for "dry" period for the flow domain cross-section of the study watershed time = 163 (Feb 2003).

# Conclusion

The objective of this study was to quantify and qualify surface and subsurface hydrological dynamics within the Slagle Farm watershed. The culmination of observed soil characteristics, hydrology, and meteorological data were used to parameterize input data for the HYDRUS 2-D transport and flow model. HYDRUS 2-D was capable of simulating the general trend of soil water content ($\theta_v$) and matched reasonably well with observed field data.

Individual soil characteristics, such as particle size distribution, bulk density, and saturated hydraulic conductivity, influenced how and when water moved through specific soil materials (series/horizon). The presence of a less permeable Bt-horizon had higher $\theta_v$ during dry conditions (function of clay content), while during wet conditions water seemed to perch above this higher density horizon.

HYDRUS 2-D was used to simulate water flow (saturated and unsaturated) during a period of approximately 8 months (August 2002 to March 2003). In an attempt to characterize periods of potentially high precipitation with low surface resistance (low vegetation surface friction, and low evapotranspiration), much of the monitoring period occurred during the fall and winter seasons. This 8-month block was used to differentiate water flow as a function of season. The seasonal interaction of precipitation, evapotranspiration, and soil $\theta_v$ influenced stream stage accordingly. In periods of high precipitation and evapotranspiration, stream stage was low. In periods of lower precipitation and evapotranspiration, stream stage generally increased.

HYDRUS 2-D was relatively successful in simulating soil $\theta_v$ compared to observed $\theta_v$. However, there were discrepancies. An average relative error for the Bt-

horizon was 11.25 %, while the Ap-horizon had an average relative error of 47.5 %. Simulated $\theta_v$ was consistently over-estimated for the Ap-horizons. This is most likely attributed to how HYDRUS 2-D regards infiltration at the surface of the flow domain. Only one boundary condition can be assigned to the surface nodes within the model flow domain. An atmospheric boundary condition was utilized in the scenario described in this paper to account for plant root water uptake. As a result, HYDRUS 2-D assumed that all rainwater was infiltrated into the surface horizon, an obvious weakness of the model. Another notable discrepancy was the root water uptake distribution. It was assumed that fescue covered the entire flow domain outside of the stream furrow. However, in the field, there are areas of low to no fescue coverage. As a result, evapotranspiration may have been over-estimated in the model. Although the model has limitations, HYDRUS 2-D was very beneficial in predicting variables that are often difficult to measure under field conditions. One such variable, evapotranspiration, was predicted through HYDRUS 2-D model. Actual Et was calculated parameterized by atmospheric conditions, precipitation, and a plant stress function, which accounts for root water uptake of prescribed species.

In general, HYDRUS 2-D simulated acceptable trends in $\theta_v$. However, as with any modeling, validation and calibration should be implemented before definitive conclusions are made. Validation and calibration were outside the scope of this specific project, but will be conducted in the near future.

The coupled use of observed field data and the HYDRUS 2-D model support the positive role that vegetation and riparian areas play in reducing water flow (and pollutants) within and across watersheds. The use of vegetation and riparian areas to

control hydrological dynamics within watersheds may prove useful in reducing non-point source pollution to receiving waters

# References


Anderson, M.G., and T.P. Burt. 1990. Subsurface Runoff, p. 368-380, *In* M.G. Anderson and T.P Burt, ed. Process Studies in Hillslope Hydrology. John Wiley and Sons Ltd., West Essex, England. p. 539.

Anderson, S.P., W.E. Dietrich, D.R. Montgomery, R. Torres, M.E. Conrad, and K. Loague. 1997. Subsurface flow paths in a steep, unchanneled catchment. Water Resourc. Res. 33:2637-2653.

Blake, G.R., and K.H. Hartge. 1986. Bulk Density, p. 364-367, *In* A. Klute, ed. Methods of Soil Analysis: Part 1- Physical and Mineralogical Methods, 2 ed. A. Klute, Madison,WI. p. 1188.

Bouyoucos, G.J. 1936. Directions for making mechanical analysis of soil by the hydrometer method. Soil Sci. 42:225-228.

Brooks, R.H., and A.T. Corey. 1966. Properties of porous media affecting fluid flow. J.Irrig. Drainage Div., ASCE Proc. 72:61-88.

Cassell, D.K., and D.R. Nielsen. 1986. Field Capacity and Available Water Capacity, p. 910-913, *In* A. Klute, ed. Methods of Soil Analysis: Part 1-Physical and Mineralogical Methods, 2 ed. ASA, Inc. and SSSA, Inc., Madison, WI. p. 1188.

Cooper, A.B. 1990. Nitrate depletion in the riparian zone and stream channel of a small headwater catchment. Hydrobiologia 202:13-26.

Corvallis Microtechnology, Inc. 1998a. PC-GPS. Release 3.7D. Corvallis Microtechnology, Inc., Corvallis, OR.

Corvallis Microtechnology, I. 1998b. GPS-HP-L4. Corvallis Microtechnology, Inc., Corvallis, OR.

Danielson, R.E., and P.L. Sutherland. 1986. Porosity, p. 450-457, *In* A. Klute, ed. Methods of Soil Analysis: Part 1-Physical and Mineralogical Methods, 2 ed. ASA, Inc. and SSSA, Inc., Madison, WI. p. 1188.

Dillaha, T.A., J.H. Sherrard, D. Lee, S. Mostaghimi, and V.O. Shanholtz. 1988. Evaluation of vegetative filter strip as a best management practice for feed lots. Journal WPCF 60:1231-1238.

Feddes, R.A., P.J. Kowalik, and H. Zaradny. 1978. Simulation of Field Water Use and Crop Yield John Wiley & Sons, New York, NY. p. 189.

Fetter, C.W. 2001. Properties of Aquifers, In P. Lynch, ed. Applied Hydrogeology, Fourth ed. Prentice Hall, Upper Saddle River, NJ. p. 598.

Fisher, R.F., and D. Binkley. 2000. Ecology and Management of Forest Soils. John Wiley and Sons, Inc., New York. p. 489.

Golden Softwrare, Inc. 1999. User's Guide: Contouring and 3D Surface Mapping for Scientists and Engineers. Release 6.04. Golden Softwrare, Inc., Golden, CO.

Harrelson, C.C., C.L. Rawlins, and J.P. Potyondy. 1994. Stream channel reference sites: an illustrated guide to field techniques. General Technical Report RM-245. U.S. Department of Agriculture, Fort Collins, CO.

Heppell, C.M., T.P. Burt, and R.J. Williams. 2000. Variations in the hydrology of an underdrained clay hillslope. J. Hydrol. 227:236-256.

Hill, A.R. 1996. Nitrate removal in stream riparian zones. J. Environ. Qual. 25:743-755.

Hubbard, R.K., and J.M. Sheridan. 1983. Water and nitrate-nitrogen losses from small, upland, coastal plain watershed. J. Environ. Qual. 12:291-295.

Jackson, R. 1992. Hillslope infiltration and lateral downslope unsaturated flow. Water Resour. Res. 28:2533-2539.

Johns, E.L. 1989. Water Use By Naturally Occurring Vegetation Including An Annotated Bibliography. American Society of Civil Engineers.

Klute, A., and C. Dirksen. 1986. Hydraulic Conductivity and Diffusivity: Laboratory Methods, p. 694-700, *In* A. Klute, ed. Methods of Soil Analysis: Part 1-Physical and Mineralogical Methods, 2 ed. ASA, Inc. and SSSA, Inc., Madison, WI. p. 1188.

Lowrance, R.R., R.L. Todd, and L.E. Asmussen. 1983. Waterborne nutrient budgets for the riparian zone of an agricultural watershed. Agric., Ecosyst., & Environ. 10:371-384.

Luxmoore, R.J., and L.A. Ferrand. 1993. Toward pore-scale analysis of preferential flow and chemical transport, p. 45-60, *In* D. Russo and G. Dagan, ed. Water Flow and Solute Transport in Soils: Developments and Applications. Springer-Verlag, New York, NY. p. 306.

Mailhol, J.C., P. Ruelle, and I. Nemeth. 2001. Impact of fertilisation practices on nitrogen leaching under irrigation. Irrig. Sci. 20:139-147.

McLaren, R.G., and K.C. Cameron. 1996. The storage of water in soils, p. 71-86, Soil Science. Oxford University Press, Oxford. p. 314.

Mosley, M.P. 1982. Subsurface flow velocities through selected forest soils, South Island, New Zealand. J. Hydrol. 55:65-92.

Pang, L., M.E. Close, J.P.C. Watt, and K.W. Vincent. 2000. Simulation of picloram, atrazine, and simazine leaching through two New Zealand soils and into groundwater using HYDRUS-2D. J. Contaminant Hydrol. 44:19-46.

Reynolds, B.C., and J.M. Deal. 1986. Procedures for Chemical Analysis at the Coweeta Hydrologic Laboratory. Coweeta Hydrologic Laboratory, Otto, NC.

Schultz, R.C., T.M. Isenhart, and J.P. Colletti. 1994. Riparian Buffer Systems in Crop and Rangelands. Agroforestry and Sustainable Systems: Symposium Proceedings August 1994. p. 13-27.

Simunek, J., M. Sejna, and M.T.v. Genuchten. 1999. The Hydrus-2D Software Package for Simulating the Two-Dimensional Movement of Water, Heat, and Multiple Solutes in Variably-Saturated Media. p. 227.

Slack, J.R., A.M. Lumb, and J.M. Landwehr. 2002. Station 03500240 Cartoogechaye Creek near Franklin, NC 93-4076. USGS Water Resources.

Smith, M. 1999. Manual of CROPWAT Computer Program (version 4.3) 52. FAO, Rome, Italy. Food and Agriculture Organization of the United Nations (FAO). 1998. CropWat 4 Windows. Release 4.2. Food and Agriculture Organization of the United Nations (FAO), Rome, Italy.

Stephens, D.B. 1996. Basic Concepts and Theory, p. 9-14, *In* D. B. Stephens, ed. Vadose Zone Hydrology. Lewis Publishers, Boca Raton, Fl. p. 339.

Topp, G.C., and J.L. Davis. 1985. Measurement of Soil Water Content using Time-domain Reflectometry (TDR): A Field Evaluation 1. Soil Sci. Soc of Am. J. 49:19-24.

United States Department of Agriculture, Natural Resources Conservation Service. 1996. Soil Survey of Macon County, North Carolina. p. 322.

van Genuchten, M.T. 1980. A closed-form equation for predicting the hydraulic conductivity of unsaturated soils. Soil Sci. Am. J. 44:892-898.

van Genuchten, M.T., F.L. Leiji, and S.R. Yates. 1991. The RETC code for Quantifying the Hydraulic Functions of Unsaturated Soils. U.S. Environmental Protection Agency, R. S. Kerr Environmental Research Laboratory Office of Research and Development, Ada, OK.

Vogel, T., and M. Cislerova. 1988. On the reliability of unsaturated hydraulic conductivity calculated from the moisture retention curve. Transp. Porous Media 3:1-15.

Vogeler, I., D.R. Scotter, S.R. Green, and B.E. Clothier. 1997. Solute movement through undisturbed soil columns under pasture during unsaturated flow. Aust. J. Soil Res. 35:1153-1163.

Walsh, L.M. 1971. Instrumental Methods for Analysis of Soils and Plant Tissue. *In* A. Klute, ed. Methods of Soil Analysis: Part 1-Physical and Mineralogical Methods, 2 ed. ASA, Inc. and SSSA, Inc., Madison, WI. p. 1188.

Wilson, G.V., P.M. Jardine, R.J. Luxmoore, and J.R. Jones. 1990. Hydrology of a forested hillslope during storm events. Geoderma 56:119-138.

Yeakley, J.A., W.T. Swank, L.W. Swift, G.M. Horneberger, and H.H. Shugart. 1998. Soil moisture and controls on a southern Appalachian hillslope from drought through recharge. Hydrology and Earth Systems Sciences 2:41-49.

# Chapter 4: Nutrient Dynamics of a Mountain Pasture

## Abstract

Soil, nutrient, and hydrological flux were characterized at the Slagle Farm watershed, located in southwestern North Carolina, to quantify surface and subsurface hydrological dynamics of nutrient transport to a developing riparian area. The physical and mechanical characteristics of these soils were studied to understand the influence these soils had on subsurface transport of nitrate and ammonium. The watershed was monitored for approximately eight months with meteorological monitoring, time domain reflectometry (TDR), soil water chemistry, and stream gaging. Simulated subsurface flow predicted in the HYDRUS 2-D flow and transport model was coupled with observed field nutrient data to characterize the interaction of precipitation, soils, and nutrient transport from an uplands pasture to a naturally developing riparian area.

The results indicated that the riparian area was efficient in removing nitrate and ammonium in subsurface flow prior to reaching the stream. Seasonal and storm influences were identified as the primary influencing mechanism of nutrient transport with the watershed.

# Introduction

A desirable function of riparian areas in both the agricultural and forest settings is to reduce the loading of non-point source (NPS) pollution. A variety of chemical and physical processes occur within these riparian areas that allow them to protect water quality. Riparian zones typically act as sinks for nutrients in solution moving along subsurface hydrologic paths (Yeakley et al., 2003) as well as for sediments and nutrients suspended or dissolved in overland flow.

There have been considerable research efforts to quantify nutrient loss from both agricultural and forested watersheds (Lowrance et al., 1983; Peterjohn and Correll, 1984; Schultz et al., 1994; Swanson et al., 1982; Yeakley et al., 2003). Research has shown that soil water chemistry changes as it moves from the upland ecosystem through riparian zones and into surface streams. Riparian zones are major sites of nutrient transformation (Dahm et al., 1998; Hedin et al., 1995; Hill, 1996; Mulholland, 1993; Triska et al., 1990). Mechanisms such as solute transport, biogeochemical transformation, nutrient sequestration, and reduction of nutrient inputs have received attention in an effort to reduce NPS pollution to receiving waters.

Nitrogen dynamics in forested and agricultural watersheds has received attention due to the high mobility and transport of nitrogen in solution. The primary sources of nitrogen input in agricultural watersheds are atmospheric deposition, organic matter decomposition, fertilizers, and livestock waste ($NO_3^-$ and $NH_4^+$) (Fisher and Binkley, 2000). However, nitrate ($NO_3^-$) and ammonium ($NH_4^+$) are often lost from agricultural watersheds through surface and groundwater transport and denitrification (Lowrance, 1992).

Studies have indicated that subsurface flow is a primary transport mechanism of nitrogen loss from agricultural watersheds (Dahm et al., 1998; Haycock and Pinay, 1993; Hubbard and Sheridan, 1983; Lowrance et al., 1983; Peterjohn and Correll, 1984). Hubbard and Sheridan (1983) found that subsurface $NO_3^-$ concentration was 19 times greater than surface $NO_3^-$ concentration in soils with significant leaching. The study also revealed that $NO_3^-$ concentration was generally low unless favorable surface runoff conditions occurred. In a study of nutrient dynamics in an agricultural watershed, Peterjohn and Correll (1984) observed that of the total nitrogen lost from a riparian forest at the bottom of the agricultural watershed, 75% was lost through groundwater flow, thus concluding that subsurface flow is a major pathway of nitrogen losses from the riparian forest to stream. Hubbard and Sheridan (1983) observed similar results in a small, upland Coastal Plain watershed. Of the total input of nitrogen, 99% of $NO_3^-$ was lost through subsurface flow.

Both nitrogen and phosphorous are efficiently removed at the ecotone between upland groundwater and surface water (Dahm et al., 1998). Bosch et al. (1994) found that the concentration and loading of nitrogen and phosphorous in both surface and subsurface runoff were reduced after moving through a riparian zone. Nitrate is often transported during overland and subsurface flow. Considerable research has been focused on the transport of nitrate ($NO_3^-$ N) due to its ability to readily dissolve in water and its negative charge. Haycock and Pinay (1993) observed that nitrate retention in groundwater was at maximum within the first few meters of both poplar and grass riparian zones on the Leach River in the United Kingdom. This study also indicated that the riparian zones were especially efficient sinks for nitrate during winter months. Biogeochemical

processes and microbial activity within the riparian area sequester and transform nitrogen into nitrogen gases such as nitrous oxide ($N_2O$) and nitric oxide (NO). Gaseous loss typically occurs through microbial denitrification (Lowrance et al., 1983).

In order to understand how nitrate and ammonium move through surface and subsoil horizons, one must consider nutrient transport as a function of hydrologic flow. As noted earlier, researchers have shown that nitrogen transport primarily occurs through surface and subsurface flow (Dahm et al., 1998; Haycock and Pinay, 1993; Hubbard and Sheridan, 1983; Lowrance et al., 1983; Peterjohn and Correll, 1984). Nitrate and ammonium transport in saturated and near-saturated soil conditions are relatively easy to monitor through tension lysimetry, but nutrient flow occurring under partially saturated (below field capacity) and unsaturated states is quite complex.

The specific nature of unsaturated flow is complex and very difficult to measure *in situ*. As a result, mathematical models have been developed to iteratively solve for unsaturated flow (Mailhol et al., 2001; Pang et al., 2000; Simunek et al., 1999). Observed nutrient field data is often coupled with model outputs of partially saturated or unsaturated flow to adequately account for nutrient transport. One such model that has received much attention in this application is the HYDRUS 2-D software package. This model was specifically designed to analyze water and solute movement in unsaturated, partially saturated or saturated porous media (Simunek et al., 1999). The HYDRUS 2-D model numerically solves Richard's equation for saturated-unsaturated water flow. Richard's equation, the governing flow and transport equation, is solved numerically using a Galerkin-type linear finite element scheme (Simunek et al., 1999). HYDRUS 2-D uses unsaturated soil hydraulic properties that are incorporated into the governing flow

equation. The user may choose from three different analytical models as described by Brooks and Corey (1966), van Genuchten (1980), and Vogel and Cislerova (1988), to solve for unsaturated soil hydraulic properties. This model incorporates a sink term for root water uptake (evapotranspiration), and uses an anisotropy tensor to account for an anisotropic medium.

Research has shown successful application of HYDRUS 2-D to simulate saturated, partially saturated, and unsaturated flow as well as the transport of various nutrients, pesticides, and chemical pollutants (Kao et al., 2001; Mailhol et al., 2001; Pang et al., 2000; Simunek et al., 1998). Pang et al. (2000) successfully used this model to simulate picloram, atrazine, and simazine pesticide leaching through two New Zealand soils to groundwater reserves. The authors noted that the HYDRUS 2-D model was capable of simulating general trends of field soil water contents and potentials, as well as trend of the pesticide leaching. However, the authors did observe discrepancies between observed data and simulated data that were primarily attributed to the lumping of soil hydraulic properties, the presence of preferential flow paths, the use of single average values of solute dispersivity, and the lack of consideration of spatial heterogeneity in hydraulic and transport parameters. Mailhol et al. (2001) successfully utilized the HYDRUS2-D model to characterize the impact of fertilization practices on nitrogen leaching under irrigation on a loamy soil plot in France. The researchers used the results from HYDRUS 2-D to validate simulated water application depths, crop yield, and nitrate leaching using the RAIEOPT and STICS models. Kao et al. (2001) used HYDRUS 2-D in a study of steady state analysis of unsaturated flow above a shallow water table aquifer. The authors showed that HYDRUS 2-D was capable of simulating unsaturated

flow in the transition zone above the water table. The use of models like HYDRUS 2-D to simulate saturated, partially saturated, and unsaturated flow and solute transport offer mathematical solutions to very complex soil physics and hydrological studies that aid in understanding flow and transport mechanisms. However, technicians of modeling packages such as HYDRUS 2-D must assert discretion on the application and efficacy of relying on such models for *in situ* applications. As Pang et al. (2000) noted, successful simulated results are a function of properly characterizing input parameters.

The specific objective of this paper is to utilize observed watershed soil, hydrological, and meteorological data to two-dimensionally model both saturated and unsaturated flow processes within a hillslope pasture and at the adjacent riparian zone interface. Saturated and unsaturated mass balances given by the HYDRUS 2-D model will be coupled with observed field nutrient data to describe nitrate and ammonium flux within the study watershed. The understanding of these flow processes will assist in understanding the hillslope hydrology of the study site, as well as the influence of water flux on nutrient transport.

# Methods

## *Site Description*

The study watershed is located approximately 13 kilometers west of the town of Franklin, Macon County, North Carolina on the Slagle Farm (Figure 2-1). This area of southwestern North Carolina is in the Blue Ridge Mountain physiographic region and is typified by steep granitic slopes to relatively level alluvial flood plains adjacent to primary rivers. The Slagle Farm watershed (N:92355.91 E:27448.47) (Figure 2-2, 2-3) incorporates approximately 5 hectares of drainage, and ranges in elevation from 646 meters at the top ridge to 628 meters at the Cartoogechaye Creek. The watershed is located on private land that has primarily been used for agriculture, with moderate cattle grazing.

The area receives an average of 132 cm of precipitation a year. Approximately 50 % of annual precipitation falls during the months of April and September, with an average relative humidity of 60% (United States Department of Agriculture, 1996). The average summer temperature is 24° C, with a maximum temperature of 29° C. The average winter temperature is 4° C, with a minimum of -3° C (United States Department of Agriculture, 1996).

## *Soil Characteristics*

The site is primarily covered with Kentucky Fescue 31 grass, with sparse woody vegetation distributed across the landscape. The pasture is primarily composed of four series of soil: the Braddock, Saunook, Rosman, and Dillsboro series (Figure 2-4) (United States Department of Agriculture, 1996). The Braddock series is usually located on the strongly sloping (8-15%) and top-slopes of the pasture as well as on the spurs within the

drainage. The Braddock clay loam is a well-drained, clayey, mixed, mesic Typic Hapludults. The surface layer is within the top 28 cm of soil and is reddish brown (Ap-horizon) (United States Department of Agriculture, 1996). The subsoil Bt-horizon is located between 28 and 109 cm, followed by a weathered C-horizon consisting primarily of mica.

The Saunook series is a very deep, well-drained, moderately permeable soil located on gently sloping (2-8%) mid-sloped areas. The Saunook loam is a fine-loamy, mixed, mesic Humic Hapludults. The surface layer (Ap-horizon) is a dark brown loam and is up to 25 cm deep. The subsoil (Bt-horizon) ranges from 25 cm to 86 cm in depth. The Bt is located atop a weathered C-horizon composed of mica with 15% gravel and 25% cobbles (United States Department of Agriculture, 1996).

The Dillsboro series is a moderately permeable, very deep, well-drained loam that is located mid-slope in the eastern most drainage of the watershed. The Dillsboro loam is a clayey, mixed, mesic Humic Hapludults found on gentle slopes ranging between 2 and 8%. The surface soil is a dark brown loam up to 30 cm in depth. The subsoil Bt-horizon is a strong brown clay up to 127 cm deep (United States Department of Agriculture, 1996).

The Rosman series is a very deep, well-drained, moderately rapid permeable sandy loam. This series is often found on nearly level (0-2%) slopes adjacent to major streams and is specifically located within the established riparian area of this site. The Rosman is a fine sandy loam that is frequently flooded. This coarse-loamy, mixed, mesic Fluventic Haplumbrepts runs the entire length of the watershed. The surface soil (Ap-horizon) is dark brown and reaches a maximum depth of 41 cm. The subsoil (Bt-horizon)

reaches a maximum depth of 145 cm and is typified as a Bt/Bw horizon (United States Department of Agriculture, 1996).

## *Watershed Delineation and Sample Transects*

The delineation of the watershed was conducted on site, with use of USGS 7.5' Franklin, NC quadrangle topographic map (Figure 2-2) and Corvallis Microtechnology, Inc. PC5-L global positioning system (GPS) receiver (Corvallis Microtechnology, 1998b). The survey was conducted to define the smaller watershed that drains into an established riparian study site. The survey established elevation gradients, slopes, and drainage reference points that aided in quantifying the total drainage area of the study riparian zone.

After the perimeter survey was completed, a more intensive survey was conducted within the watershed to develop a local topographic map for the drainage area. GPS locations were taken at every major change (> 0.5-m) in micro-topographical feature within a 10-m grid. Data collected were used to develop a topographic map, with geodetic correction. CMT PCGPS 3.7 software was used to correct and process GPS data (Corvallis Microtechnology, 1998a). X, Y, and Z data collected was then processed through Surfer Win 32 Version 6.04 (Golden Software, 1999) to create the topographic map (Figure 4-1). The watershed topographic map assisted in identifying micro-topography and its influence on both surface and subsurface drainage.

Transects were established within the primary sub-watershed drainage patterns (identified from contour map) of the watershed (Figure 4-1). A total of three transects were established within each primary sub-watershed individual drainage regimes, which drain into the study riparian area. Transects span the length of the watershed, from ridge

tops in pasture, through riparian area, to river (transects were laid in the general direction of subsurface flow to river).

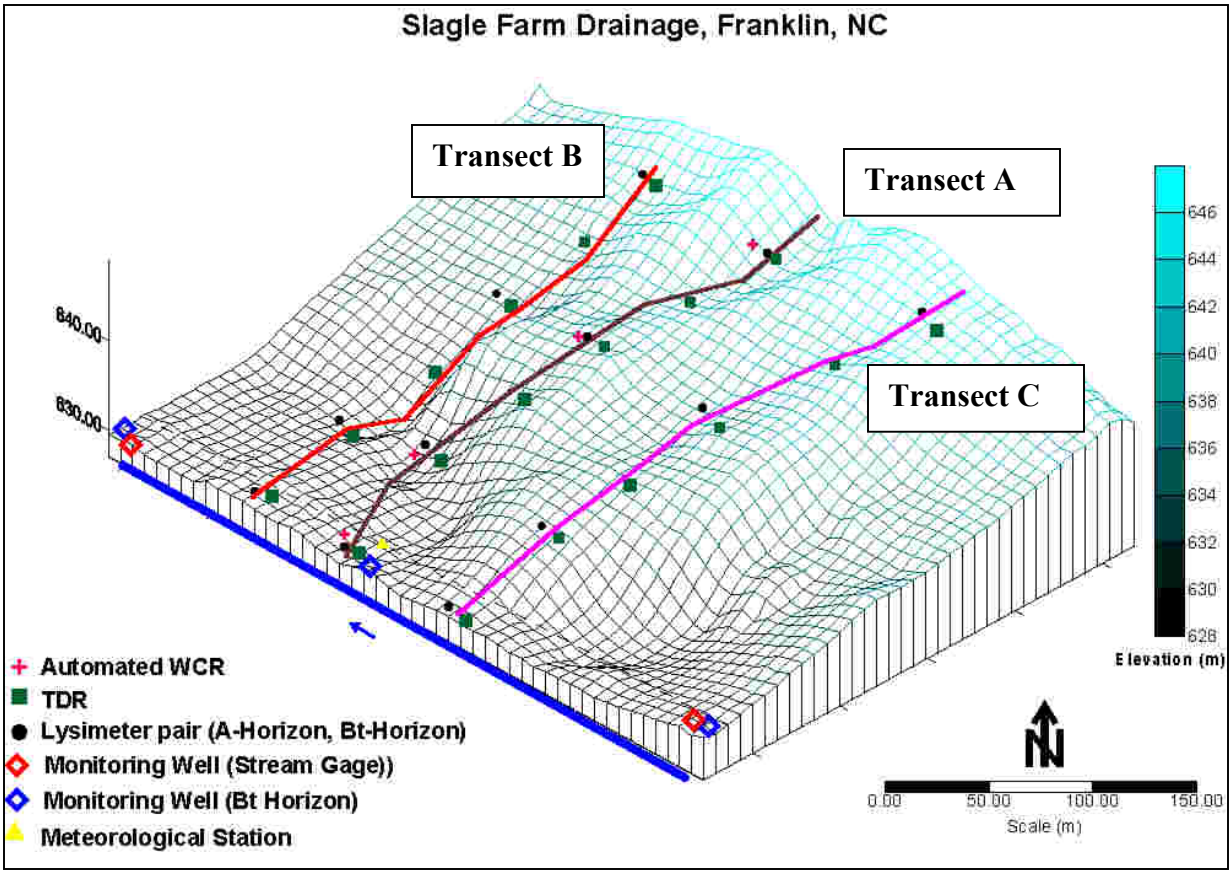


Figure 4-1: Rendered Slagle Farm watershed topographic map with instrumentation locations

## *Field and Laboratory Measurements*

Soil profile descriptions were conducted along each transect to characterize master soil horizons. Four sampling stations were located in each transect, representing top-slope, mid-slope, toe-slope, and riparian area. Profiles were delineated based on depth, color, structure, texture, mottles, and roots. A Munsell color chart and the Soil Survey of Macon County, North Carolina (United States Department of Agriculture, 1996) aided in the delineation and classification. The profile descriptions were used to

determine specific depths for the placements of lysimeters and TDR instrumentation placements. Intact soil core samples were collected from both the Ap and the Bt horizons.

Transects were instrumented with four pairs of porous-cup tension lysimeters. Lysimeters pairs, in the Ap- (20 cm) and Bt- (50 cm) horizons, were located on the top-slope, mid-slope, toe-slope, and riparian zone (approximately 125 m spacing). Lysimeter measurements were conducted bimonthly between August 2002 and March 2003. Lysimeters were evacuated to -0.03 MPa, and were analyzed for $NO_3^-$-N, and $NH_4^+$-N through procedures developed by the Coweeta Hydrologic Laboratory (Reynolds and Deal, 1986; Walsh, 1971).

## *Hydrologic Analysis*

Water transport were simulated using the HYDRUS 2-D model (Simunek et al., 1999). HYDRUS-2D is a Microsoft Windows based modeling platform for the analysis of unsaturated, variably saturated, and saturated flow and solute transport through porous media. The HYDRUS 2-D model numerically solves Richard's equation for saturated-unsaturated water flow. Richard's equation (1), the governing flow and transport equation, is solved numerically using a Galerkin-type linear finite element scheme (Simunek et al., 1999). HYDRUS 2-D uses unsaturated soil hydraulic properties that are incorporated into the governing flow equation.

$$\textit{Richard's Equation: } \frac{\partial \theta}{\partial t} = \frac{\partial}{\partial x_i}\left[K(K_{ij}^A \frac{\partial h}{\partial x_j} + K_{iz}^A) - S)\right] \quad (1)$$

where $\theta$ is the volumetric water content [$L^3L^{-3}$], $h$ is the pressure head [L], $S$ is a sink term [$T^{-1}$], $x_i$ ($i$=1,2) are the spatial coordinates [L], $t$ is time [T], $K_{ij}^A$ are components of a

dimensionless anisotropy tensor $K^A$, and $K$ is the unsaturated conductivity function [$LT^{-1}$] (2) given by

$$K(h,x,z) = K_s(x,z)\, K_r\, h,x,z) \quad (2)$$

Where $K_r$ is the relative hydraulic conductivity and $K_s$ is the saturated hydraulic conductivity [$LT^{-1}$].

The HYDRUS 2-D model also incorporates heat and solute transport equations. The heat transport equation considers movement by both conduction and convection in flowing water (Simunek et al., 1999). The governing equation for solute transport is based on a convection-dispersion equation. The governing convection-dispersion solute transport equations are presented in a very general form by including provisions for nonlinear non-equilibrium reactions between the solid and liquid phases, and a linear equilibrium reaction between the liquid and gaseous phase (Simunek et al., 1999). The authors have also included the effects of zero-order production, first-order degradation independent of other solutes, and first-order decay/production reactions that provides the required coupling between the solutes involved in the sequential first-order chain (Simunek et al., 1999). These transport models also account for convection and dispersion in the liquid phase and diffusion in the gaseous phase.

The general construction of the HYDRUS 2-D model can be seen in Figure 3.6. The desired simulation is defined in the pre-processing menus within the HYDRUS 2-D model. Geometry, time information, iteration criteria, soil hydraulic model, water flow parameters, root water uptake, time-variable boundary conditions, and mesh generation are defined within these pre-processing menus. Refer to Chapter 3, Hydrologic Analysis, for detailed model description, input parameterization, and simulation criteria.

## *Nutrient Flux*

As noted earlier, the objective of this paper is to describe and quantify soil water and nutrient flux within the Slagle Farm watershed. Research has shown that water flow is the primary transport mechanism of nitrate and ammonium (Hill, 1996; Hubbard and Sheridan, 1983; Jacobs and Gilliam, 1985; Lowrance, 1992; Vos et al., 2000). In order to address nutrient flux within the sub-soil, both saturated and unsaturated flow must be quantified.

The HYDRUS 2-D model was used to simulate saturated and unsaturated flow within the Slagle Farm watershed. Meteorological data (precipitation, evaporation), root water uptake (Et), soil hydraulic properties, and stream stage data were used to parameterize water flow in the finite element grid flow domain. Water mass balance output data from HYDRUS 2-D was used to characterize water flux within the study site. Water mass balance out put data were calculated for specific areas (sub-regions) of the flow domain, delineated by soil series and horizon, as well as for the total flow domain. The partitioning of water mass balance by sub-region was used to quantify water flow dynamics within individual soil series and horizon. Sub-region water flux was coupled with observed nutrient data from lysimeters.

Water flux by sub-region was coupled with the respective nitrate and ammonium concentrations measured from lysimeters from each sampling location (Figure 4-1). Sub-region areas (soil series and horizon) were multiplied by their respective simulated volumes to calculate total water flux within each region (input flow domain used in HYDRUS 2-D was characterized by a cross-section of average elevation values per slope location). Potential nitrate and ammonium flux were calculated per sampling location

(sub-region for water flux and lysimeter location for concentration) by the following equation:

$$[NO_3^-\text{-}N] \text{ or } [NH_4^+\text{-}N] \text{ flux (mg/L)} = V\,T^{-1} \times [Conc.]$$

where, $V$ is the volume of flux (L), $T$ is time in days, and *Conc.* is the concentration of $NO_3^-$-or $NH_4^+$ in mg/L. Nutrient flux can then be scaled to the desired resolution by:

$$\text{scaled nutrient flux} = \Sigma\,[\text{nutrient flux}] \times T$$

where $\Sigma$ *[nutrient flux]* is the total nutrient flux per time period, and $T$ is the desired time resolution.

# Results and Discussion

## *Mechanical and Physical Soil Properties*

Soil mechanical and physical properties analyzed in this study were bulk density, saturated hydraulic conductivity, total, macro-, and micro-porosity, particle size analysis, and water retention curve development. Bulk density values for the Braddock, Saunook, and Rosman series Ap- and Bt-horizons are shown in Table 4-1. Particle size analysis for the respective soil series are presented in Table 4-2.

Table 4-1: Bulk Density and saturated hydraulic conductivity (Ksat) mean values per soil series and horizon (Bra = Braddock, Sau = Saunook Ros = Rosman).

| Soil | Horizon | mean bulk density | saturated hydraulic conductivity |
|---|---|---|---|
| | | (Mg/cm3) | (cm/hr) |
| Bra | Ap | 1.28 (.09) | 8.37(10.7) |
| Bra | Bt | 1.36 (.08) | 2.22(2.2) |
| Sau | Ap | 1.12(.20) | 19.45(12.6) |
| Sau | Bt | 1.30(.09) | 3.89(4.7) |
| Ros | Ap | 1.16(.10) | 24.39(12.1) |
| Ros | Bt | 1.10(.21) | 6.89(3.8) |

(*Standard deviations in parenthesis)

Table 4-2: Mean* sand, silt, and clay percentages per soil series and horizon.

| Soil | Horizon | Sand | Silt | Clay |
|---|---|---|---|---|
| | | (%) | (%) | (%) |
| Bra | Ap | 52 (7.4) | 20 (5.0) | 27 (5.4) |
| Bra | Bt | 50 (9.5) | 23 (2.5) | 27 (8.0) |
| Sau | Ap | 55 (5.0) | 25 (6.1) | 20 (3.7) |
| Sau | Bt | 51 (11.6) | 26 (3.2) | 22 (10.3) |
| Ros | Ap | 54 (12.4) | 30 (7.9) | 16 (6.2) |
| Ros | Bt | 51 (11.5) | 26 (5.3) | 23 (6.7) |

(*Standard deviations in parenthesis)

Bulk density may influence the transport of nutrients in water by increasing (low bulk density) or decreasing (high bulk density) the flow of water through soils. The less torturous path that water moves through the soil, the faster water will transport dissolved nutrient, resulting in rapid transport of the respective nutrients. With increased bulk density, the velocity of water decreases. If the nutrient laden water is stored in the soil, plant may have an opportunity to uptake the nutrients. Bulk density values for the Bt-horizons of the Braddock and Saunook soil series were greater than the Ap-horizons. The increase of bulk density from the Ap- to the Bt-horizon may be attributed to pedogenic processes or terrestrial and microbial activity. Such processes as eluviation (movement of material out of a horizon) and illuviation (movement of a material into a horizon) can remove smaller particle of clay out of the Ap-horizon, depositing them into the Bt-horizon (Fisher and Binkley, 2000). Studies conducted by Wilson et al. (1990) in a forested hillslope and Hill (1996) in a riparian zone adjacent to agricultural land, observed similar results.

Though the particle density of clay is smaller than that of sand, clay particles have greater surface area (due to the mineralogical constitution of clay), packing more particles into a smaller area, thus increasing bulk density. Packing of soil particles also may influence bulk density. Packing refers to how soil particles align within a given soil volume (Fetter, 2001). In heterogenic soils made of sand, silt, and clay, the heavier particles (sand) settle under gravity. Smaller particles, such as silt or clay, will fill in the voids left between individual sand particles, resulting in an increase of total mass per unit volume. This can be seen in the particle size distribution of the Braddock, Saunook, and

Rosman soils (Table 4-2). Clay and silt percentages increased from the Ap- to the Bt-horizon in each of the three soils.

It is interesting to note that the bulk densities of the Ap-horizons were less than the Bt-horizons, even though this horizon receives greater compaction as a result of cattle grazing. This may be attributed to the influence of root penetration and turn over in this surface horizon. Once established in the shallow sub-soil, roots will continue to grow and slough, adding organic matter to this horizon and reducing bulk density (Fisher and Binkley, 2000). The influence of freezing and thawing cycles, as well as the shrinking and swelling of soils with mixed mineralogy may also reduce bulk density in surface horizons. Such terrestrial creatures as shrews, moles, and earthworms also aid in churning and aerating the surface soil horizon. This surface horizon may be desirable to earthworms and microbial populations due to the deposition of cattle manure and urea.

The bulk density for the Rosman series (riparian area) did not show the same trend of increased bulk density in the Bt-horizon. This phenomenon may be attributed to the influence of particle deposition within the riparian zone. As sediment is transported in overland into the riparian area, the vegetation reduces the velocity of flow, resulting in sediment deposition. Over time, fine sediments will eluviate from the surface horizon into the sub-soil. However, overland flow and sediment deposition may be episodic (function of storm frequency and intensity), resulting in a continual deposition of fine sediments in the riparian area.

Mean saturated hydraulic conductivity and porosity values are shown in Table 4-1 and 4-3, respectively. Saturated hydraulic conductivity and macro-porosity was greater in the Ap-horizon in each of the three soils. This is what was expected due to the influence

of particle size distribution and bulk density. Fisher and Binkley (2000) attributed this reduction of hydraulic conductivity to the influence of material layering with different textures. The authors noted that the influence of different parent material and pedogenic processes could result in silt or clay pans on top of a restrictive horizon, such as a Bt-horizon. This characteristic is often detected in Utlisols. As noted earlier, the clay content and bulk densities of the Bt-horizon were greater. Particle size distribution and bulk density may also influence the distribution of macro-pores to micro-pores. The increase of macro-pores directly influences saturated hydraulic conductivity by moving water under non-capillary force. Water flow in the macro-pores flows under reduced tortuosity than in micro-pores, thus increasing saturated hydraulic conductivity.

Table 4-3: Mean* total, macro-, and micro-porosity for the Braddock, Saunook, and Rosman soil series.

| Soil | Horizon | Total (%) | Macro (%) | Micro (%) |
|---|---|---|---|---|
| Bra | Ap | 51.67 (3.4) | 13.18 (1.9) | 38.49 (2.2) |
| Bra | Bt | 48.7 (3.2) | 8.02 (2.1) | 41.05 (2.4) |
| Sau | Ap | 57.94 (7.6) | 19.13 (2.6) | 38.81 (5.5) |
| Sau | Bt | 50.80 (3.5 | 12.08 (1.7) | 38.72 (2.3) |
| Ros | Ap | 56.1 (3.7) | 13.73 (3.8) | 42.37 (1.9) |
| Ros | Bt | 58.30 (7.9) | 9.56 (1.6) | 48.74 (6.4) |

(*Standard deviations in parenthesis)

## *Hydrologic Characteristics*

### *Observed*

Hydrological activity of the Slagle Farm watershed was characterized in the field through use of time domain reflectometry (TDR), stream gaging, and meteorological monitoring. These characteristics were then incorporated into HYDRUS 2-D model to

quantify subsurface water flux as a function of atmospheric conditions, soil water activity, and discharge to Cartoogechaye Creek. TDR, coupled with automated water content reflectometers (WCR), were used to monitor soil water content of the vadose zone. Observed soil volumetric water content values in Figure 4-2 are presented as observed mean $\theta_v$ for all transects for the top-slope (Braddock series), mid-slope (Braddock series), toe-slope (Saunook series), and riparian area (Rosman series) locations. Meteorological inputs per month and average evapotranspiration for the Slagle Farm watershed are presented in Table 4-4. Gross precipitation is presented in Figure 4-4, and Figure 4-6 shows monthly stream heights for Cartoogechaye Creek.

Observed soil volumetric water content ($\theta_v$) in the Bt-horizon was consistently higher than the Ap-horizon (Figure 4-7). This was expected due to the higher clay contents of the Bt-horizons (Table 4-2) and plant root water uptake. The plate-like structure of clay holds water more tightly than silt and sand. As a result, in periods with drier conditions, $\theta_v$ in soils with high clay content is often higher than soils with low clay (McLaren and Cameron, 1996). The influence of vegetation above of the Ap-horizon also may have contributed to a smaller $\theta_v$ than in the Bt-horizon. Though root density and distribution were not measured in this study, it is reasonable to assume that the Ap-horizon is primary source of water for the grass root water uptake. As a result of root water uptake, and decreased clay content (than the Bt-horizon) to hold water more tightly, the Ap-horizon water was taken up by plants through evapotranspiration. The influence of evapotranspiration can easily be seen by comparing $\theta_v$ for the Ap- and Bt-horizons of the riparian area (Figure 4-2). There is a dramatic difference of $\theta_v$ between these two horizons. $\theta_v$ for the Ap-horizon ranged from 0.15 to 0.22 $cm^3$ $cm^{3-}$, while the

Bt-horizon had values of 0.35 to 0.54 $cm^3$ $cm^{3-}$. The increase of $\theta_v$ from the Ap- to the Bt-horizon can be attributed to increased evapotranspiration in the Ap-horizon and a

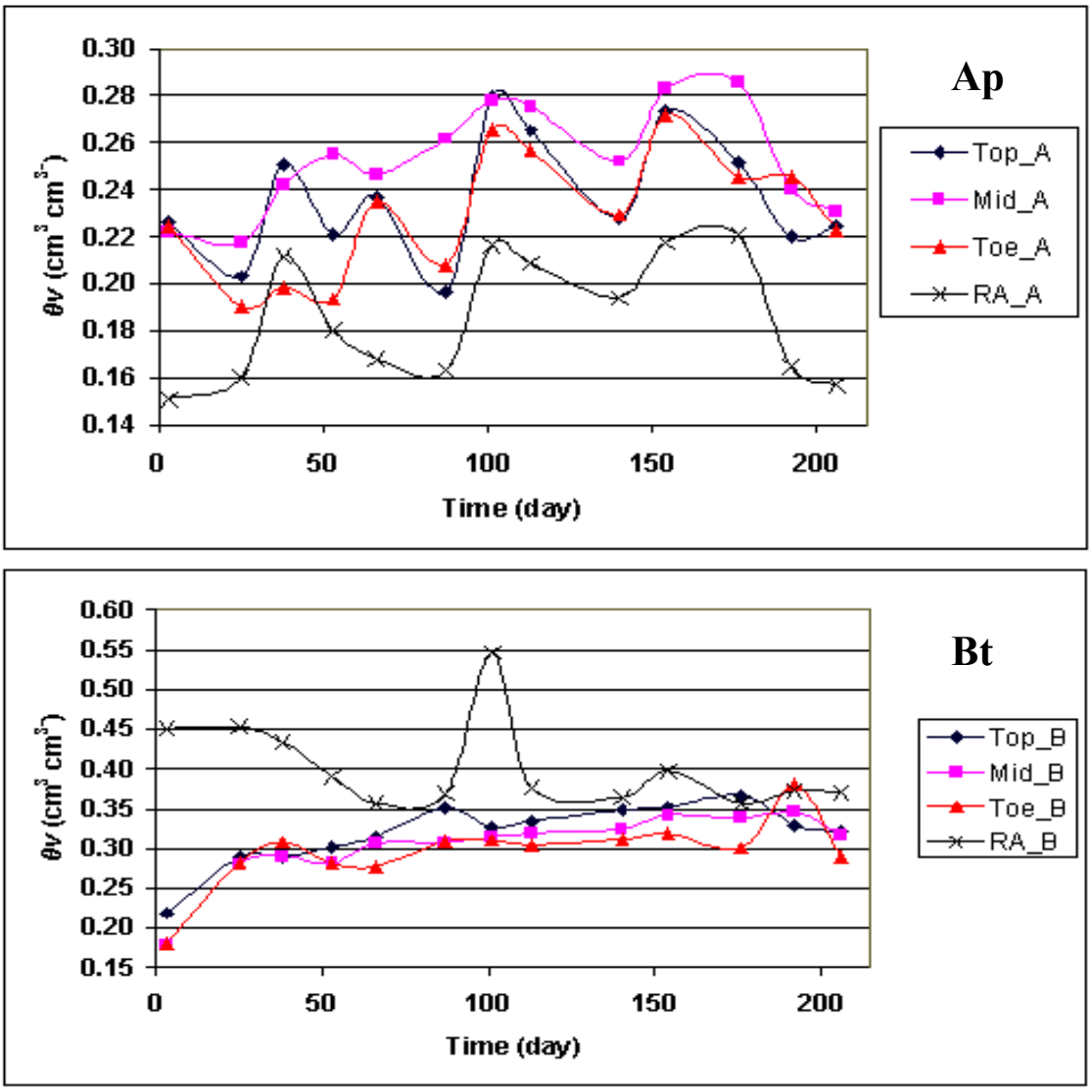


Figure 4-2: Observed $\theta_v$ by slope location (Top, Mid, Toe, RA) for the Ap- and Bt-horizons of the study watershed. Time scale: Aug. (1-18), Sep. (19-48), Oct. (49-79), Nov. (80-109), Dec. (110-134), Jan. (135-161), Feb. (162-182), and Mar. (183-212).

hyporheic recharge of water to the Bt-horizon from the stream. Vegetation in the riparian area has been excluded from cattle grazing and is less degraded than vegetation in the pasture area.

Soil $\theta_v$ for the Ap-horizon was highest for the mid-slope area of the pasture. This area is less steep than the top-slope, and is the area of preferred grazing. The top-slope Ap-horizon had the second highest $\theta_v$, followed by the toe-slope, and riparian area. The top-slope has the greatest slope that results in subsurface flow within the Ap-horizon to the mid-slope area. The low values of toe-slope $\theta_v$ may be attributed to a matrix pull of water towards the riparian area (function of root water uptake of vegetation in the riparian area). The highest $\theta_v$ for the Bt-horizons occurred in the riparian area. As noted above, this is attributed to the influence of hyporheic recharge from the stream and possibly to the greater depth of this subsurface horizon. Root depth may be limited from deep penetration due to the anaerobic conditions within this saturated area.

### *Simulated Hydrology*

Figure 4-3 suggests that simulations for water content agreed well with the general trend of observed $\theta_v$, but individual values across seasonal durations varied considerably. Simulated $\theta_v$ was consistently higher than the observed $\theta_v$ in each of the four sampling locations (top-slope, mid-slope, toe-slope, and riparian area). For following discussions, top-slope, mid-slope, toe-slope, and riparian area represent the Braddock (top and toe-slope), Saunook, and Rosman series, respectively.

In general, simulated Bt $\theta_v$ matched well with the general trend of observed $\theta_v$. However, simulated $\theta_v$ for the Ap-horizon was significantly higher than observed $\theta_v$. High simulated Ap-horizon $\theta_v$ is most likely attributed to how the HYDRUS 2-D model regards infiltration of rain water. Only one boundary condition can be assigned to specific nodes (surface nodes in this scenario) within the model flow domain. As noted in the water flow parameters section of Methods and Materials in Chapter 3, a time-variable

atmospheric condition was assigned surface horizons of the domain. When using atmospheric boundary conditions at the soil surface, HYDRUS 2-D allows all water to infiltrate (Simunek et al., 1999). As a result of this assumption, all of the water (minus evaporation) is moved into the surface horizon (Ap) thus resulting in increased soil $\theta_v$.

When one considers the hydrologic dynamics of a watershed, the entire hydrologic budget must be considered. The interaction of inputs of precipitation, removal of water by evapotranspiration, and discharge to a stream all influence the dynamics of the water budget. Soil water storage is directly affected by precipitation and evapotranspiration. The highest precipitation for the duration of the study occurred in late September 2002 (days 39-46)(Figure 4-4). The highest actual evapotranspiration rates also occurred in these months (Figure 4-5). It should be noted that "actual Et" is the simulated amount of AEt. In-field AEt was not measured in this study. High precipitation also occurred in late December (days 122-134) of the same year. However, evapotranspiration was lower in December than September. Partitioning the components of the hydrograph may help to further explain hydrologic dynamics within the watershed. Though precipitation was greatest for September 2002, soil $\theta_v$ and stream stage were the lowest. This may be attributed to the higher rates of evapotranspiration for this period. The period of November and December 2002 showed the second highest rates of precipitation, as well as increasing discharge to Cartoogechaye Creek (Figure 4-10). Though total precipitation was lower for the December period, stream stage was greater than the September event. Analysis of soil $\theta_v$ in Figure 4-7 shows that $\theta_v$ was greatest for both horizons of the pasture soils for the same period. Though the amount of total precipitation was greater

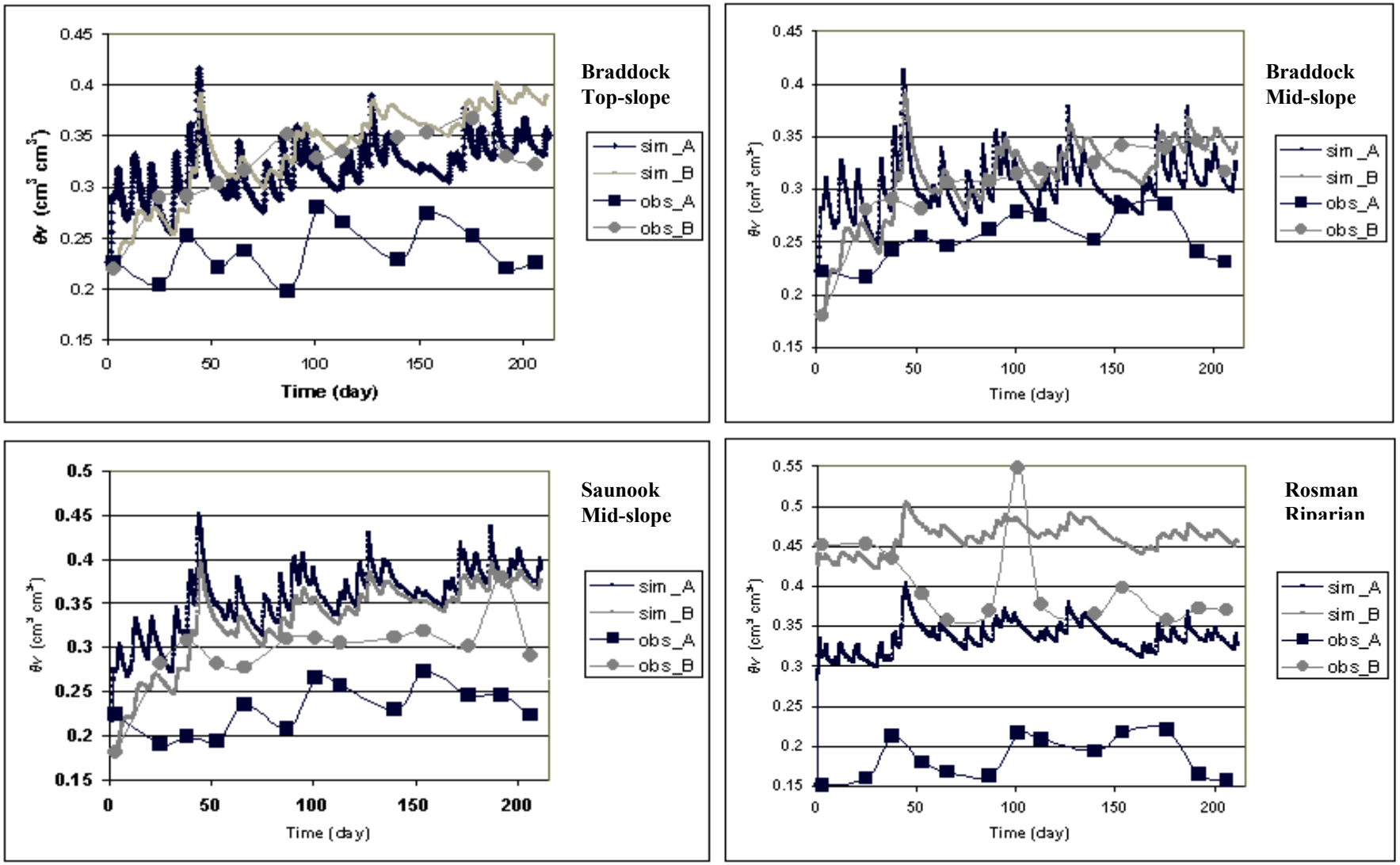


Figure 4-3: Simulated ("sim") and observed ("obs") $\theta_v$ for Braddock top-slope, Braddock mid-slope, Saunook toe-slope, and Rosman riparian. (Time scale: Aug. (1-18), Sep. (19-48), Oct. (49-79), Nov. (80-109), Dec. (110-134), Jan. (135-161), Feb. (162-182), and Mar. (183-212).)

for September than December, water in September was lost through plant water uptake (evapotranspiration).

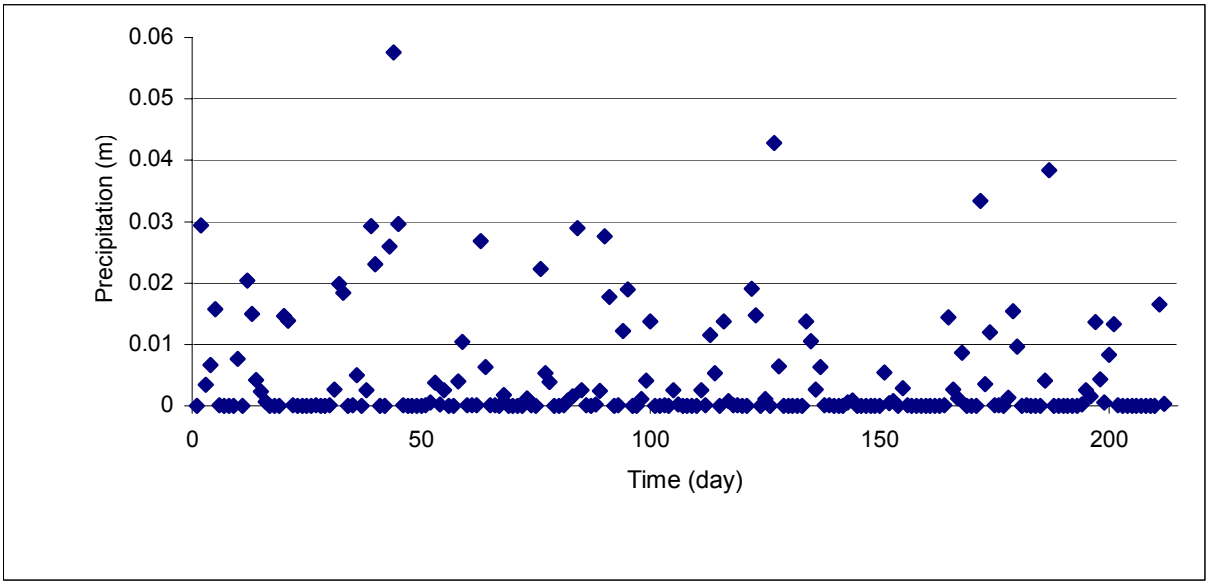


Figure 4-4: Daily precipitation for study watershed from August 2002 (day 0) to March 2003 (day 212).

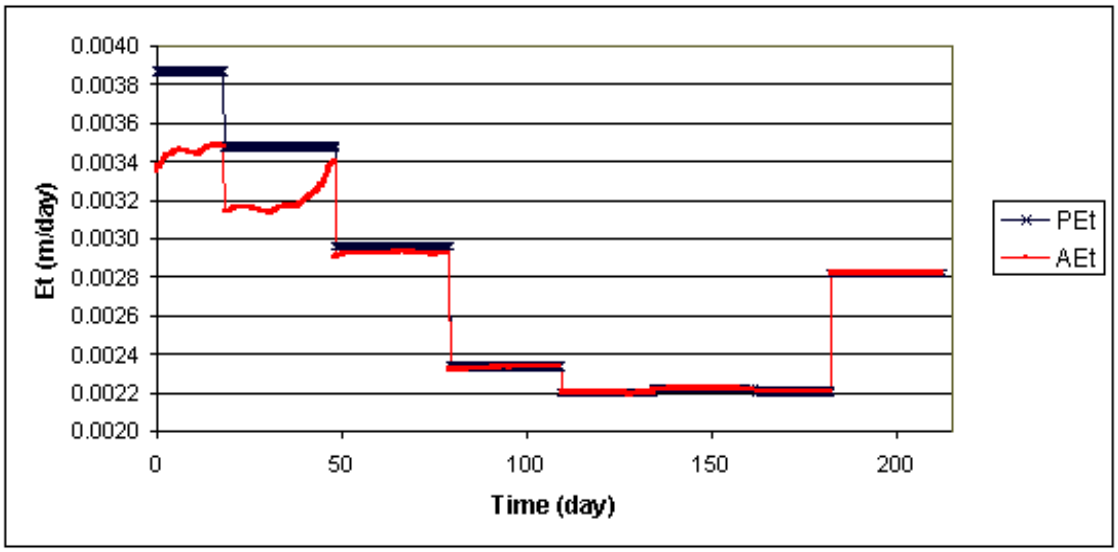


Figure 4-5: : Daily Potential (PEt) and Actual (AEt) evapotranspiration rates for the study watershed.

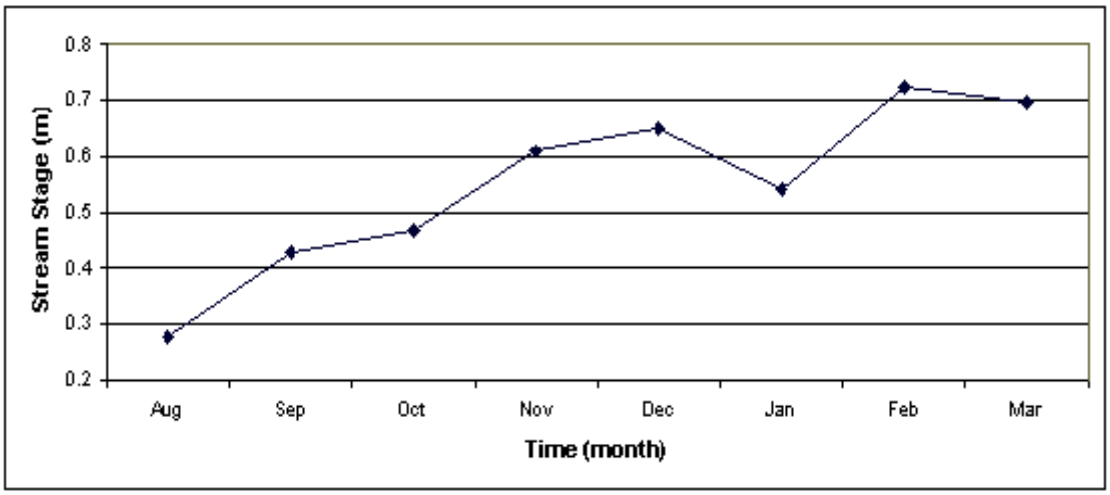


Figure 4-6: Figure 3-8: Mean monthly* stream stage of the Cartoogechaye Creek. * (Aug: day 1-18; Sep: 19-48; Oct: 49-79; Nov: 80-109; Dec: 110-143; Jan: 135-161; Feb: 162-182; Mar: 183-212)

An integral part of understanding the hydrologic dynamics of a watershed is the quantification of subsurface flow between heterogeneous soil materials and layers. To satisfy this objective, HYDRUS 2-D was utilized to simulate water volume within specific soil series and layers, as well as the flux of water between different materials. These data will help illustrate how and when water will move through the subsoil. The quantification of the volume of water and flux of water in and between different soil media may be used, among other applications, to determine flow path, water sequestration, and pollutant transport (nutrients).

Within the HYDRUS 2-D model, the user has the ability to manipulate time information to achieve desired time-step resolution or desired output print interval. For the specific scenario described in this paper, desired output print interval was scaled to the lysimeter sampling time interval, approximately 14-days, while minimum time-step interval was $1 \times 10^{-2}$ day. Recall that the print time interval is used simply to specify at which times detailed information about the pressure head, water content, flux, and water balances are printed. The time-step interval is used to define the minimum time

increment between individual calculations. A print time interval of 15 (14-day intervals for 212 days) was used in this simulation to match water volume and flux per sub-region (soil series and layer) to lysimetry data. However, water volume and flux is calculated on a 1 x $10^{-2}$ day for every day over the entire simulation period (212 days).

Figure 4-7 shows the total volume of inflow for the study watershed. Inflow is defined as the change in the volume of water per time in the total transport domain or predefined sub regions (Simunek et al., 1999). Watershed inflow in Figure 4-7 is the sum of all sub region materials (Ap- and Bt-horizon per soil series). Inflow is the summation of water (precipitation) entering (positive) the system as well as leaving (negative) the flow domain (Et, evaporation, soil water storage). Peak inflow occurred during the days leading to and on day 44 (late September). This dramatic increase of inflow into the

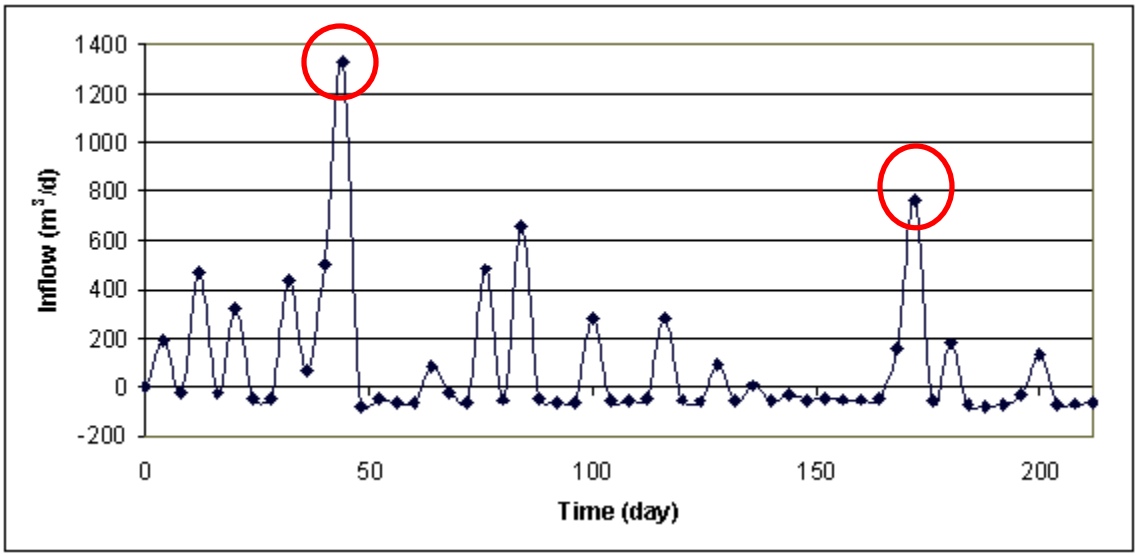


Figure 4-7: Figure 3-9: Inflow rates of water within the study watershed flow domain. (Circles show example of the increase of inflow that corresponds to increased input of precipitation.)

watershed corresponds well with precipitation input previous to, and on day 44, as well as on day 84 (Figure 4-4).

### *Seasonal Influence on Water Flow*

Due to a variety of equipment malfunctions, a complete year of sampling was not attained. However, the total monitoring period, late August 2002 to March 2003, covered four distinct seasons. Summer was covered by days 1 to 48, days 49 to 109 were used for fall, days 110 to 182 were used for winter, and spring was characterized by days 183-212. In an attempt to characterize periods of potentially high precipitation with low surface resistance (low vegetation surface friction, and low evapotranspiration), much of the monitoring period occurred during the fall and winter seasons.

Though precipitation was highest for the summer season (1-48), average stream stage was lowest (Figures 4-4 and 4-6). This is most likely attributed to high evapotranspiration during this season (Figure 4-5). The summer season was characterized as the growing season for fescue, resulting in high root water uptake. In the drier times of this season, pasture Bt-horizons generally had higher $\theta_v$ than Ap-horizons (Figure 4-3). Simulated $\theta_v$ for the pasture soils followed this general trend. However, in periods of high precipitation, simulated $\theta_v$ was often higher for Ap-horizons. This reversal of simulated Ap- and Bt-horizon $\theta_v$, again, is attributed to Et occurring primarily in the Ap-horizons during drier times, while in periods of high precipitation, water was perched above the less permeable Bt-horizon. Observed $\theta_v$ did not follow this trend, which may be attributed to a bimonthly collection interval for observed $\theta_v$. Simulated $\theta_v$ had a much higher time-step interval (calculated at $1 \times 10^{-2}$ day), which shows a higher trend of simulated $\theta_v$.

The fall season (days 49-109) showed average stream stage increasing (Figure 4-6). Though precipitation for this season was lower than the summer season, Et was significantly lower (Figures 4-4 and 4-5). The decreased rate of Et resulted in less water

uptake, resulting in increased water discharge to Cartoogechaye Creek. Again, observed $\theta_v$ for the Bt-horizon was greater than the Ap-horizon (Figure 4-7 A, B, C, D). Simulated $\theta_v$ for the pasture soils Ap- and Bt-horizons seem to alternate higher $\theta_v$, which may be attributed to wetting and drying fronts moving through the watershed (function of lower precipitation and Et).

The winter season (days 110-182) had the highest stream stage (Figure 4-6) that may be attributed to intense, sporadic storms and the lowest Et for the four seasons (Figures 4-4 and 4-5). Observed and simulated $\theta_v$ for the Bt-horizon was significantly higher than the Ap-horizon (Figure 4-3). Again, this is attributed to very low Et rates.

Average stream stage for the spring season (183-212) was still relatively high, but had decreased from the winter season (Figure 4-6). More frequent and intense precipitation events were observed during this season, and Et began to rise (Figures 4-4 and 4-5). The increased Et, a result of fescue entering the growing season, again, started to uptake water into plant roots. This, coupled with increased surface resistance (from plants reducing the velocity of surface water), resulted in the initiation of stream stage decrease. Observed $\theta_v$ for the Ap-horizon dropped below $\theta_v$ for the Bt-horizon (Figure 4-3). Simulated $\theta_v$ for the Bt-horizon again climbed significantly higher than simulated Ap-horizon $\theta_v$.

### *Storm Event vs. Dry Period*

Two specific time periods were selected to illustrate the dynamics of the Slagle Farm watershed. Days 40 to 48 (late September) will be used to illustrate the response of the watershed to high precipitation, while days 156 to 164 (late January to early February) will be used to illustrate flow dynamics under dry conditions (Table 4-4).

These two specific conditional periods represent the maximum and minimum precipitation inputs over the entire simulation period. The objective of these two scenarios is to draw correlations between precipitation, soil volumetric water content ($\theta_v$), and evapotranspiration (AEt). Graphical outputs of each period will be presented to illustrate how water moves through each soil series (material distribution) and horizon (Ap- and Bt-horizon).

The "wet" period, encompassing day 40 to 48, had a total precipitation input of 0.1364 m for the 5-ha watershed and an average AEt of 603.22 $m^3$/day. Total precipitation for the "dry" (156-164) period was 0.0002 m, with an average AEt of 121.60 $m^3$/day. Soil $\theta_v$ for the wet and dry periods be seen in Figures 4-8 and 4-9. Average $\theta_v$ per slope location and horizon are presented in Table 4-5. The day previous to each period is presented to show an "initial" condition for each scenario. Figure 4-8 shows the trend of soil $\theta_v$ during the wet period. The entire system responded to the increase of precipitation. Peak $\theta_v$ occurred on day 44, which corresponds with peak precipitation (Figure 4-4) and peak inflow (Figure 4-10). During the "wet" period, pasture Ap-horizons generally had higher soil $\theta_v$ than their respective Bt-horizons. However, the riparian Bt-horizon consistently had higher $\theta_v$, which, as discussed earlier, may be a result of hyporheic recharge from Cartoogechaye Creek, and the lack of root water uptake from riparian vegetation. The toe-slope Ap-horizon had the second highest $\theta_v$, which is most likely attributed to water contributions from upslope sources. The rate at which rainwater infiltrates into the surface horizon and percolates into the subsoil horizon is primarily a function of bulk density, macro-porosity, and antecedent moisture conditions (Anderson and Burt, 1990; Anderson et al., 1997; McLaren and Cameron, 1996).

Table 4-4: Precipitation inputs for "wet" and "dry" period. Precipitation is given for the entire watershed.

| Wet Period | | Dry Period | |
|---|---|---|---|
| Day | Precipitation | Day | Precipitation |
| | (m) | | (m) |
| 40 | 0.0231 | 156 | 0.0001 |
| 41 | 0 | 157 | 0 |
| 42 | 0 | 158 | 0 |
| 43 | 0.026 | 159 | 0 |
| 44 | 0.0576 | 160 | 0 |
| 45 | 0.0296 | 161 | 0 |
| 46 | 0.0001 | 162 | 0 |
| 47 | 0 | 163 | 0 |
| 48 | 0 | 164 | 0.0001 |

Table 4-5: Average simulated soil $\theta_v$ per slope location and horizon for "wet" and "dry" period.

| Period | top A | top B | mid A | mid B | toe A | toe B | ra A | ra B |
|---|---|---|---|---|---|---|---|---|
| | $cm^3\ cm^{3-}$ | $cm^3\ cm^{3-}$ | $cm^3\ cm^{3-}$ | $cm^3\ cm^{3-}$ | $cm^3\ cm^{3-}$ | $cm^3\ cm^{3-}$ | $cm^3\ cm^{3-}$ | $cm^3\ cm^{3-}$ |
| **Wet** | 0.3525 | 0.3430 | 0.3491 | 0.3398 | 0.3931 | 0.3463 | 0.3628 | 0.4783 |
| **Dry** | 0.3133 | 0.3537 | 0.2837 | 0.3100 | 0.3555 | 0.3452 | 0.3202 | 0.4457 |

If precipitation is greater than infiltration, overland flow or subsurface lateral flow (above a less permeable horizon) may occur (Anderson et al., 1997; Heppell et al., 2000). The top and mid-slope locations consistently had lower soil $\theta_v$. This is mostly likely the result of the influence of slope and increased clay content within the Bt-horizon. As noted above, increased clay creates a less impermeable horizon, resulting in slower percolation and possibly perching of water above the subsoil horizon. This perched water is moved downslope, above the Bt-horizon, under gravity.

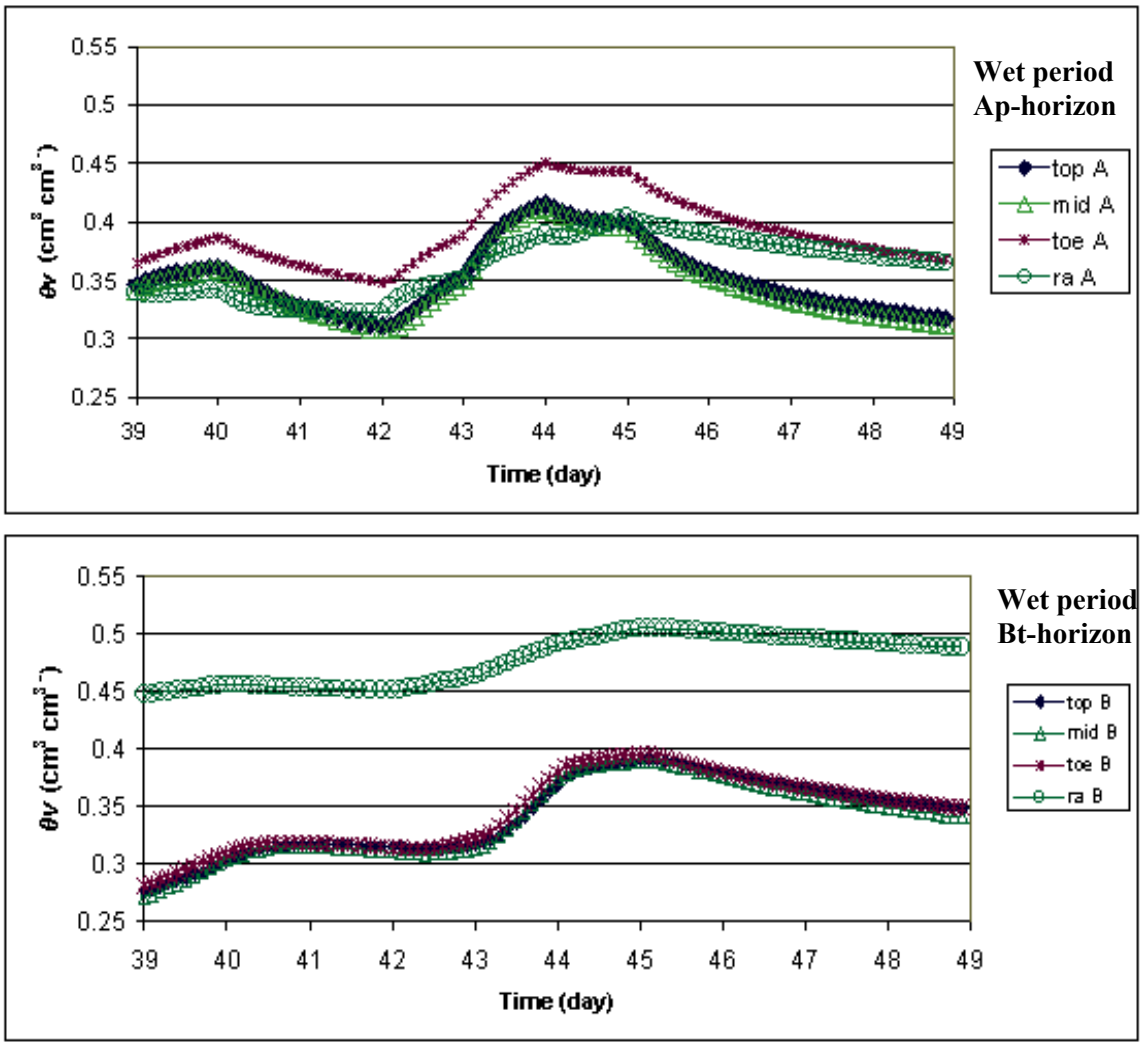


Figure 4-8: Simulated soil $\theta_v$ for watershed during "wet" period per horizon and slope location *.

* Slope locations are defined for Braddock top-slope (top), Braddock mid-slope (mid), Saunook toe-slope (toe), and Rosman riparian (ra).

Figure 4-9 shows the trend of soil $\theta_v$ during the "dry" period. In general, the Bt-horizons had greater soil $\theta_v$ than Ap-horizons. This was expected due to the tighter bond clay particles have with water molecules. The plate-like structure of clay holds water more tightly than silt and sand. As a result, in periods with drier conditions, $\theta_v$ in soils with high clay content is often higher than soils with low clay (McLaren and Cameron, 1996). Higher $\theta_v$ may also be attributed to the absence of dense rooting within this layer. The

high clay content may restrict vertical penetration of fescue roots, thus restricting root water uptake to the Ap-horizons.

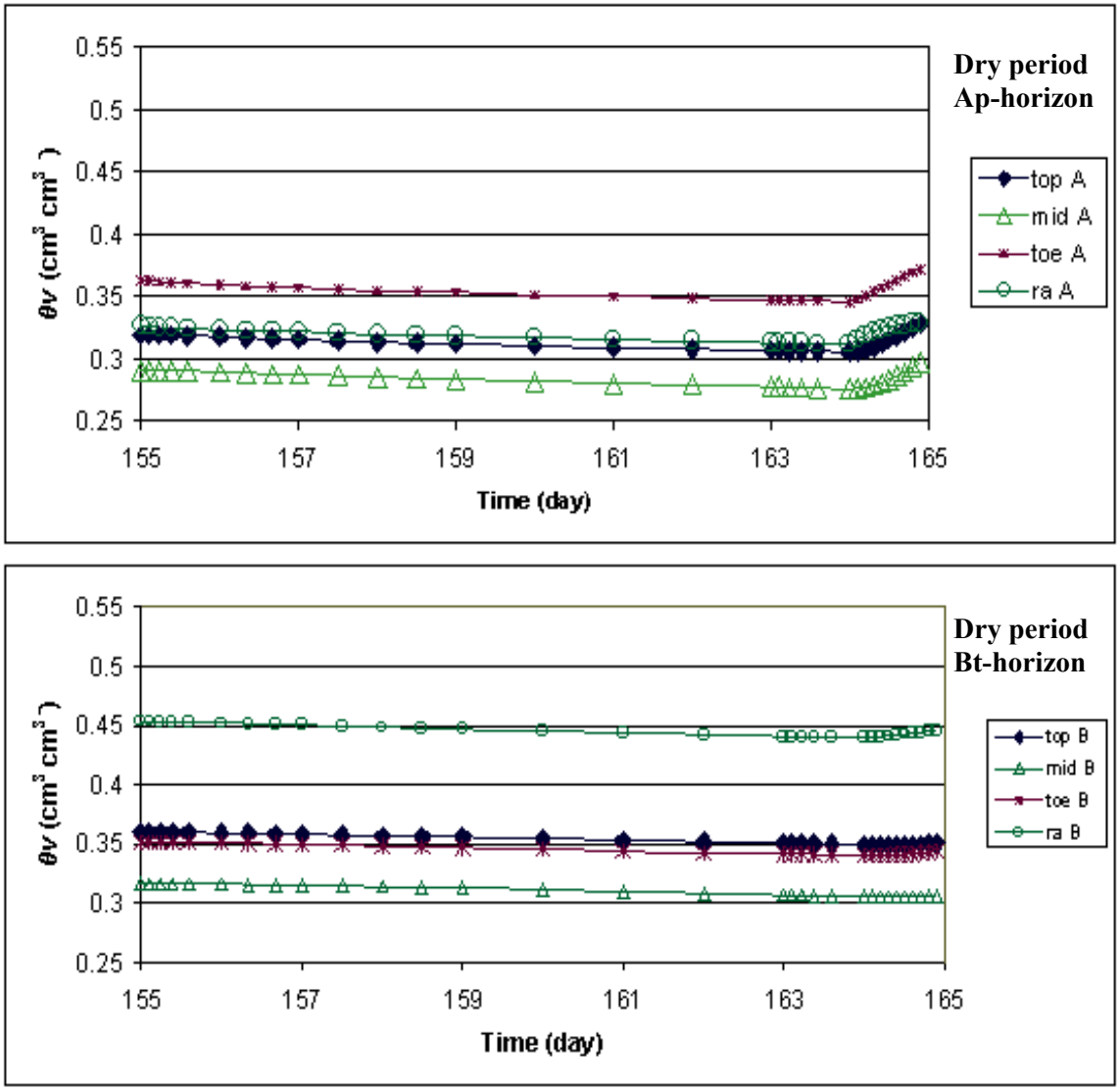


Figure 4-9: Simulated soil $\theta_v$ for watershed during "dry" period per horizon and slope location *.

* Slope locations are defined for Braddock top-slope (top), Braddock mid-slope (mid), Saunook toe-slope (toe), and Rosman riparian (ra).

An analysis of inflow volumes for these two periods helps to illustrate water flow dynamics within the flow domain. Figure 4-10 shows the inflow volume change for the wet (day 40-48) and the dry (156-164) periods. Inflow volumes are displayed by soil

series and horizon for Transect A (Figure 4-1). The general trend of inflow for each slope location increases during the storm, then falls towards an "equilibrium" after the storm has succeeded (day 47-48). The Bt- horizons are consistently higher than Ap-horizons (contrary to $\theta_v$),but this is attributed to the total modeled depth of the Bt-horizon. Average Bt-horizon depth distributed in the model flow domain was approximately 1.5 m, while Ap-horizon depth was 0.2 m. The dry period has inflow values that are slightly negative or at equilibrium for days 155-163, reflecting the absence of precipitation input.

## *Nutrient Flux*

Nitrate ($NO_3^-$ -N) and ammonium ($NH_4^+$ -N) were measured through tension-cup lysimeters located at the top-slope, mid-slope, toe-slope, and riparian area along three transects of the Slagle Farm watershed (Figure 4-5) (Reynolds and Deal, 1986; Walsh, 1971). Paired lysimeters were located in both the Ap- and Bt-horizons. Pasture lysimeters were evacuated bimonthly, while riparian area lysimeters were evacuated weekly and composited to monthly values. Mean monthly nitrogen (mean of three transects by slope locations) are displayed in Tables 4-6 and 4-7. Individual values of $NO_3^-$ -N and $NH_4^+$ -N by transect can be found in Appendix A.

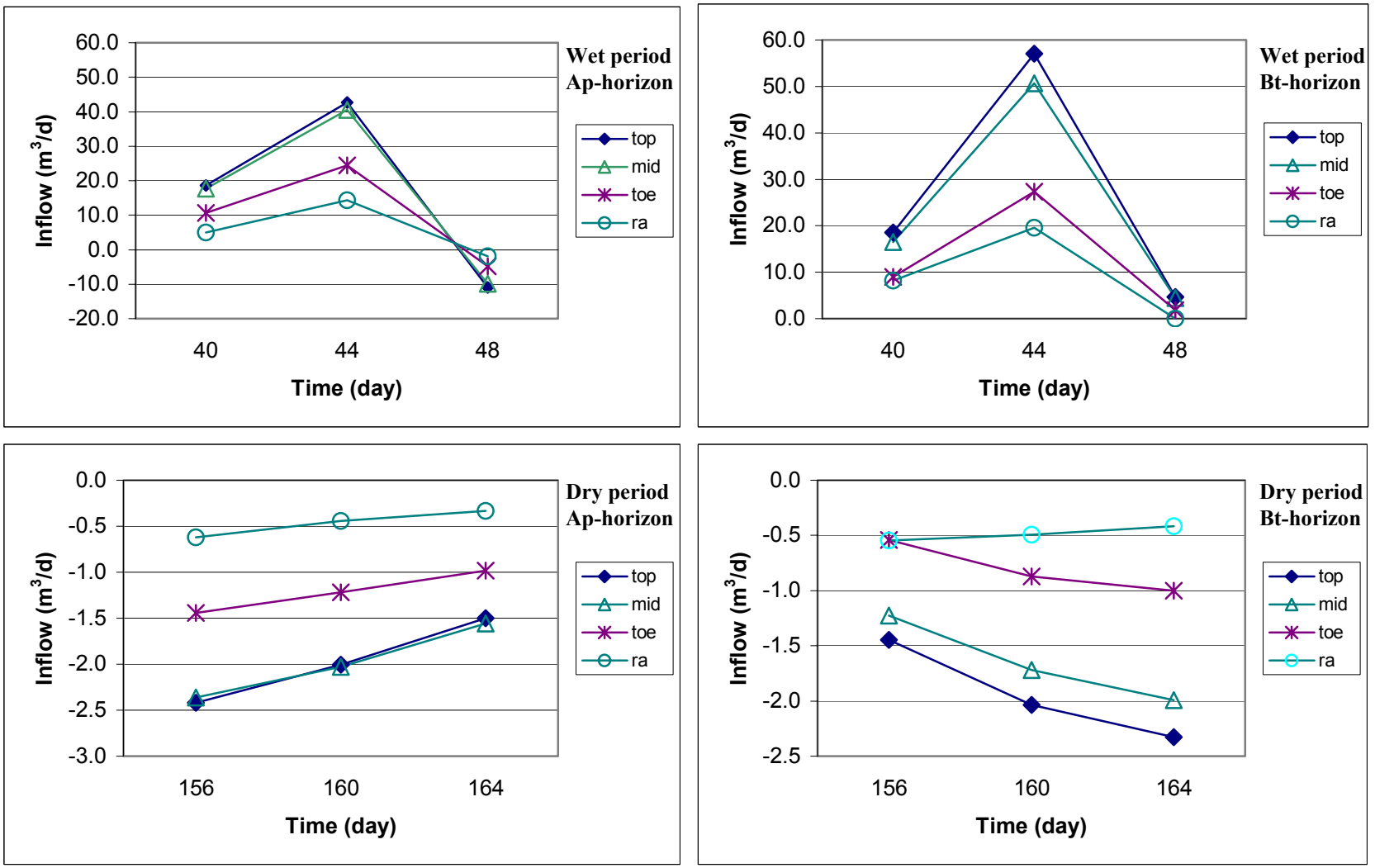


Figure 4-10: Inflow water volumes of study watershed during the "wet" and "dry" periods.

Figures 4-11 and 4-12 show the general trend of $NO_3^-$ -N and $NH_4^+$ -N during the monitoring period. Bt-horizons generally had higher $NO_3^-$ -N than Ap-horizons. This is counter-intuitive to the findings of Gaskin et al. (1989). The authors found that fluxes of $NO_3^-$ -N and other soluble ions ($SO_4$, Cl, etc.) generally decreased with depth. However, the Ap-horizons of the pasture soils in this study are relatively well drained, thus moving $NO_3^-$ out of the surface horizon. The higher $NO_3^-$ -N are most likely attributed to vertical leaching of $NO_3^-$ -N into the soil profile and higher levels of nitrification in the Ap-horizons. Nitrogen did increase over the monitoring duration, which may be a function of seasonal fluctuation. Fescue is relatively dormant during late fall and winter (November, December, January) resulting in less plant uptake of $NO_3^-$.

Higher $NO_3^-$ -N were primarily found in the mid-slope and toe-slope areas of the pasture. $NH_4^+$ -N measurements were slightly higher in the Bt-horizons than for the Ap-horizons. $NH_4^+$ -N were lower than $NO_3^-$ -N, which was expected, due to the readily available state of $NH_4^+$ uptake by vegetation. Similar to $NO_3^-$ -N, $NH_4^+$ -N values were significantly higher for Transect C, than for Transect A and B. These areas seem to be the primary grazing regions for the cattle. It should be noted that Transect C (Figure 4-5) had significantly higher values of $NO_3^-$ -N and $NH_4^+$ -N than Transects A and B (Appendix A) that may be attributed to the proximity of the lysimeters to the primary path of travel for the cattle and the presence of a "hay drop". The hay drop was used by the farm manager to feed the cattle with additional hay from other pastures.

Table 4-6: Monthly mean $NO_3^-$ -N and $NO_3^-$ concentration per horizon of three transects.

Ap-Horizon

| Month | Top-slope | | Mid-slope | | Toe-slope | | Riparian | |
|---|---|---|---|---|---|---|---|---|
| | $NO_3^-$ -N | $NO_3^-$ | $NO_3^-$ -N | $NO_3^-$ | $NO_3^-$ -N | $NO_3^-$ | $NO_3^-$ -N | $NO_3^-$ |
| | (kg/ha) | (mg/L) | (kg/ha) | (mg/L) | (kg/ha) | (mg/L) | (kg/ha) | (mg/L) |
| Aug | 0.03 | 0.30 | 43.13 | 252.56 | 0.62 | 21.79 | 0.004 | 0.11 |
| Sep | 0.12 | 1.21 | 80.35 | 339.75 | 0.78 | 16.26 | 0.000 | 0.01 |
| Oct | 0.19 | 1.65 | 27.99 | 105.68 | 1.93 | 20.11 | 0.006 | 0.16 |
| Nov | 1.43 | 14.15 | 19.48 | 93.22 | 6.26 | 19.69 | 0.004 | 0.12 |
| Dec | 2.14 | 23.26 | 7.81 | 77.63 | 10.47 | 10.17 | 0.007 | 0.21 |
| Jan | 0.88 | 9.05 | 3.12 | 33.34 | 3.21 | 5.19 | 0.018 | 0.48 |
| Feb | 0.36 | 3.59 | 2.24 | 13.61 | 1.03 | 5.74 | 0.037 | 0.84 |
| Mar | 0.06 | 0.57 | 1.40 | 10.24 | 8.28 | 12.00 | 0.016 | 0.36 |

Bt-Horizon

| Month | Top-slope | | Mid-slope | | Toe-slope | | Riparian | |
|---|---|---|---|---|---|---|---|---|
| | $NO_3^-$ -N | $NO_3^-$ | $NO_3^-$ -N | $NO_3^-$ | $NO_3^-$ -N | $NO_3^-$ | $NO_3^-$ -N | $NO_3^-$ |
| | (kg/ha) | (mg/L) | (kg/ha) | (mg/L) | (kg/ha) | (mg/L) | (kg/ha) | (mg/L) |
| Aug | 0.26 | 0.91 | 1.16 | 7.10 | 0.73 | 6.05 | 0.000 | 0.01 |
| Sep | 0.36 | 4.38 | 10.35 | 34.39 | 1.10 | 12.30 | 0.012 | 0.38 |
| Oct | 0.82 | 3.65 | 43.93 | 121.15 | 1.07 | 17.75 | 0.014 | 0.37 |
| Nov | 1.93 | 10.58 | 45.58 | 123.27 | 1.44 | 31.87 | 0.034 | 0.97 |
| Dec | 6.39 | 35.07 | 17.04 | 48.16 | 0.83 | 62.81 | 0.059 | 1.84 |
| Jan | 4.40 | 32.28 | 8.65 | 19.85 | 0.79 | 16.53 | 0.058 | 1.81 |
| Feb | 5.04 | 25.37 | 4.26 | 10.86 | 0.83 | 4.64 | 0.058 | 1.75 |
| Mar | 1.59 | 8.57 | 1.26 | 2.18 | 1.30 | 44.46 | 0.088 | 2.44 |

Table 4-7: Mean monthly $NH_4^+$ -N and $NH_4^+$ concentration per horizon of three transects.

Ap-Horizon

| Month | Top-slope | | Mid-slope | | Toe-slope | | Riparian | |
|---|---|---|---|---|---|---|---|---|
| | $NH_4^+$ -N | $NH_4^+$ | $NH_4^+$ -N | $NH_4^+$ | $NH_4^+$ -N | $NH_4^+$ | $NH_4^+$ -N | $NH_4^+$ |
| | (kg/ha) | (mg/L) | (kg/ha) | (mg/L) | (kg/ha) | (mg/L) | (kg/ha) | (mg/L) |
| Aug | 0.0013 | 0.017 | 42.1534 | 246.846 | 0.0003 | 0.011 | 0.0003 | 0.009 |
| Sep | 0.0023 | 0.025 | 19.2171 | 85.027 | 0.0005 | 0.012 | 0.0014 | 0.011 |
| Oct | 0.0026 | 0.026 | 2.2260 | 18.513 | 0.0062 | 0.075 | 0.0021 | 0.009 |
| Nov | 0.0012 | 0.010 | 1.5958 | 19.180 | 0.0003 | 0.013 | 0.0034 | 0.009 |
| Dec | 0.0047 | 0.045 | 0.0556 | 0.591 | 0.0004 | 0.011 | 0.0022 | 0.005 |
| Jan | 0.0013 | 0.012 | 0.0225 | 0.085 | 0.0008 | 0.015 | 0.0012 | 0.011 |
| Feb | 0.0004 | 0.004 | 0.0081 | 0.033 | 0.0002 | 0.004 | 0.0007 | 0.006 |
| Mar | 0.0009 | 0.008 | 0.0053 | 0.020 | 0.0010 | 1.332 | 0.4780 | 0.002 |

Bt-Horizon

| | Top-slope | | Mid-slope | | Toe-slope | | Riparian | |
|---|---|---|---|---|---|---|---|---|
| | $NH_4^+$ -N | $NH_4^+$ | $NH_4^+$ -N | $NH_4^+$ | $NH_4^+$ -N | $NH_4^+$ | $NH_4^+$ -N | $NH_4^+$ |
| | (kg/ha) | (mg/L) | (kg/ha) | (mg/L) | (kg/ha) | (mg/L) | (kg/ha) | (mg/L) |
| Aug | 0.0010 | 0.011 | 0.3179 | 1.622 | 0.0009 | 0.012 | 0.0000 | null |
| Sep | 0.0012 | 0.010 | 0.0152 | 0.068 | 0.0009 | 0.015 | 0.0004 | 0.010 |
| Oct | 0.0140 | 0.081 | 0.0102 | 0.033 | 0.0015 | 0.014 | 0.0002 | 0.006 |
| Nov | 0.0009 | 0.004 | 0.0051 | 0.015 | 0.0009 | 0.007 | 0.0003 | 0.007 |
| Dec | 0.0042 | 0.021 | 0.0068 | 0.019 | 0.0040 | 0.026 | 0.0002 | 0.004 |
| Jan | 0.0022 | 0.009 | 0.0101 | 0.020 | 0.0017 | 0.013 | 0.0004 | 0.011 |
| Feb | 0.0011 | 0.005 | 0.0011 | 0.004 | 3.6347 | 21.182 | 0.0002 | 0.004 |
| Mar | 0.0029 | 0.011 | 0.0034 | 0.008 | 8.7555 | 47.331 | 0.0001 | 0.004 |

It is very evident that the presence of the riparian area vegetation significantly reduced $NO_3^-$ -N and $NH_4^+$ -N throughout the entire monitoring period. Results from similar studies coincide with this reduction of readily soluble ions such as $NO_3^-$ in subsurface waters (Gaskin et al., 1989; Hubbard and Sheridan, 1983; Hubbard and Lowrance, 1997; Jacobs and Gilliam, 1985; Lowrance et al., 1983). Hubbard and Lowrance (1997) found that an estimated 96 % of $NO_3^-$ was retained, utilized, or transformed in heavily vegetated riparian areas of the Coastal Plain. The authors also found that stream outflow loads of $NO_3^-$ on a mixed agricultural and forested watershed were lower than $NO_3^-$ inputs by rainfall. The findings of these and other studies have repeatedly shown that riparian forests are efficient in assimilating $NO_3^-$ -N that enter from upslope agricultural fields (Hubbard and Lowrance, 1997).

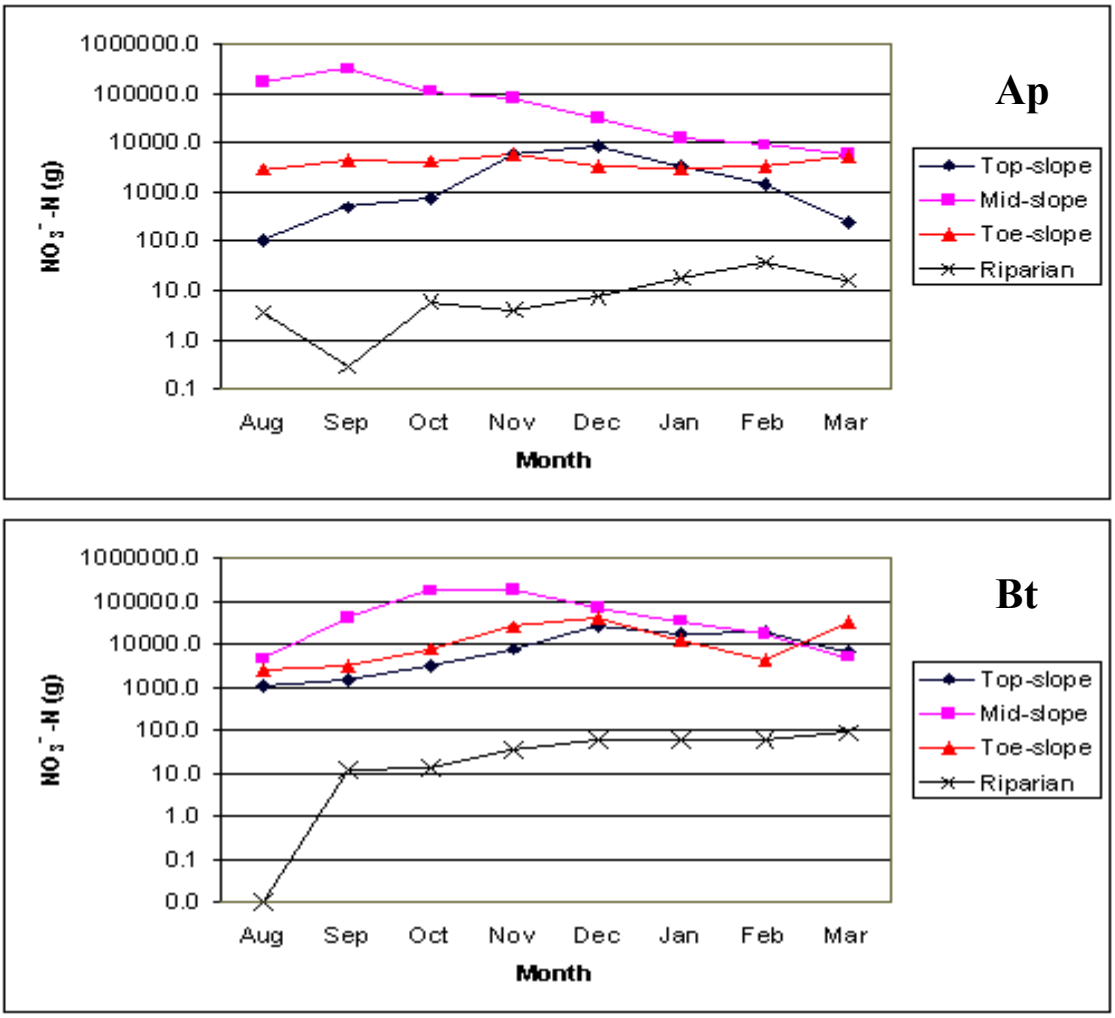


Figure 4-11: Study watershed monthly mean $NO_3^-$ -N for Ap- and Bt-horizons.

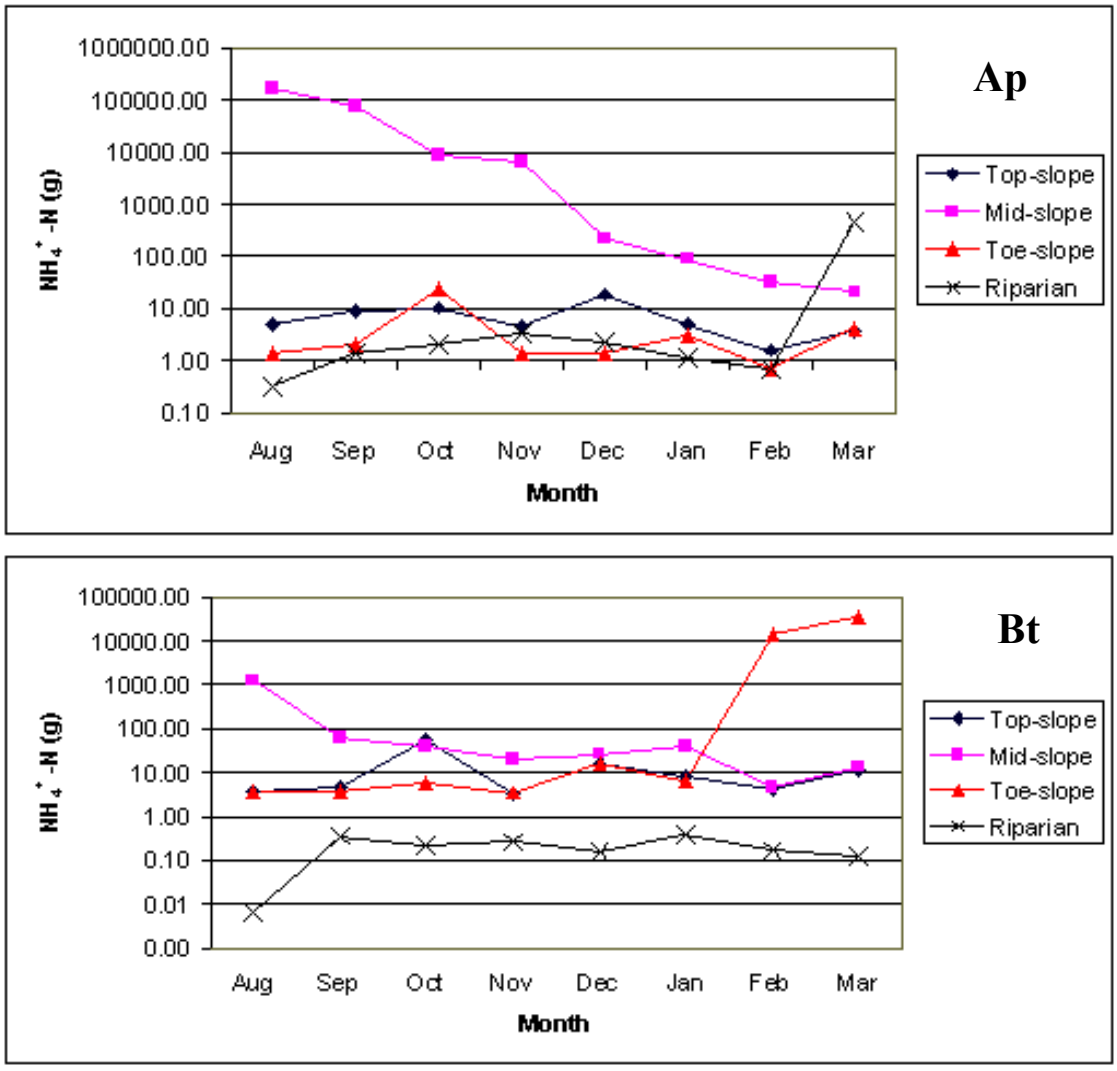


Figure 4-12: Study watershed monthly mean $NH_4^+$ -N for Ap- and Bt-horizons.

The assimilation of nitrogen in subsurface water has been attributed to two primary mechanisms: plant uptake and denitrification. Lowrance (1992) observed that the combination of year-round root growth, concentration of leaf litter and fine root biomass in or near the soil surface were responsible for the nitrogen filtering capacity of a Coastal Plain riparian forest ecosystem. The efficiency of vegetation uptake of $NO_3^-$ -N, however, is influenced by season and requires considerable fine root biomass (< 2 mm diameter (Hill, 1996; Schnabel, 1986). Schnable (1986) also noted that some riparian

zones exhibit storm event variability, and can be influenced by flow duration and intensity. In a small Pennsylvania watershed, Schnable observed that during low flow periods (June and September), $NO_3^-$ concentrations in groundwater decreased by 40 to 70 % during lateral transit through a 16-m grass riparian zone. It is interesting to note in Figures 4-11 and 4-12, that during late January, both $NO_3^-$ -N and $NH_4^+$ -N had relatively decreasing trends for both the Ap- and Bt-horizons in the pasture area. However, $NO_3^-$ concentrations tended to increase in the riparian area. This may be attributed to an increase of microbial nitrification and a decrease of denitrification within this area. Denitrification, which is dependent upon anaerobic conditions, the supply of $NO_3^-$, and high carbon content, may have decreased as a result of decreasing stream stage (Figure 4-6). Through the process of denitrification, where $NO_3^-$ is reduced to the gaseous forms of NO, $N_20$, and $N_2$, nitrogen is lost to the atmosphere as gas (Fisher and Binkley, 2000; Hill, 1996).

Many researchers have pointed to denitrification as the primary mechanism of nitrogen loss (Haycock and Pinay, 1993; Hill, 1996; Hubbard and Sheridan, 1983; Hubbard and Lowrance, 1997; Jacobs and Gilliam, 1985; Lowrance, 1992). Jacobs and Gilliam (1985), in their study of riparian losses of nitrate from agricultural drainage waters, suggested that a substantial part of the $NO_3^-$ in drainage water was denitrified in buffer strips and that uptake by vegetation was insufficient. The authors also observed that almost all of the nitrogen in drainage waters was removed from the subsurface waters prior to reaching the stream. The rate and quantity of denitrification within the Slagle Farm watershed was not measured, but the occurrence of denitrification may be assumed in the riparian area soil during higher stages of Cartoogechaye Creek (Figure 4-6). The

influence of perching of water in and above the Bt-horizons of the pasture soils may have created fluctuating saturated (anaerobic) conditions, resulting in suitable environmental conditions for denitrification.

### *Seasonal Nutrient Flux*

Individual amounts of $NO_3^-$ -N for Transect B will be used to illustrate $NO_3^-$ -N flux within the watershed. $NO_3^-$ -N flux and water volume for Ap- and Bt-horizons, as a function of slope location, are presented in Figure 4-13. $NO_3^-$ -N for the Bt-horizons were consistently higher than Ap-horizons at each slope location (top-slope, mid-slope, toe-slope, and riparian area). The top-slope location Ap-horizon showed an increase of $NO_3^-$ -N from August to November, and August to December for the Bt-horizon. Both the mid-slope and toe-slope locations had an increase of $NO_3^-$ -N from August to October for the Ap-horizon, and an increase of $NO_3^-$ -N from August to December. Water volumes for the Ap-horizon pasture locations were relatively steady during the monitoring period, while Bt-horizon water volumes steadily increased. Though peak $NO_3^-$ -N in the pasture Bt-horizons generally lagged behind Ap-horizon $NO_3^-$ -N, they were significantly higher. This may be attributed to the vertical leaching of $NO_3^-$ -N into the soil profile. Again, the influence of plant uptake may be attributed to lower $NO_3^-$ -N in the Ap-horizons.

The riparian area Ap-horizon had an increase of $NO_3^-$ -N during September and October, and again from January to March. The Bt-horizon showed a similar increase of $NO_3^-$ -N from August to November and January to March. The increase of $NO_3^-$ -N may be related to precipitation inputs upslope within the pasture (Figure 4-4). Intense precipitation events occurred in late September and again in late January through March.

Results of simulated subsurface flow calculated in HYDRUS 2-D revealed that preferential lateral flow occurred in and above the pasture Bt-horizons. This storm dependent rapid transport of $NO_3^-$ -N may have moved the readily soluble $NO_3^-$ -N through the pasture and into the riparian area before assimilation or transformation could occur.

The increasing amount of $NO_3^-$ -N for all sampling locations during August, September, and October may be attributed to bacterial nitrification. Bacterial activity is sensitive to aeration, soil water content, pH, and temperature (Barnes et al., 1998). During these warmer months, bacterial activity is greatest, resulting in higher rates of nitrification. As conditions become cooler during winter months (November, December, January) bacterial nitrification populations generally decrease, resulting in a reduction of nitrification produced $NO_3^-$. However, microbial denitrification is also relatively low during winter months, resulting in lower rates of nitrogen transformation. Removal of $NO_3^-$ in plant uptake is also reduced during the dormant season. The combined affect of high precipitation, low evapotranspiration, low denitrification, and low uptake by vegetation can result in rapid transport of high $NO_3^-$ in both surface and subsurface water (Groffman et al., 1996; Hill, 1996).

Regressional analysis was conducted to identify a statistically significant relationship between $NO_3^-$ -N and water volume. The objective of this regression was to determine if $NO_3^-$ -N transport increased as a function of increased water volume. The analysis revealed no significance (p-value = 0.64) between $NO_3^-$ -N and water volume. Many other processes, such as biological activity, soil pH, and soil temperature, influence the release of $NO_3^-$ (Groffman et al., 1996).

The amount of $NO_3^-$ -N in the riparian area was significantly lower than $NO_3^-$ -N within the pasture. Figure 4-14 shows monthly $NO_3^-$ -N flux per slope location throughout the monitoring period. Each month shows an increase of $NO_3^-$ -N at the toe-slope location. This increase is less distinct for the Ap-horizons, but much more

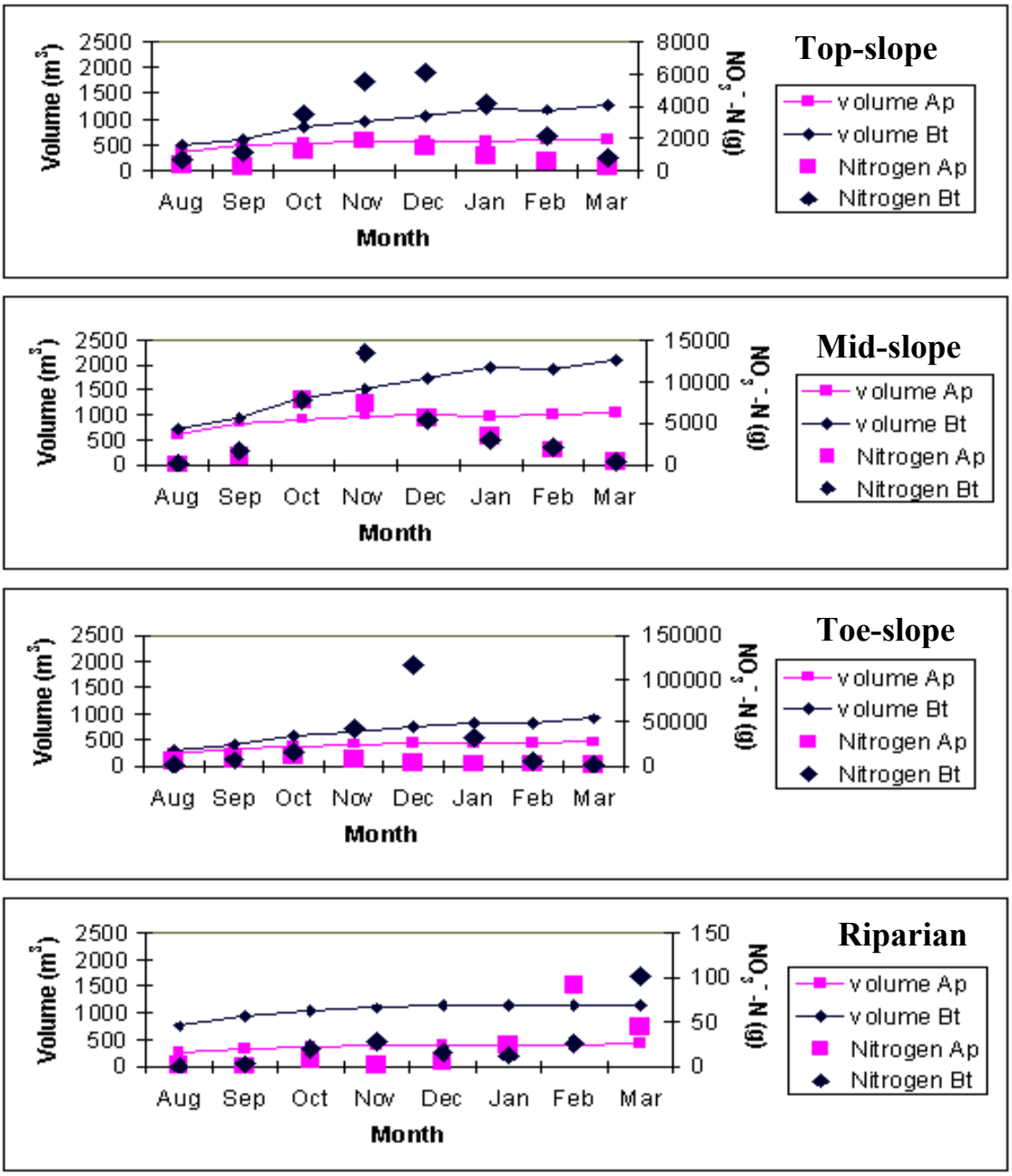


Figure 4-13: $NO_3^-$ -N and water volumes for Top-slope, Mid-slope, Toe-slope, and riparian for Transect B.

pronounced for Bt-horizons. This increase may be attributed to the increased accumulation of $NO_3^-$ -N as water moved vertically into the soil profile as well as from upslope positions to the more gentle slopes of the toe-slope area. $NO_3^-$ -N is greatly reduced in the riparian area, which may be a result of both assimilation and denitrification.

Figure 4-15 shows monthly $NH_4^+$ -N flux per slope location. The overall amount of $NH_4^+$ -N was significantly lower than $NO_3^-$ -N. This is trend is most likely attributed to the transformation of $NH_4^+$ to $NO_3^-$ through nitrification (Fisher and Binkley, 2000). $NH_4^+$ is released directly from organic nitrogen pools (manure, urea, vegetation) through mineralization and is often oxidized to nitrite ($NO_2^-$) then to $NO_3^-$ through nitrification. As a result, much of the available $NH_4^+$ is assimilated into plants or transformed in $NO_3^-$.

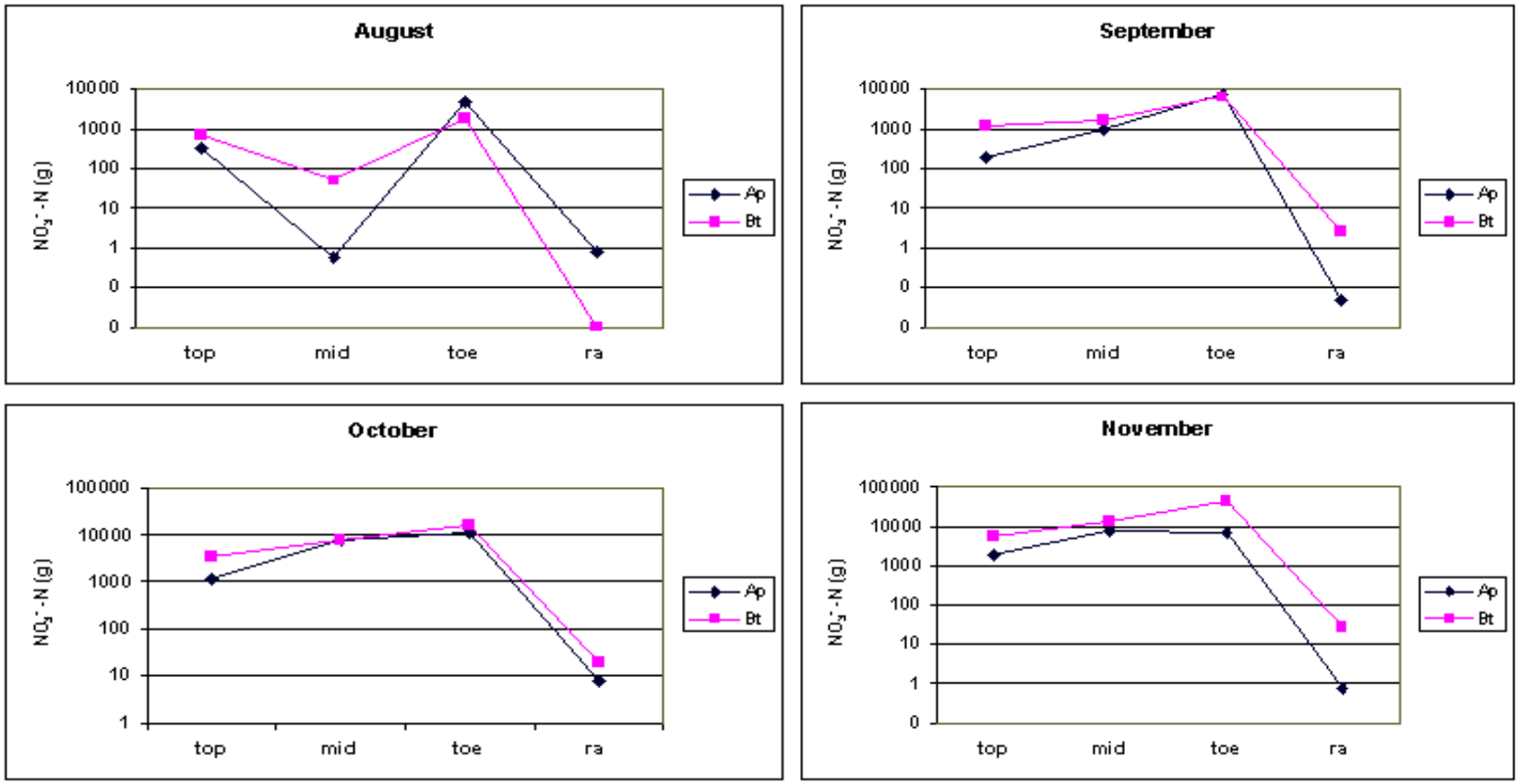


Figure 4-14: Monthly $NO_3^-$-N per horizon and slope location for Transect B.

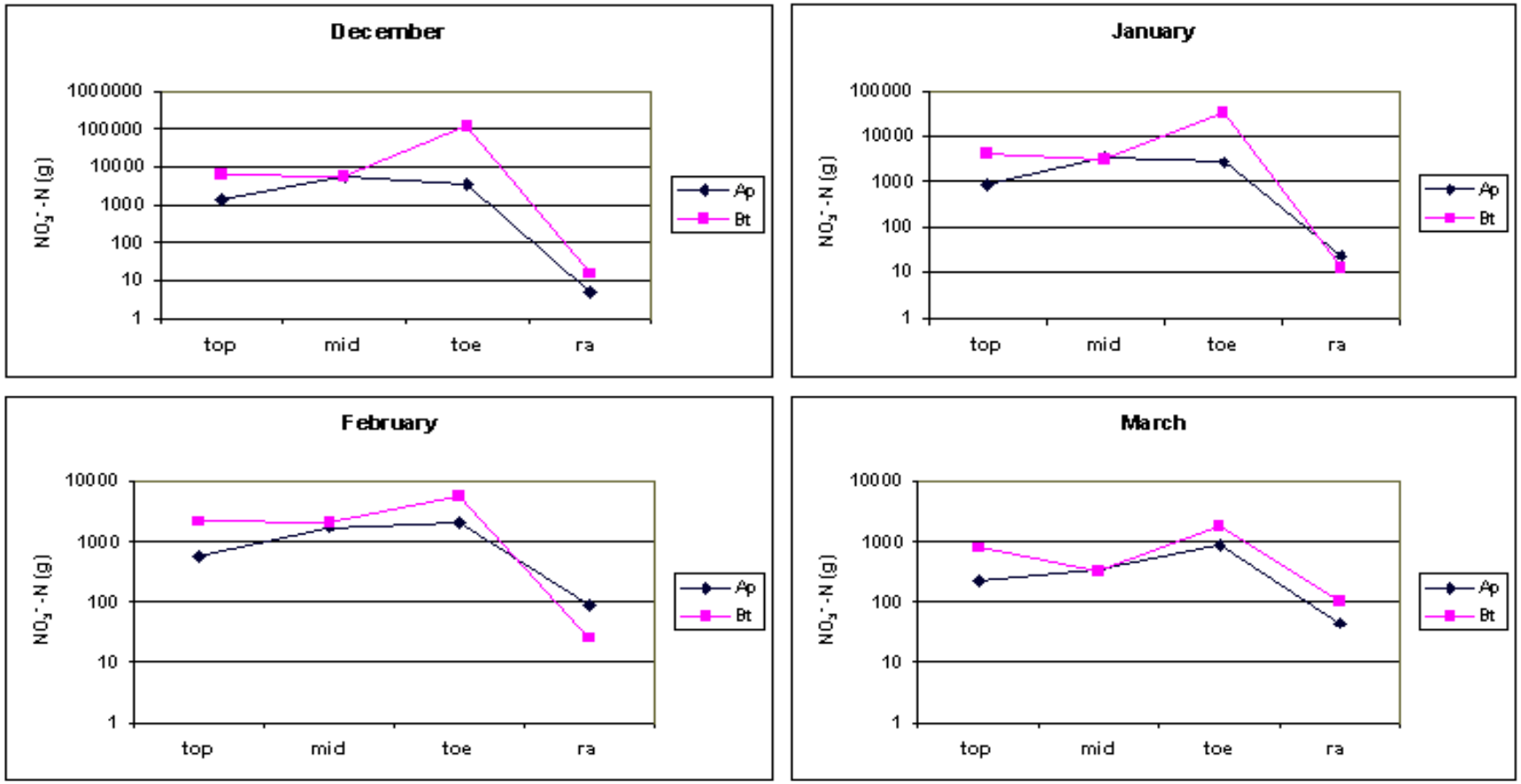


Figure 4-14 Con't: Monthly $NO_3^-$ -N per horizon and slope location for Transect B.

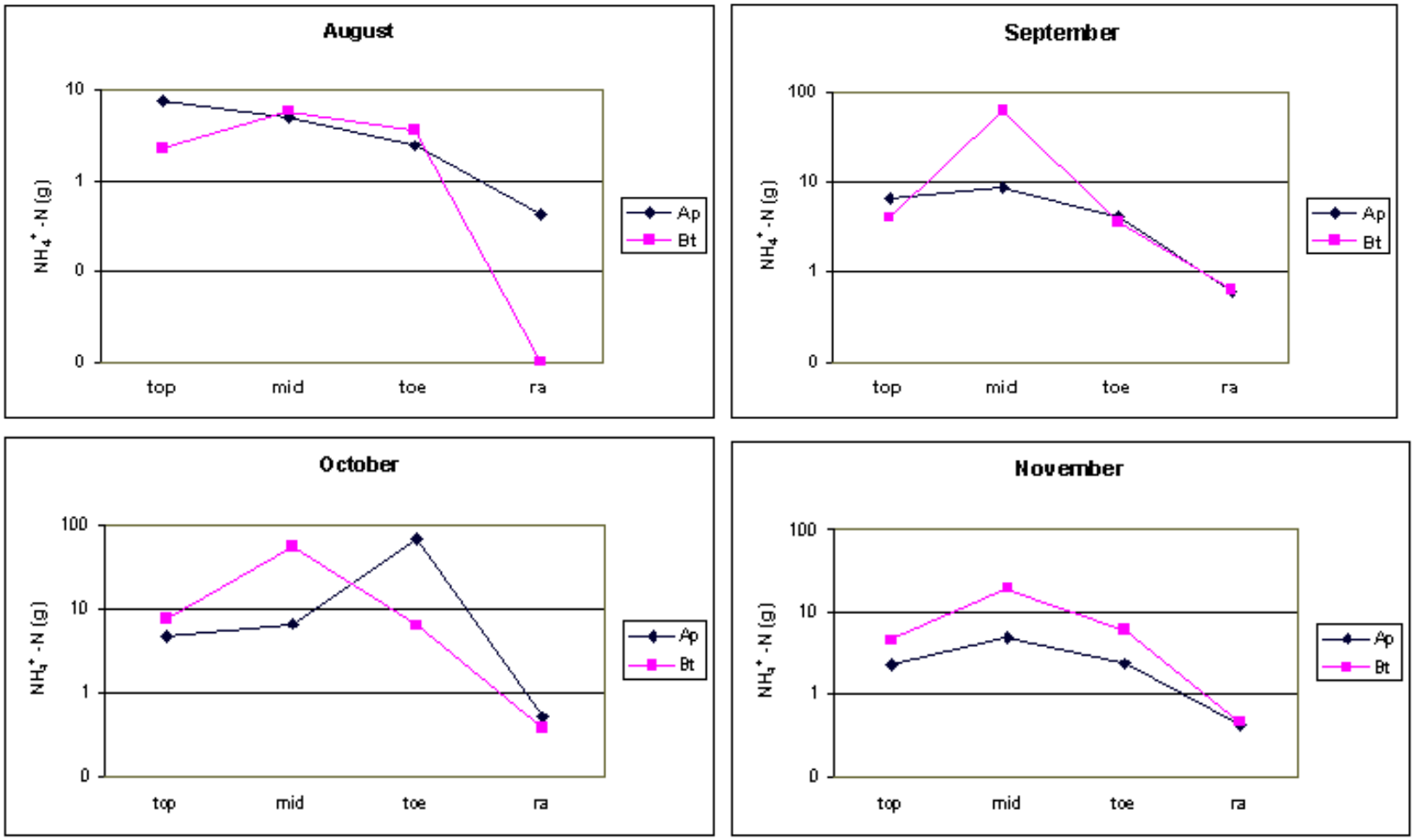


Figure 4-15: Monthly $NH_4^+$ per horizon and slope location for Transect B.

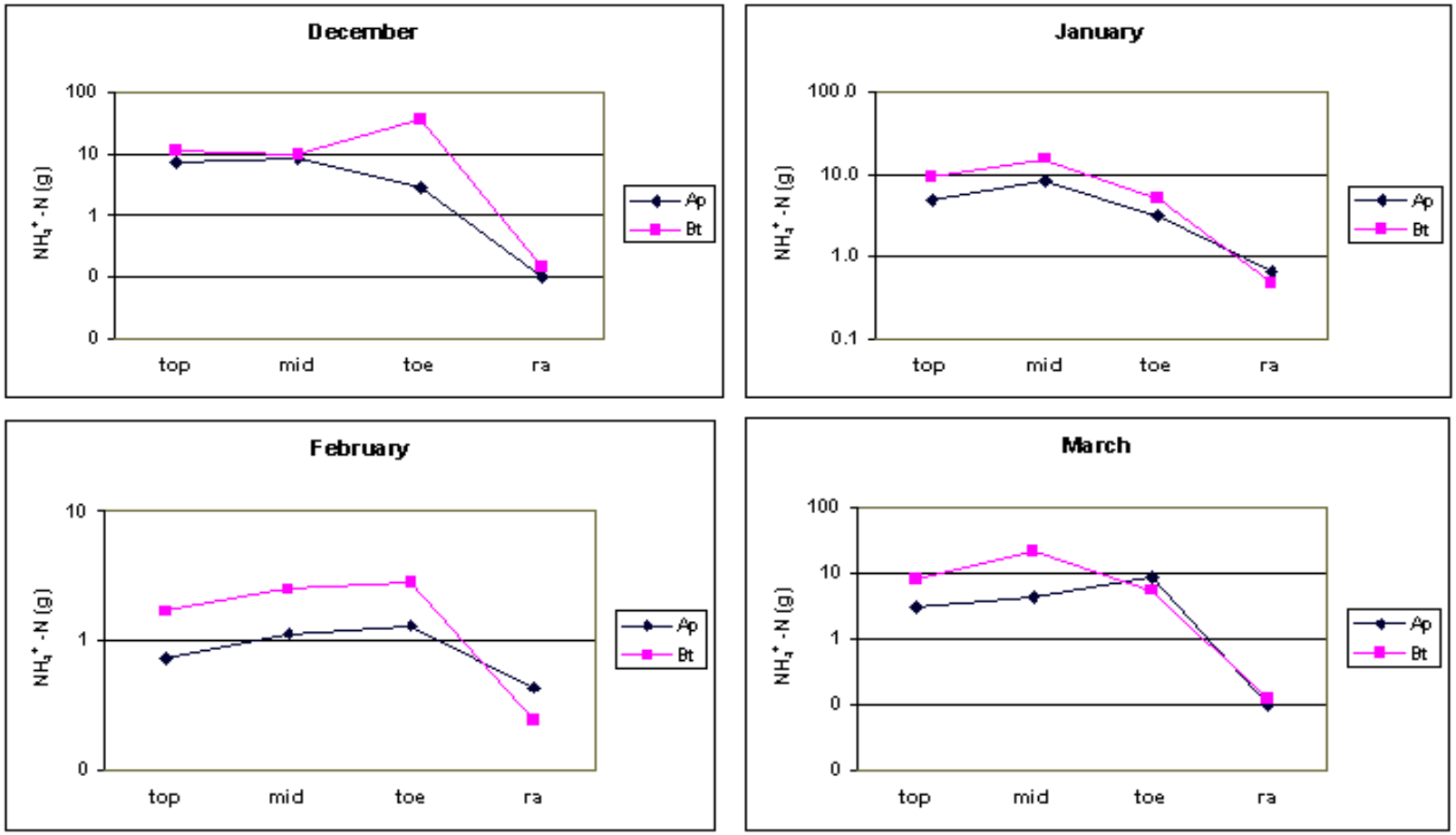


Figure 4-15 Con't: Monthly $NH_4^+$ per horizon and slope location for Transect B.

## Conclusion

The objective of this paper was to quantify and qualify surface and subsurface hydrological transport of nitrate and ammonium within the Slagle Farm watershed. Field observed data was used to characterize nutrient concentrations as a function of slope location, while the HYDRUS 2-D transport model was used to simulate and predict subsurface water flux as a function on precipitation input. The most significant finding of this paper was the dramatic reduction of observed $NO_3^-$ and $NH_4^+$ within the riparian area.

$NO_3^-$ -N and $NH_4^+$ -N showed distinct seasonal trends in soil water with higher values in winter months and lower $NO_3^-$ -N and $NH_4^+$ -N during summer months. Both $NO_3^-$ -N and $NH_4^+$ -N in the pasture soils showed increasing amounts in late summer, while $NO_3^-$ -N and $NH_4^+$ -N in the riparian area had a second peak during winter. $NO_3^-$ -N and $NH_4^+$ -N during the warmer months were attributed to higher rates of nitrification and lower rates of denitrification (drier conditions). During the cooler months, $NO_3^-$ -N and $NH_4^+$ -N increased most likely as a result of decreased denitrification (gaseous loss to atmosphere) and lower assimilation of nutrients through vegetative uptake. The amount of $NO_3^-$ -N and $NH_4^+$ -N seemed to be influenced by both season and storm events. During the warmer periods with high precipitation, $NO_3^-$ -N and $NH_4^+$ -N were lower due to assimilation, while during cooler months and high precipitation, $NO_3^-$ -N and $NH_4^+$ -N were mobilized and transported through subsurface flow.

The presence of the riparian zone drastically reduced the amount of $NO_3^-$ -N and $NH_4^+$ -N in subsurface water traveling from upslope pasture areas. This reduction of nutrient content from receiving waters supports the need for the implementation of

riparian areas as streamside management zones to reduce non-point source pollutions to aquatic ecosystems.

# References


Anderson, M.G., and T.P. Burt. 1990. Subsurface Runoff, p. 368-380, *In* M.G. Anderson and T.P Burt, ed. Process Studies in Hillslope Hydrology. John Wiley and Sons Ltd., West Essex, England. p. 539.

Anderson, S.P., W.E. Dietrich, D.R. Montgomery, R. Torres, M.E. Conrad, and K. Loague. 1997. Subsurface flow paths in a steep, unchanneled catchment. Water Resourc. Res. 33:2637-2653.

Barnes, B.V., D.R. Zak, S.R. Denton, and S.H. Spurr. 1998. Nutrient Cycling, p. 524-575, *In* B. V. Barnes, et al., eds. Forest Ecology, Fourth ed. John Wiley & Sons, Inc., New York. p. 774.

Bosch, D.D., R.K. Hubbard, L.T. West, and R.R. Lowrance. 1994. Subsurface flow patterns in a riparian buffer systems. Trans. Am. Soc. Agric. Engrs. 37:1783-1790.

Brooks, R.H., and A.T. Corey. 1966. Properties of porous media affecting fluid flow. J.Irrig. Drainage Div., ASCE Proc. 72:61-88.

Corvallis Microtechnology, Inc. 1998a. PC-GPS. Release 3.7D. Corvallis Microtechnology, Inc., Corvallis, OR.

Corvallis Microtechnology, I. 1998b. GPS-HP-L4. Corvallis Microtechnology, Inc., Corvallis, OR.

Dahm, C.N., N.B. Grimm, P. Marmonier, H.M. Valett, and P. Vervier. 1998. Nutrient dynamics at the interface between surface waters and groundwaters. Freshwater Biol 40:427-451.

Fetter, C.W. 2001. Properties of Aquifers, In P. Lynch, ed. Applied Hydrogeology, Fourth ed. Prentice Hall, Upper Saddle River, NJ. p. 598.

Fisher, R.F., and D. Binkley. 2000. Ecology and Management of Forest Soils. John Wiley and Sons, Inc., New York. p. 489.

Gaskin, J.W., J.F. Dowd, W.L. Nutter, and W.T. Swank. 1989. Vertical and lateral components of soil nutrient flux in a hillslope. J. Environ. Qual. 18:403-410.

Golden Softwrare, Inc. 1999. User's Guide: Contouring and 3D Surface Mapping for Scientists and Engineers. Release 6.04. Golden Softwrare, Inc., Golden, CO.

Groffman, P.M., G. Howard, A.J. Gold, and W.M. Nelson. 1996. Microbial Nitrate Processing in Shallow Groundwater in a Riparian Forest. J. Environ. Qual. 25:1309-1316.

Haycock, N.E., and G. Pinay. 1993. Groundwater nitrate dynamics in grass and poplar vegetated riparian buffer strips during winter. J. Environ. Qual. 22:273-278.

Hedin, L.O., J.J. Armesto, and A.H. Johnson. 1995. Patterns of nutrient loss from unpolluted, old-growth temperate forests: Evaluation of biogeochemical theory. Ecology 76:493-509.

Heppell, C.M., T.P. Burt, and R.J. Williams. 2000. Variations in the hydrology of an underdrained clay hillslope. J. Hydrol. 227:236-256.

Hill, A.R. 1996. Nitrate removal in stream riparian zones. J. Environ. Qual. 25:743-755.

Hubbard, R.K., and J.M. Sheridan. 1983. Water and nitrate-nitrogen losses from small, upland, coastal plain watershed. J. Environ. Qual. 12:291-295.

Hubbard, R.K., and R.R. Lowrance. 1997. Assessment of forest management effects on nitrate removal by riparian buffer systems. Transactions of the ASAE 40:383-391.

Jackson, R. 1992. Hillslope infiltration and lateral downslope unsaturated flow. Water Resour. Res. 28:2533-2539.

Jacobs, T.J., and J.W. Gilliam. 1985. Riparian losses of nitrate from agricultural drainage waters. J. Environ. Qual. 14:472-478.

Kao, C., S. Bouarfa, and D. Zimmer. 2001. Steady state analysis of unsaturated flow above shallow water-table aquifer drained by ditches. J. Hydrol. 250:122-133.

Lowrance, R.R. 1992. Groundwater nitrate and denitrification in a coastal plain riparian forest. J. Environ. Qual. 21:401-405.

Lowrance, R.R., R.L. Todd, and L.E. Asmussen. 1983. Waterborne nutrient budgets for the riparian zone of an agricultural watershed. Agric., Ecosyst., & Environ. 10:371-384.

Mailhol, J.C., P. Ruelle, and I. Nemeth. 2001. Impact of fertilisation practices on nitrogen leaching under irrigation. Irrig. Sci. 20:139-147.

McLaren, R.G., and K.C. Cameron. 1996. The storage of water in soils, p. 71-86, Soil Science. Oxford University Press, Oxford. p. 314.

Mulholland, P.J. 1993. Hydrometric and stream chemistry evidence of three storm flowpaths in Walker Branch Watershed. J. Hydrol. 151:291-316.

Pang, L., M.E. Close, J.P.C. Watt, and K.W. Vincent. 2000. Simulation of picloram, atrazine, and simazine leaching through two New Zealand soils and into groundwater using HYDRUS-2D. J. Contaminant Hydrol. 44:19-46.

Peterjohn, W.T., and D.L. Correll. 1984. Nutrient dynamics in an agricultural watershed: Observations on the role of riparian forests. Ecology 65:1466-1475.

Reynolds, B.C., and J.M. Deal. 1986. Procedures for Chemical Analysis at the Coweeta Hydrologic Laboratory. Coweeta Hydrologic Laboratory, Otto, NC.

Schnabel, R.R. 1986. Bitrate concentrations in a small stream as affected by chemical and hydrologic interactions in the riparian zone, *In* D. L. Correll, ed. Watershed research perspectives. Smithsonian Institute, Washington, DC. p. 263-281.

Schultz, R.C., T.M. Isenhart, and J.P. Colletti. 1994. Riparian Buffer Systems in Crop and Rangelands. Agroforestry and Sustainable Systems: Symposium Proceedings August 1994. p. 13-27.

Simunek, J., M. Sejna, and M.T.v. Genuchten. 1999. The Hydrus-2D Software Package for Simulating the Two-Dimensional Movement of Water, Heat, and Multiple Solutes in Variably-Saturated Media. p. 227.

Simunek, J., M.T. van Genuchten, M.M. Gribb, and J.W. Hopmans. 1998. Parameter estimation of unsaturated soil hydraulic properties from transient flow processes. Soil & Tillage Research 47:27-36.

Swanson, F.J., S.V. Gregory, J.R. Sedell, and A.G. Campbell. 1982. Land-Water Interactions: The Riparian Zone, p. 267-291, *In* R. L. Edmonds, ed. Analysis Of Coniferous Forest Ecosystems In The Western United States. Hutchinson Ross Publishing Company, Stroudsburg, PA. p. 419.

Triska, F.J., J.H. Duff, and R.J. Avanzino. 1990. Influence of exchange flow between the channel and hyporheic zone on nitrate production in a small mountain stream. Can. J. Fish. Aquat. Sci. 47:2099-2111.

United States Department of Agriculture, Natural Resources Conservation Service. 1996. Soil Survey of Macon County, North Carolina. p. 322.

van Genuchten, M.T. 1980. A closed-form equation for predicting the hydraulic conductivity of unsaturated soils. Soil Sci. Am. J. 44:892-898.

Vogel, T., and M. Cislerova. 1988. On the reliability of unsaturated hydraulic conductivity calculated from the moisture retention curve. Transp. Porous Media 3:1-15.

Vos, J.A., D. Hesterberg, and P.A. Raats. 2000. Nitrate Leaching in a Tile-Drained Silt Loam Soil. Soil Sci. Soc. Am. J. 64:517-527.

Walsh, L.M. 1971. Instrumental Methods for Analysis of Soils and Plant Tissue. *In* A. Klute, ed. Methods of Soil Analysis: Part 1-Physical and Mineralogical Methods, 2 ed. ASA, Inc. and SSSA, Inc., Madison, WI. p. 1188.

Wilson, G.V., P.M. Jardine, R.J. Luxmoore, and J.R. Jones. 1990. Hydrology of a forested hillslope during storm events. Geoderma 56:119-138.

Yeakley, J.A., B.W. Argo, D.C. Coleman, J.M. Deal, B.L. Haines, B.D. Kloeppel, J.L. Meyer, W.T. Swank, and S.F. Taylor. 2003. Hillslope nutrient dynamics following upland riparian vegetation disturbances. Ecosystems 6:154-167.

# Chapter 5: Summary and Conclusions

The objective of this project was to utilize observed watershed soil, nutrient, hydrological, and meteorological data to quantify and qualify subsurface hydrological dynamics and nutrient transport within the Slagle Farm watershed. The culmination of observed soil characteristics, observed and simulated hydrology, nutrient concentration, and meteorological were used to characterize water and nutrient flux across heterogeneous soil materials.

Individual soil characteristics, such as particle size distribution, bulk density, and saturated hydraulic conductivity, influenced how and when water moved through specific soil materials (series/horizon). The presence of a less permeable Bt-horizon had higher $\theta_v$ during dry conditions (function of clay content), while during wet conditions water seemed to perch above this higher density horizon.

HYDRUS 2-D was used to simulate water flow (saturated and unsaturated) during a period of approximately 8 months (August 2002 to March 2003). In an attempt to characterize periods of potentially high precipitation with low surface resistance (low vegetation surface friction, and low evapotranspiration), much of the monitoring period occurred during the fall and winter seasons. This 8-month block was used to differentiate water flow as a function of season. The seasonal interaction of precipitation, evapotranspiration, and soil $\theta_v$ influenced stream stage accordingly. In periods of high precipitation and evapotranspiration, stream stage was low. In periods of lower precipitation and evapotranspiration, stream stage generally increased.

HYDRUS 2-D was capable of simulating the general trend of soil water content ($\theta_v$) and matched reasonably well with observed field data. However, there were

discrepancies. Simulated $\theta_v$ was consistently over-estimated for the Ap-horizons. This is most likely attributed to how HYDRUS 2-D regards infiltration at the surface of the flow domain. Only one boundary condition can be assigned to the surface nodes within the model flow domain. An atmospheric boundary condition was utilized in the scenario described in this paper to account for plant root water uptake. As a result, HYDRUS 2-D assumed that all rainwater was infiltrated into the surface horizon. Though this may be contrary to actual field conditions, one must make rational assumptions when using modeling programs such as HYDRUS 2-D. Another notable discrepancy was the root water uptake distribution. It was assumed that fescue covered the entire flow domain outside of the stream furrow. However, in the field, there are areas of low to no fescue coverage. As a result, evapotranspiration may have been over-estimated in the model. HYDRUS 2-D was very beneficial in predicting variables that are often difficult to measure under field conditions. One such variable, evapotranspiration, was predicted through HYDRUS 2-D model. Actual Et was calculated parameterized by atmospheric conditions, precipitation, and a plant stress function, which accounts for root water uptake of prescribed species.

In general, HYDRUS 2-D simulated acceptable trends in $\theta_v$. However, as with any modeling, validation and calibration should be implemented before definitive conclusions are made. Validation and calibration were outside the scope of this specific paper, but will be conducted in the near future.

Field observed data was used to characterize nutrient flux as a function of slope location, while the HYDRUS 2-D transport model was used to simulate and predict subsurface water flux as a function on precipitation input. The most significant finding of

this paper was the dramatic reduction of observed $NO_3^-$ and $NH_4^+$ within the riparian area.

$NO_3^-$ -N and $NH_4^+$ -N showed distinct seasonal trends in soil water with higher values in winter months with lower values during summer months. Both $NO_3^-$ -N and $NH_4^+$ -N in the pasture soils showed increases in late summer, while the riparian area had a second peak of nitrogen during winter. $NO_3^-$ -N and $NH_4^+$ -N during the warmer months were attributed to higher rates of nitrification and lower rates of denitrification (drier conditions). During the cooler months, $NO_3^-$ -N and $NH_4^+$ -N increased most likely as a result of decreased denitrification (gaseous loss to atmosphere) and lower assimilation and uptake of nutrients by vegetation. $NO_3^-$ -N and $NH_4^+$ -N seemed to be influenced by both season and storm events. During the warmer periods with high precipitation, $NO_3^-$ -N and $NH_4^+$ -N were lower due to assimilation, while during cooler months and high precipitation, $NO_3^-$ -N and $NH_4^+$ -N were mobilized and transported through subsurface flow.

The presence of the riparian zone drastically reduced the amount of $NO_3^-$ -N and $NH_4^+$ -N in subsurface water traveling from upslope pasture areas. This reduction of nutrient content from receiving waters supports the need for the implementation of riparian areas as streamside management zones to reduce non-point source pollutions to aquatic ecosystems.

The most significant findings of this research are as follows:

- The presence of a less permeable subsurface soil horizon resulted in rapid transport of subsurface lateral flow of water and nitrogen downslope

- HYDRUS 2-D was capable of simulating subsurface flow (saturated and unsaturated) as a function of observed soil physical properties (bulk density, saturated hydraulic conductivity, particle size distribution, water retention characteristics) and climatic data (precipitation, air temperature, wind speed, etc.).
- HYDRUS 2-D was successful in predicting complex processes, such as evapotranspiration, hyporheic exchange of riparian area and Cartoogechaye Creek, and the transition of water flow from saturated to unsaturated flow, that are often difficult to measure *in situ*.
- $NO_3^-$ -N and $NH_4^+$ -N decreased significantly as subsurface water moved from upslope pasture to riparian area.
- $NO_3^-$ and $NH_4^+$ were removed from subsurface water in the riparian area through plant uptake and possibly denitrification, prior to reaching Cartoogechaye Creek.
- The riparian area was effective in reducing the amount of nonpoint source pollution to a naturally developing riparian area from an agricultural watershed.

As with any research project, many questions were created from answers. There are many potential future studies that can be conducted within the Slagle Farm watershed to quantify and qualify nutrient and hydrologic dynamics within the watershed. A comprehensive study of denitrification and nitrification within the pasture and riparian area may assist in understanding the rate of nitrogen transformation and a refinement of a comprehensive nitrogen budget.

An integral component of the hydrologic and nutrient transport cycle not measured in this study was overland flow (surface flow) and the interaction of overland flow water with subsurface flow. Though the component of overland was dismissed for this specific

study, research has shown that overland flow may be a significant process of nutrient transport. The use of piezometers and tensiometers may be implemented to observe *in situ* saturated and unsaturated flow within the watershed. Measurements of saturated and unsaturated flow can be coupled with an extensive array of overland flow collectors to describe the interaction of soil water content, saturated and unsaturated flow, and overland flow.

The use of HYDRUS 2-D may be used (as in this study) to predict subsurface water flow dynamics, but may also be used to predict solute transport. The HYDRUS 2-D model platform will be used by the author in the near future to simulate $NO_3^-$ and $NH_4^+$ as a function of water transport and compared to observed nutrient dynamics.

A study of stream water chemistry may also be used to quantify actual nitrogen export from the agricultural watershed and riparian area to Cartoogechaye Creek. The export of nutrients to the stream can be quantified through use of automatic stream samplers (Sigma waste-water samplers) located at the top and bottom of the Cartoogechaye Creek drained by the Slagle Farm watershed. This study can assist in understanding further dynamics of the riparian/aquatic ecosystem interface and the mechanisms influencing nitrogen transport in fully saturated systems.

# Appendix A: $N0_3^-$-N and $NH_4^+$ -N for three transects

Table 1: Individual values of $NO_3^-$ -N for each transect

| Month | Top-slope Ap | Mid-slope Ap | Toe-slope Ap | Riparian Ap | Top-slope Bt | Mid-slope Bt | Toe-slope Bt | Riparian Bt |
|---|---|---|---|---|---|---|---|---|
| | $NO_3^-$ -N per horizon and slope location for three transects | | | | | | | |
| | N (g) | N (g) | N (g) | N (g) | N (g) | N (g) | N (g) | N (g) |
| **Transect A** | | | | | | | | |
| Aug | 0.24 | 28.32 | 833.25 | 0.06 | 113.75 | 2721.23 | 3136.245 | 0 |
| Sep | 269.31 | 3611.76 | null | 0.03 | 2415.99 | 36783.615 | 2076.575 | 16.53 |
| Oct | 871.105 | 2548 | 83.765 | 0.03 | 3037.91 | 85151.31 | 2958.22 | 5.55 |
| Nov | 15188.075 | 37688.92 | null | 0.12 | 9825.47 | 27437.58 | null | 16.725 |
| Dec | 24136.975 | 70168.875 | 3171.325 | 0.045 | 44704.755 | 11541.145 | 2508.9 | 50.46 |
| Jan | 9637.465 | 25700.585 | 5098.3 | 0.51 | 48224.335 | 7088.28 | 4268.3 | 58.545 |
| Feb | 3091.17 | 15225.43 | 5659.61 | 0.765 | 58019.79 | 1806.925 | 5423.515 | 23.43 |
| Mar | 511.2 | 8492.26 | 2688.96 | 0.18 | 17851.04 | null | 4917.48 | 65.64 |
| **Transect B** | | | | | | | | |
| Aug | 311.95 | 0.59 | 4977.53 | 0.768 | 675.43 | 49.05 | 1787.72 | 0.01 |
| Sep | 191.16 | 967.815 | 7174.38 | 0.048 | 1141.09 | 1617.005 | 6311.275 | 2.52 |
| Oct | 1163.42 | 7747.69 | 10937.715 | 7.512 | 3520.77 | 7782.715 | 15787.425 | 19.824 |
| Nov | 1867.915 | 7292.995 | 6896.175 | 0.768 | 5529.38 | 13481.53 | 43620.85 | 27.864 |
| Dec | 1409.205 | 5580.105 | 3626.305 | 4.872 | 6128.91 | 5397.755 | 115808.945 | 15.024 |
| Jan | 868.88 | 3428.23 | 2674.3 | 23.64 | 4212.855 | 2930.52 | 31697.17 | 12.48 |
| Feb | 559.495 | 1737.675 | 2094.255 | 90.72 | 2193.05 | 2057.92 | 5797.75 | 25.008 |
| Mar | 224.585 | 334.555 | 886.345 | 44.496 | 794.575 | 329.98 | 1871.515 | 101.28 |
| **Transect C** | | | | | | | | |
| Aug | 0.29 | 514903.73 | null | 9.76 | 2322.16 | 11026.01 | null | 0 |
| Sep | 1029.49 | 954758.155 | 1567.48 | 0.784 | 783.255 | 85214.355 | 974.23 | 17.504 |
| Oct | 195.01 | 323857.765 | 1739.69 | 9.936 | null | 431542.885 | 4282.36 | 16.448 |
| Nov | 2.675 | 187607.805 | 4603.955 | 11.2 | null | 503348.5 | 6182.645 | 56.672 |
| Dec | 55.22 | 17553.66 | 3141.105 | 16.816 | null | 186473.125 | 6683.465 | 112.416 |
| Jan | 10.12 | 8143.56 | 1629.305 | 30.192 | 61.84 | 93254.39 | 2405.405 | 103.392 |
| Feb | 609.615 | 9789.7 | 2155.405 | 19.584 | 2.2 | 46992.335 | 1062.785 | 126.784 |
| Mar | 0.685 | 7937.4 | 11964.2 | 4.48 | 366.7 | 9691.255 | 92126.795 | 96.512 |

Table 2: Individual values of $NH_4^+$ -N for each transect

| Month | Top-slope Ap | Mid-slope Ap | Toe-slope Ap | Riparian Ap | Top-slope Bt | Mid-slope Bt | Toe-slope Bt | Riparian Bt |
|---|---|---|---|---|---|---|---|---|
| | $NH_4^+$ -N per horizon and slope location for three transects | | | | | | | |
| | N (g) | N (g) | N (g) | N (g) | N (g) | N (g) | N (g) | N (g) |
| **Transect A** | | | | | | | | |
| Aug | 4.45 | 15.21 | null | 0.21 | 7 | null | null | 0.01 |
| Sep | 9.315 | 2.195 | 1.805 | 0.24 | 3.44 | 3.12 | 3.81 | 0.18 |
| Oct | 18.745 | 15675.47 | 5.185 | 0.09 | 3.955 | 9.725 | 4.975 | 0.015 |
| Nov | 4.77 | 18848.5 | 1.305 | 0.135 | 2.275 | 5.52 | 1.67 | 0.135 |
| Dec | 27.315 | 550.365 | 1.27 | 0.09 | 22.52 | 12.02 | 5.62 | 0.105 |
| Jan | 7.235 | 8.21 | 6.15 | 0.195 | 7.935 | 5.005 | 9.43 | 0.39 |
| Feb | 3.14 | 3.01 | null | 0.15 | 8.53 | 3.98 | 3.535 | 0.075 |
| Mar | 5.18 | 3.11 | 3.525 | 0.045 | 9.365 | 6.64 | 3.225 | 0 |
| **Transct B** | | | | | | | | |
| | B1A | B2A | B3A | RA_30 | B1B | B2B | B3B | RA_90 |
| Aug | 7.52 | 5.06 | 2.43 | 0.432 | 2.27 | 5.89 | 3.58 | 0.01 |
| Sep | 6.51 | 8.825 | 4.13 | 0.6 | 4.03 | 62.89 | 3.59 | 0.624 |
| Oct | 4.7 | 6.595 | 68.945 | 0.504 | 7.46 | 54.475 | 6.345 | 0.384 |
| Nov | 2.245 | 4.825 | 2.335 | 0.432 | 4.55 | 19.61 | 5.975 | 0.456 |
| Dec | 7.46 | 8.175 | 2.785 | 0.096 | 11.195 | 9.605 | 35.045 | 0.144 |
| Jan | 4.82 | 8.22 | 3.095 | 0.648 | 9.5 | 15.55 | 5.12 | 0.48 |
| Feb | 0.735 | 1.125 | 1.3 | 0.432 | 1.685 | 2.485 | 2.8 | 0.24 |
| Mar | 3.105 | 4.255 | 8.78 | 0.096 | 8.06 | 21.415 | 5.49 | 0.12 |
| **Transect C** | | | | | | | | |
| Aug | 3.51 | 503290.98 | 0.336 | null | 2.4 | 2524.52 | null | 0 |
| Sep | 12.105 | 229440.84 | 0.384 | 3.48 | 6.65 | 115.725 | null | 0.304 |
| Oct | 7.72 | 10896.835 | 0.384 | 5.57 | 156.23 | 57.985 | 5.995 | 0.272 |
| Nov | 6.715 | 200.595 | 0.448 | 9.75 | null | 35.58 | 2.99 | 0.176 |
| Dec | 21.225 | 104.875 | 0.304 | 6.455 | null | 59.95 | 7.115 | 0.208 |
| Jan | 3.15 | 251.735 | 0.368 | 2.675 | null | 99.535 | 5.175 | 0.32 |
| Feb | 1.005 | 92.46 | 0.144 | 1.59 | 2.415 | 7.11 | 43392.455 | 0.176 |
| Mar | 2.55 | 56.26 | 0.096 | 1433.745 | 16.62 | 12.635 | 104531.59 | 0.256 |

# Vita

Nicolas P. Zegre was born in Newton, New Jersey on January 1, 1975. Upon graduating from high school in 1993, he fulfilled a three-year enlistment in the United States Army as a Nuclear, Biological, and Chemical Warfare specialist. After military service, he received his Bachelor of Science in Forestry Management from West Virginia University. After employment with the U.S. Forest Service at the Coweeta Hydrologic Laboratory in western North Carolina, Nicolas began work on a Master of Science focusing on forest hydrology. Nicolas is now headed west to Oregon State University, fulfilling his professional dream of working in research forest hydrology.

He passes time outside of research with his extremely supportive family and friends, and can often be found exploring the virgin cave passage in the subterranean world and the vertical world of big wall climbing.